

# Practical and scientific aspects of injection molding simulation

**Citation for published version (APA):**

Kennedy, P. K. (2008). *Practical and scientific aspects of injection molding simulation*. [Phd Thesis 2 (Research NOT TU/e / Graduation TU/e), Mechanical Engineering]. Technische Universiteit Eindhoven.  
<https://doi.org/10.6100/IR634914>

**DOI:**

[10.6100/IR634914](https://doi.org/10.6100/IR634914)

**Document status and date:**

Published: 01/01/2008

**Document Version:**

Publisher's PDF, also known as Version of Record (includes final page, issue and volume numbers)

**Please check the document version of this publication:**

- A submitted manuscript is the version of the article upon submission and before peer-review. There can be important differences between the submitted version and the official published version of record. People interested in the research are advised to contact the author for the final version of the publication, or visit the DOI to the publisher's website.
- The final author version and the galley proof are versions of the publication after peer review.
- The final published version features the final layout of the paper including the volume, issue and page numbers.

[Link to publication](#)

**General rights**

Copyright and moral rights for the publications made accessible in the public portal are retained by the authors and/or other copyright owners and it is a condition of accessing publications that users recognise and abide by the legal requirements associated with these rights.

- Users may download and print one copy of any publication from the public portal for the purpose of private study or research.
- You may not further distribute the material or use it for any profit-making activity or commercial gain
- You may freely distribute the URL identifying the publication in the public portal.

If the publication is distributed under the terms of Article 25fa of the Dutch Copyright Act, indicated by the "Taverne" license above, please follow below link for the End User Agreement:

[www.tue.nl/taverne](http://www.tue.nl/taverne)

**Take down policy**

If you believe that this document breaches copyright please contact us at:

[openaccess@tue.nl](mailto:openaccess@tue.nl)

providing details and we will investigate your claim.

# **Practical and Scientific Aspects of Injection Molding Simulation**

CIP-DATA LIBRARY TECHNISCHE UNIVERSITEIT EINDHOVEN

Kennedy, P.K.

Practical and Scientific Aspects of Injection Molding Simulation /  
by P.K. Kennedy. - Eindhoven: Technische Universiteit Eindhoven, 2008.  
Proefschrift. - ISBN 978-90-386-1275-1

This thesis was prepared with the  $\text{\LaTeX}2_{\epsilon}$  documentation system.  
Reproduction: University Press Facilities, Eindhoven, The Netherlands.  
Cover design: P.K. Kennedy and Oranje.

# **Practical and Scientific Aspects of Injection Molding Simulation**

PROEFSCHRIFT

ter verkrijging van de graad van doctor aan de  
Technische Universiteit Eindhoven, op gezag van de  
Rector Magnificus, prof.dr.ir. C.J. van Duijn, voor een  
commissie aangewezen door het College voor  
Promoties in het openbaar te verdedigen  
op woensdag 11 juni 2008 om 14.00 uur

door

**Peter Kenneth Kennedy**

geboren te Melbourne, Australië

Dit proefschrift is goedgekeurd door de promotor:

prof.dr.ir. H.E.H. Meijer

Copromotoren:

dr.ir. G.W.M. Peters

en

dr.ir. P.D. Anderson

# Contents

---

<b>Summary</b>	<b>ix</b>
<b>1 Introduction</b>	<b>1</b>
1.1 The Injection Molding Process . . . . .	2
1.2 The Problem . . . . .	2
1.2.1 Basic Physics of the Process . . . . .	3
1.2.2 Material Properties . . . . .	3
1.2.3 Geometric Complexity of Mold and Part . . . . .	4
1.3 Why Simulate Injection Molding? . . . . .	4
1.4 Early Academic Work on Simulation . . . . .	5
1.5 Early Commercial Simulation . . . . .	6
1.6 Simulation in the Eighties . . . . .	9
1.6.1 Academic Work in the Eighties . . . . .	9
Mold Filling . . . . .	9
Mold Cooling . . . . .	12
Warpage Analysis . . . . .	13
1.6.2 Commercial Simulation in the Eighties . . . . .	13
Codes Developed by Large Industrials and Not for Sale . . . . .	16
Codes Developed by Large Industrials for Sale in the Marketplace . . . . .	16
Companies Devoted to Developing and Selling Simulation Codes . . . . .	17
1.7 Simulation in the Nineties . . . . .	18
1.7.1 Academic Work in the Nineties . . . . .	19
1.7.2 Commercial Developments in the Nineties . . . . .	21
SDRC . . . . .	21
Moldflow . . . . .	21
AC Technology/C-MOLD . . . . .	22
Simcon . . . . .	23
Sigma Engineering . . . . .	23
Timon . . . . .	23
Transvalor . . . . .	24

CoreTech Systems . . . . .	24
1.8 Simulation Science Since 2000 . . . . .	24
1.8.1 Commercial Developments Since 2000 . . . . .	26
Moldflow . . . . .	27
Timon . . . . .	28
Core Tech Systems . . . . .	28
1.9 Outline of Thesis . . . . .	29
1.10 Background of Candidate . . . . .	30
<b>2 Simulation of Injection Molding</b>	<b>33</b>
2.1 Introduction . . . . .	33
2.2 Filling and Packing Analysis(2.5D) . . . . .	34
2.2.1 Material Assumptions . . . . .	35
2.2.2 Geometric Considerations . . . . .	36
2.2.3 Simplification by Mathematical Analysis . . . . .	37
2.2.4 Boundary Conditions and Solidification . . . . .	39
2.2.5 Solution of the Governing Equations . . . . .	40
2.3 Mold Cooling Analysis . . . . .	41
2.4 Warpage Analysis . . . . .	41
2.4.1 Residual Strain Methods . . . . .	41
2.4.2 Residual Stress Models . . . . .	43
2.5 Material Testing Techniques . . . . .	48
2.6 Two Critical Issues . . . . .	49
<b>3 The Geometry Problem</b>	<b>51</b>
3.1 Modeling for Analysis . . . . .	51
3.2 Midplane Generation . . . . .	52
3.3 3D Analysis . . . . .	54
3.4 Dual Domain FEA . . . . .	54
3.5 Dual Domain Structural Analysis . . . . .	56
3.6 Warpage Analysis Using the Dual Domain FEM . . . . .	60
<b>4 Overcoming Material Data Limitations</b>	<b>67</b>
4.1 The Material Data Problem . . . . .	67
4.2 Hybrid Model . . . . .	68
4.2.1 The Contracted Notation . . . . .	69
4.2.2 Prediction of the $b_i$ . . . . .	71
4.2.3 Using the Model . . . . .	73
4.3 Results for Unfilled Polypropylene . . . . .	74
4.4 Results on Other Materials . . . . .	76
4.4.1 ABS . . . . .	77

---

4.4.2	PC . . . . .	77
4.4.3	PC+ABS Blend . . . . .	78
4.4.4	PBT . . . . .	78
4.5	Filled Materials . . . . .	79
4.5.1	Glass Reinforced PA66 . . . . .	79
4.5.2	Talc Filled PBT . . . . .	80
4.6	Conclusion . . . . .	81
<b>5</b>	<b>Improving Simulation Models</b>	<b>87</b>
5.1	Crystallization in Flowing Melts . . . . .	88
5.2	A FIC Crystallization Model . . . . .	90
5.2.1	Rheological Aspects . . . . .	93
5.2.2	Amorphous Phase . . . . .	94
5.2.3	The Semi-Crystalline Phase . . . . .	97
5.3	Viscosity Modeling . . . . .	99
5.4	Crystallization Model Performance . . . . .	100
	The Effect of Shear . . . . .	101
<b>6</b>	<b>Implementation in Molding Simulation</b>	<b>107</b>
6.1	Governing Equations . . . . .	107
6.2	Effect of Crystallization on Rheology . . . . .	108
6.3	Crystallization and Thermal Properties . . . . .	109
6.4	Crystallization and the Equation of State . . . . .	110
6.5	Numerical Scheme . . . . .	111
6.6	Validation of the Model . . . . .	112
6.6.1	Pressure . . . . .	112
6.6.2	Temperature . . . . .	112
<b>7</b>	<b>Conclusions and Further Work</b>	<b>117</b>
7.1	The Geometry Problem . . . . .	117
7.2	The Material Data Problem . . . . .	118
7.3	Future Development . . . . .	118
7.3.1	The Geometry Problem . . . . .	119
7.3.2	Prediction of Properties . . . . .	119
7.3.3	Thermal Conductivity . . . . .	119
7.3.4	Thermal Expansion Coefficient . . . . .	120
7.3.5	Mechanical properties . . . . .	120
7.3.6	Viscosity . . . . .	121
7.4	Additives . . . . .	121



<b>Bibliography</b>	<b>123</b>
References . . . . .	123
<b>Acknowledgment</b>	<b>137</b>
<b>Curriculum Vitae</b>	<b>139</b>
<b>Notes</b>	<b>140</b>

# Summary

---

## Practical and Scientific Aspects of Injection Molding Simulation

Simulation of injection molding is, arguably, the most successful example of simulation for any plastic forming process. The expense associated with creating an injection mold and the likelihood that a problem discovered in production will result in costly retooling and lost time, make molding simulation of high value to industry. This may be contrasted with other polymer forming processes where tooling costs are much lower or where problems may be overcome by varying process conditions.

Despite the apparent success of injection molding simulation, too few parts are subject to any simulation. Moreover, the prediction of shrinkage and warpage is subject to increasingly higher standards of accuracy. This thesis identifies some areas of improvement and provides solutions to increase usage of simulation and to improve accuracy of shrinkage and warpage prediction.

A commercial issue arises from the commonly used Hele-Shaw approximation. This reduces the conservation equations for mass and force to a single equation for pressure in which the pressure is assumed constant across the part thickness. Adopting a coordinate system with  $z$  in the local thickness direction and  $x$  and  $y$  in the plane of the part, this means that pressure is a function of  $x$  and  $y$  only. Such an equation is readily solved by a finite element approach and a mesh of triangles located at the midplane of the part geometry. While elegant and efficient in terms of solution, this approach requires a user with a true 3D geometry to create a representation of the midplane of the 3D geometry. This requirement can be costly in terms of time, as it typically involves some interaction with the user to create the mesh for analysis. We refer to this problem as the geometry problem.

Injection molding simulation requires data for viscosity, specific heat, thermal conductivity and density. These may be measured under controlled laboratory conditions, However, simulation may require the data under very different conditions. Consequently, a problem arises. How do we use data measured under a specific set of conditions in simulation? We refer to this problem as the material data problem.

This thesis examines the geometry and material data problem. The first chapter provides an introduction to the history of injection molding simulation from both academic and commercial viewpoints. We see that the evolution of software is influenced by external factors such as the hardware available to compute solutions and certain approximations made on the governing equations.

Chapter 2 reviews the Hele-Shaw approximation and discusses material data that is relevant to simulation. The chapter identifies the two problems introduced above, namely, the geometry and the material data problems.

Chapter 3 proposes a solution to the geometry problem. We describe a method for analysis of 3D solid models known as Dual Domain Finite Element Analysis. Originally developed for flow analysis, the extension to structural analysis is described, thereby enabling warpage analysis of a solid geometry. The method is much faster than a true 3D solution and makes use of the fact that injection molded products are typically thin walled.

Chapter 4 defines a practical method that overcomes some aspects of the material data problem as it relates to prediction of shrinkage. The technique is called the Corrected Residual In-Mold Stress (CRIMS) method. Essentially, we use a very simple theoretical model for predicting shrinkage and adjust it, using measured shrinkages on molded parts. The technique is shown to dramatically improve shrinkage prediction for a range of materials.

Chapter 5 presents recent attempts to further improve warpage simulation by means of improved physical modeling of injection molding. This is accomplished by predicting crystallization kinetics and morphology of semi-crystalline material. The idea is to first predict a morphology and then use this to predict a property.

Chapter 6 presents some models to predict material properties using crystallization kinetics and morphology prediction. This enables transformation of data obtained under laboratory conditions to the conditions experienced in simulation. We also

provide some validation of an injection molding simulation that incorporates the models.

Chapter 7 summarizes the previous chapters and proposes some area for future investigation.



## CHAPTER ONE

# Introduction

---

Injection molding is an ideal process for fabricating large numbers of geometrically complex parts. Many everyday items are injection molded: mobile phone housings, automobile bumpers, television cabinets, compact discs and lunch boxes are all examples of injection molded parts. Parts produced by the process are also becoming commonplace in less obvious applications. For example the relatively new area of micro-injection molding is providing new methods of drug delivery and optical couplers [91].

In terms of total plastic usage, injection molding is second only to extrusion. Resin consumption, for USA injection molders alone, is expected to grow at 3.2% per annum for the next few years. At this rate the resin consumed by the US injection molding industry in 2008 will be valued at US\$10.5 billion [65].

An important characteristic of molding is that it may not be possible to fix a problem in production by varying process conditions. Consequentially simulation of injection molding is industrially valuable. It is far better to avoid problems in the design phase than to fix them in production. Simulation of injection molding, particularly flow analysis, has had a major impact on industry. Indeed the editors of *Plastics Technology* magazine, a leading industrial journal, recently proposed a list of the fifty most important innovations in the plastic industry [1]. Number one was the reciprocating screw injection molding machine while simulation of injection molding was listed nineteenth. Whether one agrees with the editor's ranking or not, simulation of injection molding has been an outstanding aid to industry.

Despite this apparent success, there are significant problems in simulation of injection molding. Some of these problems are addressed in this thesis. In this chapter we review the molding process, consider the history of simulation from the commercial and scientific viewpoint and finally state the scope of the thesis.

## 1.1 The Injection Molding Process

Injection molding is a cyclic process. Initially, the mold is closed to form the cavity into which the material is injected. The screw then moves forward as a piston, forcing molten material ahead of it into the cavity. This is the injection or filling phase. When filling is complete, pressure is maintained on the melt and the packing phase begins. The purpose of the packing phase is to add further material to compensate for shrinkage of material as it cools in the cavity. At some time during packing, the gate freezes and the cavity is effectively isolated from the pressure applied by the melt in the barrel. This marks the beginning of the cooling phase in which the material continues to cool until the component has sufficient mechanical stiffness to be ejected from the mold. During cooling, the screw starts to rotate and moves back. The rotation assists plastication of the material and a new charge of melt is created at the head of the screw. When the molded part is sufficiently solid, the mold opens and the part is ejected. The mold then closes and the cycle begins again.

In summary the injection molding process is characterized by the following phases:

1. Mold closing
2. Injection
3. Packing
4. Cooling
5. Plastication and screw back
6. Ejection

Most effort in computer simulation has been devoted to phases 2-4. There have been significant advances in modeling plastication ([149], [82], [175], [120]) but generally, for molding simulation, it is assumed that the melt enters the cavity with a prescribed flow rate or pressure and a uniform temperature. Simulation of the ejection phase requires accurate shrinkage analysis and complex boundary conditions for the frictional resistance of the part on the core. Again advances have been made in these areas [59] but today no simulation combines all these effects.

## 1.2 The Problem

While the description of the process in the previous section appears straightforward there are complications, namely,

- the nature of injection molding, in particular the basic physics of the process;
- the properties of the material and
- geometric complexity of the mold

Each of these is briefly discussed as background to the problems tackled later in this thesis.

### 1.2.1 Basic Physics of the Process

The filling phase is characterized by high flow rates and hence high shear rate. During mold filling, the molten material enters the mold and convection of the melt is the dominant heat transfer mechanism. Due to the rapid speed of injection, heat may also be generated by viscous dissipation. Viscous dissipation depends on both the viscosity and deformation rate of the material. It may be most apparent in the runner system and gates where flow rates are highest however, it can also occur in the cavity if flow rates are sufficiently high or the material is very viscous.

In addition to forming the shape of the part to be made, the mold causes solidification of the material. Heat is removed from the melt by conduction through the mold wall and out to the cooling system. As a result of this heat loss, a thin layer of solidified material is formed as the melt contacts the mold wall. Depending on the local flow rate of the melt, this "frozen layer" may rapidly reach equilibrium thickness or continue to grow thereby restricting the flow of the incoming melt. This has a significant bearing on the pressure required to fill the mold and an important role in warpage prediction. When the cavity is volumetrically filled, the filling phase is complete but pressure is maintained by the molding machine. This begins the packing or holding phase.

Since the cavity is now full, mass flow rate into the cavity is much smaller than during injection and consequently both convection and viscous dissipation are minor effects – though they can be important locally. During packing, conduction becomes the major heat transfer mechanism and the frozen layer continues to increase in thickness. At some time, the gate will freeze thereby isolating the cavity from the applied pressure. Conduction is still the dominant heat transfer mechanism as the material solidifies and shrinks in the mold. It is possible that the material will pull away from the mold wall during this time ([21], [36]) - a condition that greatly complicates the calculation of the temperature of the material whilst in the mold. Finally, when the part is sufficiently solidified it is ejected from the mold.

To summarize then, we see the injection molding process involves several heat transfer mechanisms, is transient in nature, and involves a phase change and time varying boundary conditions at the frozen layer in filling, packing and during cooling. While these considerations are substantive, the process is further complicated by material properties and the geometry of the part.

### 1.2.2 Material Properties

Polymers for injection molding can be classified as semi-crystalline or amorphous. Both have complex thermo-rheological behavior which has a bearing on the molding



process. Thermoplastics typically have a viscosity that decreases with shear and increasing temperature while increasing with pressure. Their thermal properties are temperature dependent and may depend on the state of stress [138]. In the case of semi-crystalline materials, properties also depend on the flow history and rate of temperature change.

An additional complexity, in injection molding simulation, is the need to incorporate an equation of state to calculate density variation as a function of temperature and pressure. The equation of state relates the material's specific volume (inverse of density), pressure and temperature. This is referred to as the material's PVT characteristic. It too is complex and depends on the type of material.

### 1.2.3 Geometric Complexity of Mold and Part

Injection molded parts are generally thin walled structures and may be of extremely complex shape. The combination of thin walls and rapid injection speeds leads to significant flow rates and shear rates and these, coupled with the material's complex viscosity characteristics, lead to large variations in material viscosity and so variation in fill patterns.

The mold has two functions in injection molding. The first is to form the shape of the part to be manufactured and the second is to remove heat from the mold as quickly as possible. An injection mold is a complex mechanism with provision for moving cores and ejection systems. This complexity influences the positioning of cooling channels which can lead to variations in mold temperature. These variations affect the material viscosity and so the final flow characteristics of the material.

## 1.3 Why Simulate Injection Molding?

The previous section provides some feeling for the complexity of the molding process. It is no surprise that part quality is related to processing conditions. Indeed, the notion that processing has a dramatic affect on the properties of the manufactured article has been known since plastic processing began. In practice, the relationship between process variables and article quality is extremely complex. It is very difficult to gain an understanding of the relationship between processing and part quality by experience alone. It is for this reason that simulation of molding was developed and it is interesting to note that CAE has been much more successful in injection molding than in other areas of polymer processing.

The last point requires some explanation. Many polymer forming processes are continuous and, although the process physics may be complex, the die is generally quite simple and inexpensive to make. Moreover, there is considerable flexibility in changing process conditions. For blow molding and thermoforming, the cost of tooling is relatively inexpensive. In fact the cost of a blow-molding mold can be as low as one

tenth that of an injection mold for a similar article [64]. Moreover, blow-molding machines provide the operator with enormous control so problems can often be solved on the factory floor. By contrast, in injection molding, problems experienced in production may not be fixed by varying process conditions as with other processes. While there is scope to adjust process conditions to solve one problem, often the change introduces another. For example, increasing the melt temperature and so decreasing the viscosity of the melt may cure a mold that is difficult to fill and which is flashing slightly. The increase in temperature may, however, cause gassing or degradation of the material which may cause unsightly marks on the product. The fix may be to increase the number of gates or mold the part on a larger machine. Both of these are economically unfavorable - the first, involving significant retooling, is also costly in terms of time and the second will erode profit margins as quotes for the job were based on the original machine which would be cheaper to operate. On the other hand, simulation can be performed relatively cheaply in the early stages of part and mold design and offers the ability to evaluate different design options in terms of part, material and mold design.

## 1.4 Early Academic Work on Simulation

Injection molding was practiced a long time prior to the advent of simulation. While the observation that part quality was affected by processing was well known, due to the complex interplay of the factors involved, injection molding was something of an art. Experience was the only means of dealing with problems encountered in the process. An overview of this approach is given by Rubin [133]. The bibliography of this book cites hundreds of empirical studies each contributing to the relationship between processing and part quality.

Early work on simulation began in the late 1950's with the work of Toor et al. [157] where the authors introduced a scheme to calculate the average velocity of a polymer melt filling a cold rectangular cavity and so obtain the maximum flow length of the polymer. These results could then be used to deduce the time to fill a cavity of given length. Their calculations accounted for conductional heat loss and used experimentally determined parameters for the effect of temperature and shear rate on viscosity. No viscous dissipation effects were accounted for and the pressure equations solved were obtained by a force balance. It is interesting to note that the equations were solved on an IBM 702 computer with an average run time per simulation of 20 hours!

Demand for increased quality of molded parts in the 1970's saw an increased interest in mathematical modeling of the injection molding process. During this time many pioneering studies were published. In the early seventies there was some interest by mathematicians in Hele-Shaw flow [132]; however, these works focused on mathematical issues and did not consider application to injection molding.

In 1971 Barrie [11] gave an analysis of the pressure drop in both delivery system and a disk cavity. He avoided the need for temperature calculations by assuming

the frozen layer had uniform thickness that is proportional to the cube root of the filling time. Interestingly, Barrie remarked that a tensile (extensional) viscosity may be required for prediction of cavity pressure in the region near the sprue due to the extension rate there. It is a sobering thought that to this day no commercial package includes such terms in the cavity although pressure losses at sudden contractions such as gates are often included.

The work of Kamal and Kenig [88] was especially noteworthy as they considered filling, packing and cooling phases in their analysis. They used finite differences to solve for the pressure and temperature fields.

Williams and Lord [174] analyzed the runner system using the finite difference method. This was extended to analysis of the cavity in the filling phase again using finite differences [110].

In Germany, the Institut für Kunststoffverarbeitung (IKV), formed at the University of Aachen in 1950, produced a method for simulation called the Füllbildmethode. This was based on simple flow paths, (similar to the layflat method described in Section 1.5) and assumed the melt was isothermal [135].

The formation of the Cornell Injection Molding Program (CIMP) at Cornell University in 1974 saw a focus on the scientific principles of injection molding. Early work focused on the filling stage [146]. This consortium had a significant effect on injection molding simulation.

All of the above work focused on rather simple geometries and while of academic interest, offered little assistance to engineers involved with injection molding. Nevertheless, these studies provided the scientific base for commercial simulation tools.

## 1.5 Early Commercial Simulation

Development of commercial software for injection molding simulation relied on the scientific understanding of the process as well as the state of the CAD and computer industries.

The first company devoted to simulation of injection molding was founded, in Australia, by Colin Austin in 1978. In explaining the greatest influences on his early thinking [7] Austin named the works of Kamal and Kenig [88], Lord and Williams [110], [174] and Barrie [11]. Austin named his company Moldflow and it continues under this name today. As computers were extremely costly in the early 1980's, Moldflow's first products were distributed primarily by timeshare services whereby users could buy access to the programs via satellite links to central computers. Consequently users around the world were granted access to the software. An important part of the Moldflow product at that time was the Moldflow Design Principles [6]. These were a set of guidelines for improving the design of plastic parts and runner systems. The Design Principles defined what people should do, while the software gave a quantitative indication of how closely they achieved these goals. Moldflow

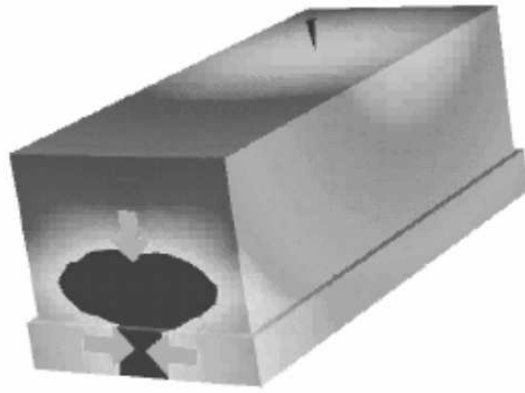


**Figure 1.1:** Flow progresses faster in the thick rim of the box and creates an airtrap on the front (shown) and rear ends.

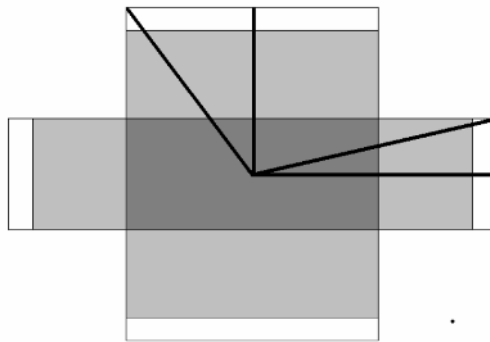


**Figure 1.2:** The "layflat" is created by unfolding the box to lie in a plane. Note though that correct thickness of each surface is retained. Dark lines represent possible flow paths for analysis.

Design Principles are still valuable and were recently reprinted [143].

Early Moldflow software used the "layflat" approach developed by Austin [5]. The layflat was a representation of the part under consideration that reduced the problem of flow in a three-dimensional thin walled geometry to flow in a plane. For example, consider an open box with a thickened lip at the open end. If the box is to be injected at the center of its base, a potential problem could arise from polymer flowing around the rim of the box and forming an air trap as shown in Figure 1.1.

The lay flat of the box is shown in Figure 1.2. As can be seen, the box has been "folded out" to form the layflat.

Analysis could be performed on the various flow paths on the layflat (the dark lines). The analysis was essentially one-dimensional with regard to pressure drop, although temperature variation through the thickness and along the flow path was accounted for.

While the box seems simple, considerable skill was required to produce the layflat for more complex parts. Figure 1.3 shows the layflat for an early automotive component. It can be seen that unfolding the part and determining the flow paths is not straightforward.

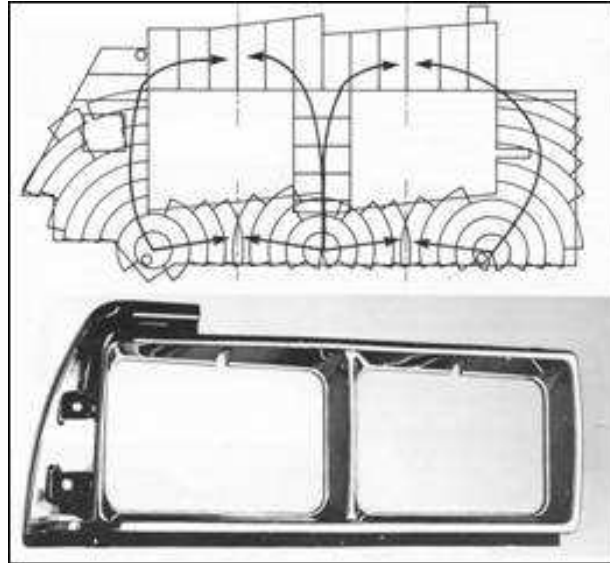


**Figure 1.3:** An automotive component and its associated layflat model.

Thermal calculations used either a method similar to that proposed by Barrie [11] for calculation of frozen layer thickness, or a finite difference scheme with grid points through the thickness and along the flow path. A constant mold temperature was assumed at the plastic mold interface. While the melt temperature at injection points was assumed constant, viscous dissipation, convection of heat due to incoming melt and conduction to the mold were accounted for. Viscosity of the melt was modeled with a power law or second order model as used by Williams and Lord [110] and included shear thinning and temperature effects. Pressure drop was calculated using analytic functions for flow in simple geometries – parallel plates or round tubes. Results from the analysis were displayed in tabular form for each of the analyzed flow paths. Due to the relatively simple assumptions made, the analysis was sufficiently fast to allow users to interactively modify thicknesses to achieve their design goal. By determining the pressures and times to fill along each flow path, the user could increase (or decrease) the thickness of the component so as to balance the fill time along each flow path and eliminate the airtrap. While this type of analysis was undoubtedly of benefit, it required the user to analyze an abstraction (the layflat) of the real geometry. For complex parts, the determination of the layflat required considerable skill. However a solution to this problem was not far away.

Giorgio Bertacchi formed *Plastics & Computer*, an Italian company devoted to molding software, in 1978. Products from *Plastics & Computer* were also distributed by

timeshare systems. These products were aimed at all aspects of injection molding. While there was some simulation capability, the software also dealt with costing estimation.

## 1.6 Simulation in the Eighties

Apart from research on molding simulation, the eighties saw the introduction of CAD as a mainstream part of product design. CAD systems of the period were predominantly surface or wireframe based. This meant that geometry was represented as surfaces with no thickness displayed. However, when meshed the local thickness information was assigned to elements. It was thus a time ripe for the introduction of finite element methods using the Hele-Shaw approximation. Indeed the Hele-Shaw approximation enabled the advancement of both academic and commercial software. Such is its importance that we provide an outline of the derivation of the equations in Chapter 2.

This decade saw a rapid evolution of computer hardware. In the early eighties, large mainframe systems and time share distribution of software were common. In the mid eighties the hardware moved to the super mini, while at the end of the decade the UNIX workstation was introduced. The latter provided vastly improved graphics and higher computational speed.

### 1.6.1 Academic Work in the Eighties

In the eighties, academic and commercial interest extended to other aspects of the process. Certainly there were further advances in simulating the filling phase but interest shifted to other phases of the process. Consequently we find a broadening of simulation to the packing and cooling phases. Another feature of this period is the formation of several centers focusing on the injection molding process. Each center was based around a university department and each produced its own computer code to further research on simulation of molding.

#### Mold Filling

McGill University had a team lead by Musa Kamal. As well as academic work on foundations, the McGill group developed the McKam software for molding simulation [87]. McKam used the finite difference method for numerical calculations and utilized the most advanced algorithms available. Analysis of both filling and packing phases was possible and the program focused on the long term goal of determining product properties such as birefringence and tensile modulus. In 1986 Lafleur and Kamal [106] presented an analysis of injection molding that included the filling, packing and cooling phases with a viscoelastic material model.



The Cornell Injection Molding Program (CIMP) led by K.K. Wang was also very active in the eighties. The work of Hieber and Shen in 1980 [74] was arguably the most influential work from the Cornell Injection Molding Program. Assuming an incompressible material, a symmetric flow field about the cavity centre line and adopting the Hele-Shaw approximation, the pressure equation solved was

$$\frac{\partial}{\partial x} \left( S \frac{\partial p}{\partial x} \right) + \frac{\partial}{\partial y} \left( S \frac{\partial p}{\partial y} \right) = 0. \quad (1.1)$$

A more general form of this equation is derived in Chapter 2. The above equation results by setting the RHS eqn.(2.17) in accord with the assumption of incompressibility.

The important point is that the pressure field is two-dimensional – there is no pressure variation in the thickness (local  $z$ ) direction. Under the same assumptions, the energy equation was

$$\rho c_p \frac{DT}{Dt} = \eta \dot{\gamma}^2 + \frac{\partial}{\partial z} \left( k \frac{\partial T}{\partial z} \right) \quad (1.2)$$

(see eqn. (2.11) in Chapter 2).

A finite element scheme using quadratic elements was used to solve the pressure equation. As there was no need to calculate pressure in the local  $z$  direction, the mesh required was located on a local  $x - y$  plane. Finite differences were used to solve the temperature field which was assumed to be symmetric about the cavity center line. After solving for the pressure field, the velocities in the  $x$  and  $y$  directions could be obtained using

$$v_x(x, y, z) = \frac{\partial p}{\partial x} \left[ \int_{-H}^H \frac{z'}{\eta} dz' - C(x, y) \int_{-H}^H \frac{dz'}{\eta} \right] \quad (1.3)$$

$$v_y(x, y, z) = \frac{\partial p}{\partial y} \left[ \int_{-H}^H \frac{z'}{\eta} dz' - C(x, y) \int_{-H}^H \frac{dz'}{\eta} \right] \quad (1.4)$$

For details, see equations (2.12) and (2.13) in Chapter 2.

With the velocity field known, the total flow into a nodal control volume could be determined. In this way the flow front could be propagated at each time step until the part was filled.

Most importantly, this paper introduced the idea of analyzing the thin-walled geometry as a set of shell elements, with the required model being much closer to the original geometry than the one-dimensional flow paths analyzed in the layflat method and finite difference codes using simplified geometry. Figure 1.4 shows an example of a 3D component and a midplane shell element mesh.

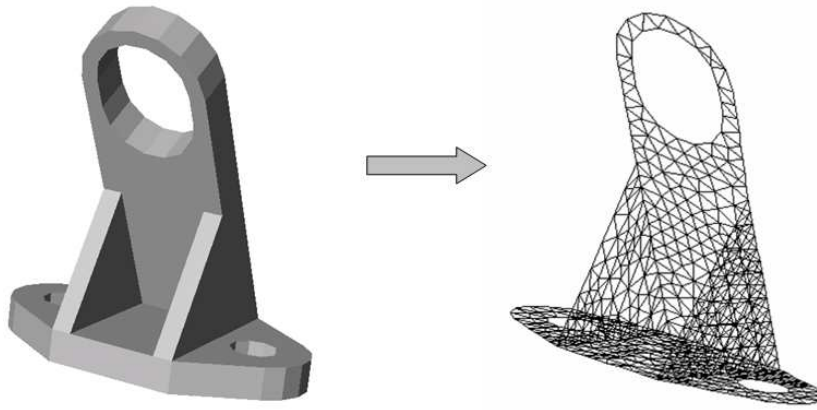


**Figure 1.4:** A 3D object (left) and its corresponding meshed midplane model. Each triangle in the mesh is assigned a thickness.

The use of finite elements and finite differences lead to this approach being described as a “hybrid” approach. Moreover, as the pressure field was two-dimensional and the velocity and temperature field three-dimensional, this method of molding simulation was often referred to as 2.5D analysis.

We will use the term “2.5D midplane” analysis in the sequel by which we mean the use of a finite element solution of a 2D pressure solution using a mesh at the centerline of the product and the 3D solution of the temperature equation using finite differences with a control volume approach to the propagation of the flow front.

The CIMP produced several software codes based on this work. In 1980 the code TM-2 was completed. It used the 2.5D midplane method of Hieber and Shen [74] and was limited to single-gated analysis of one cavity. TM-2 was extended to TM-7 in 1986. This code allowed analysis of the runner system and a variable thickness cavity, using beam and triangular elements respectively. Viscosity was modeled with temperature, shear rate and pressure dependence. The final code from the CIMP in this period was distributed in 1989 and called TM-10-C. This software offered 2.5D midplane analysis in the filling and packing stage of injection molding. It was applicable to thin-walled geometry with variation in thickness and used a compressible fluid model.

In Germany, the Institut für Kunststoffverarbeitung (IKV) at Aachen, continued to research all aspects of plastic processing – not just injection molding. However, they too developed an injection molding code called CADMOULD. This was also a 2.5D midplane analysis code.

A group lead by J. Vlachopoulos at McMaster University in Canada formed the Centre for Advanced Polymer Processing and Design (CAPPA-D). Generally CAPPA-D dealt with processes other than injection molding but they did fundamental work on the so-called fountain flow that takes place in injection molding [113], [114]. The importance of this work was that all prior work had assumed the melt flow in injection



molding is two-dimensional. That is, there was no pressure variation through the thickness of the part and hence no velocity gradient in the thickness direction. Consequently, when considering the energy equation, there was no explicit convection calculation of temperature in the thickness direction. Researchers openly stated that these assumptions were invalid at the flow front, but it was generally accepted that the assumption was appropriate once the flow front passed a given point. Interestingly it has only recently been demonstrated that the stability of the flow front has an important role in the surface defect known as “tiger stripes” [17].

The late eighties also saw the Eindhoven group, lead by H.E.H Meijer and F.P.T. Baaijens, begin work on molding simulation. In conjunction with the Philips Centre for Fabrication Technology (Philips CFT) they introduced a series of codes called Inject-I and Inject-2. Sitters [145] and Boshouwers and van der Werf [20] introduced simulations using the 2.5D midplane approach which led to Inject-3 the first 2.5D midplane analysis from the collaboration. This code dealt rigorously with the filling phase for amorphous materials.

## Mold Cooling

People familiar with the injection molding process realized the cooling phase accounted for the majority of time in any given cycle. Naturally, there was an interest in optimizing the cooling system so as to reduce cooling time and increase productivity. Industrial interest in cooling was also motivated by the effect of cooling on warpage of injection molded parts. Several groups contributed to development of mold cooling software. Interestingly development of cooling simulation was lead by commercial companies rather than academia. This was perhaps due to the lack of new science involved in cooling simulation.

Despite this, the CIMP did make some major contributions. Kwon et al. [105] introduced a relatively simple solution to mold cooling. This was extended by Himasekhar et al. [75]. By considering a 1D problem conduction problem with a finite difference scheme in the mold and melt, and several different numerical methods, the authors concluded that a cycle averaged temperature was sufficiently accurate for mold design purposes. Himasekhar et al. [75] then implemented a 3D solution for which the temperature in the mold was determined using a boundary element method (BEM), similar to that proposed by Burton and Rezayat [27], and a finite difference method for heat transfer in the polymer. This became the most common approach to cooling simulation. That is, use a finite difference or semi-analytical solution in the polymer and conduct a full 3D heat transfer analysis in the mold using the BEM.

The work of Karjalainen [89] was a noteworthy but little-known contribution to the field. Here a finite element solution in the plastic and the mold metal was employed, unlike the boundary element approach used by others. Moreover, interface elements were used to model heat transfer between mold blocks and inserts.

It is worth remarking that the trend to use the BEM method for the 3D mold cooling

problem was due to the need to mesh only the outer surface of the mold. It is unlikely that the mesh generators of the day would have been able to produce a 3D mesh of the mold. It is for this reason that the BEM method became the standard solution.

### **Warpage Analysis**

One of the great problems in injection molding is part warpage. Some major steps toward simulation of this phenomenon were made in this period. We make no attempt to detail all of this work here but note the work of greatest impact on simulation.

To understand the development of warpage simulation, it is important to appreciate that warpage results from inhomogeneous polymer shrinkage. While all polymers shrink on cooling from the melt to solid phase, processing causes variation in shrinkage and it is this variation that results in part deformation. One can break the problem into two parts - prediction of isotropic shrinkage and prediction of anisotropic effects. The former is influenced greatly by the pressure and temperature history of the part. Consequently the packing phase is important. Development of anisotropic shrinkage effects is related to structure development of the material as it solidifies. For an amorphous polymer, molecular orientation is important. The problem is more difficult for semi-crystalline materials.

It follows then, that warpage simulation rests on our ability to model the filling, packing and cooling phases of the molding process.

There is little work in the literature on the prediction of warpage specifically. Instead, research focused on understanding the residual stress in injection molded products. The early work in this area was influenced by the literature on residual stress in glass [108]. While this accounted for residual stresses due to cooling, it neglected the effect of the pressure applied in the packing phase.

Isayev et al. [84] considered the residual stress in an amorphous polymer. They showed that the flow-induced stresses tended to be tensile and of maximum value at the surface of a molded strip. On the other hand, purely thermal stresses are compressive at the surface. An excellent review of this and the work of others is provided in Isayev [83].

The link between packing pressures and the development of residual stresses was investigated by Titomanlio et al. [154]. A simple model for residual stress was used to calculate stress distributions in rectangular plate moldings of polystyrene. Results compared reasonably with experimental data.

### **1.6.2 Commercial Simulation in the Eighties**

The eighties saw a big increase in commercially available programs for simulation of injection molding. In the early eighties, the only commercial companies involved in molding simulation were Moldflow and Plastics & Computer. By the end of the

decade there were simulation codes from

- General Electric
- Philips/Technical University of Eindhoven
- Graftek Inc.
- Structural Dynamics Research Corporation (SDRC)
- AC Technology
- Moldflow Pty. Ltd.
- Simcon GmbH

These offerings may be grouped into three categories,

1. Codes developed by large industrials and used for internal advantage - but not for sale in the open marketplace;
2. Codes developed by large industrials and available for sale in the open marketplace;
3. Codes developed by companies devoted to developing and selling simulation codes.

We consider each later in this section.

Some general remarks are in order regarding the development of commercial software in this period. By far the most important development was the general acceptance of the 2.5D midplane solution for flow analysis. The use of finite elements immediately provided the advantage of displaying results on something that resembled the actual geometry. This was a great advantage over lay flats and tabular results. Generally, triangular shaped elements were used to model the cavity – due to ease of mesh generation. Runners were modeled with beam elements of circular section.

While software was chiefly distributed by timeshare in the early eighties, some large companies purchased mainframe systems. These included the VAX VMS, Control Data CDC Cyber, and IBM machines running the VM operating system. These systems started to reduce in popularity as the decade wore on due to inroads by PC's and UNIX workstations.

Aside from any technological advance in the modeling of injection molding, the power of computers increased dramatically. Gordon Moore [119] published a paper in 1965, suggesting that the number of transistors per chip would double every 18 months or so. Nobody at the time could have imagined that this prediction would remain in force for so long – particularly when you look at the scant data on which it was based. As well as the predicted changes in fundamental semiconductor technology, there were enormous changes in commercially available hardware – approximately a doubling of speed every 18 months.

An important change in hardware was heralded by IBM's introduction of a personal computer in 1981 [78]. An improved model, the AT, was introduced in 1983 [77]. For the first time a computer with worldwide support was available at a reasonable price and led to simulation software being distributed on media such as floppy disks. These machines had 16 bit processors and required extenders to increase addressable memory for molding simulation. However, it was not until 1985 when Intel introduced the 386 chip – a 32 bit processor – that the PC showed its true potential.

Toward the end of the decade, a new hardware platform was introduced - the UNIX workstation. Manufacturers such as Apollo, Silicon Graphics International (SGI), Hewlett Packard (HP), SUN and Digital Electronics Corporation (DEC) introduced machines running variants of UNIX. These machines had 32 bit operating systems, were aimed at the scientific computing industry, were faster than PC's and offered very high graphics performance. The latter was a major factor in the acceptance of 2.5D midplane analysis as the standard for molding simulation. Importantly, the graphics capability of these machines enabled the development of photorealistic rendering of parts in the CAD systems of the day.

The major CAD systems of the eighties were Computervision (CADD5), Intergraph (IGDS and Interact), McDonnell-Douglas (Unigraphics), GE/CALMA, IBM/Dassault (CADAM and CATIA). All of these systems offered wireframe and surface modeling. Consequently they were ideally suited to production of the model required for the 2.5D midplane analysis employed in commercial simulation software.

Commercial simulation was extended to the packing and cooling phases of the molding process. A significant impediment to introduction of this software was the lack of PVT data. In the eighties the largest source of data was a German work published by VDMA – an industrial association of German plastic processing machine makers [159]. Fortunately, two commercial machines were introduced later in the decade. One was developed by Paul Zoller [197] and sold under the name Gnomix. This machine immersed the sample in a confining fluid – silicon oil or mercury. Pressure was applied to the confining fluid, which in turn applied a uniform pressure to the sample. The temperature and pressure of the fluid and the change in volume were measured from which the PVT characteristics were derived.

The other machine was developed by SWO Polymertechnik GmbH. Rather than a confining fluid, the sample was compressed by a piston. Measurement of the pressure and temperature of the melt and the volume change allowed calculation of the PVT behavior of the material.

Wiegmann and Oehmke [173] describe each method and the associated advantages and disadvantages.

Against this background we now discuss the available simulation codes.

## Codes Developed by Large Industrials and Not for Sale

**General Electric** As mentioned in a previous section, cooling phase simulation was considered commercially important. Singh [144] described a system developed within General Electric in the early eighties that used one-dimensional heat transfer theory to optimize the design of cooling circuits. This code was known as POLYCOOL. It was further developed within GE and then commercialized by SDRC (see later section).

GE also developed some flow analysis software. Named FEMAP, this code used the 2.5D midplane approach [166]. Unlike the work of Hieber and Shen [74], linear finite elements were used for pressure calculation. Post processing of results was done in the SDRC environment.

**Philips/Technical University of Eindhoven** The Inject-3 code mentioned earlier [20] was used within Philips for simulation. It dealt with the filling phase using the hybrid 2.5D midplane approach. Its academic roots meant it was capable of detailed analysis when used by experts. While developed for internal use, there was an attempt to commercialise it. This failed when another Philips division adopted C-Flow (see Section entitled "Companies Devoted to Developing and Selling Simulation Codes" later in this chapter).

## Codes Developed by Large Industrials for Sale in the Marketplace

**SDRC** Structural Dynamics Research Corporation (SDRC) was an early pioneer of finite element dynamics analysis and a major CAD company. They became involved in CAE for injection molding when they commercialized the POLYCOOL code from GE. In 1982, SDRC offered its first product called POLYCOOL 1. This was a two-dimensional quasi-static thermal analysis of mold cooling. The program used shape factors to describe the mold geometry [144]. In 1984 SDRC embarked on a new development for a cooling analysis code that did not have the drawbacks of POLYCOOL 1, namely the lack of a true 3D description of the mold, part and cooling line system. This culminated in the limited release of POLYCOOL 2.0 in late November 1984 and a wider release of POLYCOOL 2.1 in 1985. This code used a one-dimensional transient finite difference method for heat conduction in the plastic coupled with a 3D boundary element method for heat transfer in the mold [27]. Heat transfer from the mold to the cooling circuits was steady state. At that time, SDRC also distributed flow analysis software produced by Moldflow. SDRC developed interfaces so that POLYCOOL 2.1 could accept the initial temperature distribution of the plastic in the mold calculated from Moldflow flow analysis and then commence cooling analysis. POLYCOOL 2.1 was the state of the art in cooling analysis software at the time. Indeed the approach used, or an approximation to it, became the standard method for mold cooling analysis.

**GRAFTEK** GRAFTEK was formed in 1980 and believed the plastics injection molding market would be best served by an integrated CAD/CAM and CAE system. The company sold a turnkey system for 3D mechanical design and numerical control machining. Its first filling simulation product was called SIMUFLOW. This was a finite difference branching flow program not unlike that offered by Moldflow. A 2.5D midplane analysis called SIMUFLOW 3D, which was based on code developed by the CIMP, was offered later [30]. GRAFTEK also supplied SIMUCOOL for mold cooling analysis. In 1984 GRAFTEK was acquired by the Burroughs Corporation. It underwent further changes of ownership and disappeared in the 1990's. SIMUFLOW 3D has recently reappeared in the market place due to reinvestment in the technology by another company.

### **Companies Devoted to Developing and Selling Simulation Codes**

**AC Technology** The Cornell Injection Molding Program gave rise to AC Technology - an incorporated company formed in 1986. AC Technology marketed the C-Flow filling code in 1986 [168]. Based on the work of Hieber and Shen [74], this code sought to make the 2.5D midplane analysis more tractable on the computer systems of the day by using linear finite elements for the pressure equation. It also incorporated a high-level graphical user interface (GUI) to facilitate use by people who were not expert in the field of analysis.

The original C-MOLD product performed only filling analysis but did not assume symmetry about the cavity centre line and so used a finite difference grid for temperature calculation over the entire thickness.

Analysis of the packing phase [167] and mold cooling analysis were introduced in 1988. The cooling analysis used the BEM in the mold [75]. Heat fluxes calculated by the cooling analysis were used as boundary conditions for the filling and packing analyses thereby coupling the flow and cooling phases.

**Moldflow** Moldflow developed a finite element flow analysis program in the early eighties. While it used linear elements for pressure, it differed from the approach used by other companies in that it did not use the finite difference method for temperature calculations. Instead it used a proprietary scheme based on the ideas of Barrie [11] for frozen layer thickness and a semi-analytic method for temperature. From a commercial viewpoint the big problem was the lack of suitable mesh generation and graphical display of results. This was overcome in 1982 when the first finite element software with meshing and graphical display software was released by Moldflow [5].

Moldflow began development of a 3D cooling analysis in the early eighties. The development was completed in 1986 [148]. This code was similar to the SDRC POLY-COOL 2 development. However, it was never released. Unlike finite element methods, the boundary element method required solution of a full matrix. The company



decided solution of such matrices was too computer-intensive for the time. Consequently, Moldflow developed a near node boundary element method. Rather than calculate the effect of each plastic element on every other plastic element and each cooling line element, this technique considered only those elements near the element under consideration. This resulted in much smaller matrices and reduced computer requirements greatly. It was released for sale in 1985.

In 1987, Moldflow started an industrial consortium with the acronym SWIS – Shrinkage Warpage Interface to Stress. It was aimed at predicting the warpage of injection molded parts. For this project, Moldflow adopted a 2.5D midplane analysis for flow analysis that was similar to that used in C-MOLD – that is, linear finite elements for pressure and finite differences for temperatures. A packing analysis was also introduced. In order to reduce the necessary computer requirements, the filling and packing analyses assumed the flow field was symmetric about the cavity centre line.

The near node boundary element mold cooling analysis was extended to give asymmetric temperatures and these were averaged to interface to the filling and packing analysis. Shrinkage calculations used the results from flow and cooling analysis to determine shrinkage strains calculated from an equation [118] (see equations 2.19 and 2.20 in Chapter 2). These strains were calculated on the top and bottom of each element in the model, thereby accounting for differential temperature effects, and in directions parallel and transverse to flow. The deformation of the part was then determined by converting these strains to thermal strains and inputting them to commercial structural analysis solvers such as ABAQUS, ANSYS, NASTRAN and ADINA. It should be noted that this approach does not involve calculation of residual stress – rather, residual strains are calculated and these are then “corrected” with measured values of shrinkage. Chapter 2 provides more details on this procedure.

**Simcon Kunststofftechnische Software GmbH** Simcon was founded in 1988. Located in Aachen the company maintained a close relationship with IKV and commercialized the Cadmould program that was developed within IKV.

Simcon’s products used 2.5D midplane analysis with their own pre and post processing. They allowed analysis of filling and cooling phases of the molding process.

## 1.7 Simulation in the Nineties

Toward the end of the 1980’s, the UNIX workstation became the machine of choice for simulation. However PC development continued. In 1990, the Windows operating system was introduced. This enabled better user interfaces and improved graphics performance.

Apart from the hardware advances, another important factor was the development of computer aided drafting (CAD) software. Many users of design software saw immediate benefits in CAD systems rather than simulation. The rationale was that

CAD systems offered a single design environment in which product development could occur. The notion that designs were captured on disk and available for change quickly displaced many drafting boards with computer screens. In the eighties CAD was restricted by computer power and industrial needs. In 1985 the formation of Parametric Technology Corporation led to the introduction of 3D modeling with parametric constraints on geometry. Suddenly the entire CAD landscape changed. Surface and wireframe modeling were no longer the state of the art. Three-dimensional modeling became the norm in the CAD world. However, injection molding simulation was focused on the Hele-Shaw approximation and required midplane representations of the 3D geometry. The notion of performing full 3D analysis on 3D geometry in the early nineties was not viable with the available computer resources. Nevertheless, the nineties can be described as the period in which 3D geometry started to dominate the injection molding simulation industry.

An important side effect of this move to 3D was the general trend of all CAE companies to introduce analysis products that could be used by non-specialists. These were targeted at product designers rather than specialist analysts. Development of these “design” products was fuelled by the recognition that analysis was more beneficial when used early in product development. In regard to molding simulation this trend signaled a change in emphasis from troubleshooting to preliminary analysis of initial designs. This was reflected in the products for molding simulation developed in this decade.

### 1.7.1 Academic Work in the Nineties

For the first five years of the decade, there was little recognition from academia on the fundamental change that occurred in the CAD industry namely, the move to 3D modeling systems. Instead the focus was on calculating the effects of processing on residual stress and properties – both necessary for improved shrinkage and warpage prediction.

The CIMP published several early papers on warpage of molded parts. Santhanam and Wang [137] considered the warpage due to temperature differences across the mold halves. Using both thermo-elastic and thermo-viscoelastic models their study showed that both models could calculate similar deflections. The effect of packing pressure was not considered however. Chiang et al. developed models for the packing phase in the early nineties [33]. Around the same time Hieber et al. [29] showed the effect of packing on warpage of a center gated disk. All work from CIMP during this period used the 2.5D midplane analysis method.

Significant contributions from the Technical University of Eindhoven also emerged at this time. They always had a focus on properties, and offered sophisticated simulations of residual stress as the first step to prediction of properties. Douven [46] simulated the development of residual stresses using viscoelastic models for an amorphous polymer. Using analysis of the filling and packing phases, Douven used a compressible Leonov model to determine the residual stress in a molded part. Two



methods of implementing the viscoelastic model were investigated. The first, known as decoupled, used a generalized Newtonian fluid model to determine the kinematics of the flow to drive the viscoelastic stress model, the assumption being that the flow induced stress does not affect the rheology of the material. A fully coupled scheme was also used. Douven showed that the results from the decoupled solution were comparable to the fully coupled approach for a simple flow. Consequently the decoupled approach, requiring far less computer resources, was adopted by several authors. Similar findings were reported by Baaijens [9]. Caspers [31] used the decoupled approach to compute shrinkage, warpage and the elastic recovery of a molded amorphous material. He used an ageing term in the PVT model to determine the density as a function of time. As for the CIMP, all work at Eindhoven utilized the 2.5D midplane analysis method and resulted in the code VIp (6p) which was an abbreviation for Polymer Processing and Product Properties Prediction Program.

Contributions to simulation were also made by the group of Titomanlio in Italy. Using a Williams and Lord approach ([110], [174]), that was extended to the packing phase, they studied the decay of pressure during the packing phase using a crystallization model [155] and concluded that it was necessary to link crystallization to flow. In [156] the theory was further developed to allow the crystallization kinetics to be a function of the shear stress. Moreover the viscosity was related to the degree of crystallization.

In Canada the Industrial Materials Institute of the National Research Council of Canada (CNRC IMI) also developed 2.5D software for injection molding simulation. This was also based on the 2.5D midplane approach. More importantly, they undertook development of a true 3D code for filling analysis. The first of its type, the IMI code was first described in [73]. Using a finite element solution for pressure and temperature, the code used tetrahedral discretization of the mold geometry and solved a Navier Stokes equation for pressure and three velocity components at each node. Instead of the control volume approaches used to propagate the flow front in 2.5D midplane analysis, they used a pseudo-fluid method. This involved solution of a further equation:

$$\frac{DF}{Dt} = \frac{\partial F}{\partial t} + \mathbf{v} \cdot \nabla F \quad (1.5)$$

where  $F \in [0, 1]$  and represents the concentration of polymer. When  $F = 0$  the cavity is unfilled, whereas  $F = 1$  corresponds to a filled region. Of course for numerical implementation some intermediate value must be chosen for partially filled regions.

The Centre de Mise en Forme des Matériaux (CEMEF) at the Ecole Nationale Supérieure des Mines des Paris was also active during this period. Boitout et al. [18] used a simple thermo-elastic constitutive model for development of residual stresses in a simple geometry and considered the effect of mold deformation. Like the CNRC IMI, CEMEF recognized the importance of a true three-dimensional approach and developed a 3D code [128]. This code solved the non-isothermal Stokes equations with eqn. (1.5) for flow front advancement. It also used a tetrahedral discretization.

## 1.7.2 Commercial Developments in the Nineties

### SDRC

In the 1980's SDRC distributed Moldflow flow analysis code and developed its own mold cooling analysis. Early in the nineties, however, the company decided to offer its own flow analysis and warpage analysis products. The flow analysis was based on 2.5D midplane analysis and they included residual stress calculations for warpage prediction [131].

In 1994, SDRC decided to stop the development of their proprietary molding simulation software. Moldflow and SDRC entered into an agreement in which Moldflow solvers for flow, cooling and warpage were embedded in the SDRC CAD environment. This product was then marketed and sold by SDRC and its distributors.

### Moldflow

Moldflow's SWIS consortium resulted in a commercial warpage product in 1990. This used a 2.5D midplane analysis of the filling and packing phase with linear finite elements for pressure prediction. However, to save time and memory, it assumed the flow and temperature fields were symmetric about the midplane. The symmetry assumption was only possible because of the approach to warpage prediction used. While all other commercial codes used the residual stress method, Moldflow used a strain based approach [118] to calculate shrinkage in each finite element in directions parallel and perpendicular to flow. Bending moments, due to temperature differences on the mold halves, were introduced by modifying the parallel and perpendicular shrinkages on the top and bottom of each element according to the temperature calculated by cooling analysis. Details of this approach are provided in Chapter 2.

The trend to 3D solid modeling was taken very seriously by Moldflow and lead to developments on three fronts:

- Automatic midplane generation
- Dual Domain Finite Element Analysis and
- Full 3D analysis

Moldflow released an automatic mid plane generator in 1995. Kennedy and Yu [93] described the system, in which a representation of the geometry was input in stereolithography format (STL), re-meshed and converted to a mesh of triangular elements with assigned thicknesses, located at the midplane of the geometry. The method was useful for many parts, but could lead to a model that required some manual cleanup from the operator. The decision to use the STL format was to facilitate integration with CAD systems. Whereas mesh generators were frequently an expensive add on to a CAD system, almost all CAD systems could output STL to

facilitate rapid prototyping.

In 1997, Moldflow introduced dual domain finite element analysis (DDFEA) technology for filling analysis. Here the idea was to use a mesh on the exterior of the 3D geometry for the flow analysis. This method again used STL input of solid geometry. The exterior skin of the part was then meshed with triangles. Each triangle was assigned a local thickness when it could be matched to another parallel triangle on the other side of the mesh. Special boundary conditions were applied to ensure that the flow on each side of the part was synchronized. The essential idea is to introduce connections at strategic points such that the flows on each surface mesh remain synchronized. This method is discussed in detail in Chapter 3. The dual domain approach allowed a simple means of providing flow analysis on a solid geometry. DDFEA was extended to the Moldflow advanced products for filling, packing and cooling analysis. Once again the popularity of the method pushed Moldflow to extend the dual domain approach to shrinkage and warpage analysis. To achieve this, it was necessary to develop a structural analysis that used the mesh on the exterior of the 3D geometry. We discuss this in detail in Chapter 3.

Moldflow undertook a large development effort in the nineties to develop its 3D analysis software [61]. Full 3D filling analysis was introduced to the marketplace by Moldflow in 1998 [129] and was extended to packing in 1999 [150]. However, as noted earlier, the first report of true 3D filling analysis was reported by workers at the Industrial Materials Institute, National Research Council Canada (Institut des Matériaux Industriels Conseil National de Recherches Canada) in [73].

## **AC Technology/C-MOLD**

During the nineties AC Technology adopted a more commercial stance to the market place and renamed the company C-MOLD, thereby emphasizing its primary business. Having developed filling packing and cooling analysis, C-MOLD introduced a residual stress calculation module called C-PACK/W in 1991. This was based on the CIMP work ([137], [33], [29], [136]) and performed a viscous-elastic residual stress analysis using packing and cooling analysis results. Calculated residual stresses were then used as input to the structural analysis package ABAQUS®, which calculated the deformed shape of the component after ejection from the mold using linear or nonlinear geometric analysis. In 1992, C-MOLD released C-STRESS, a linear structural analysis program for calculation of the warpage from the residual stresses computed in C-PACK/W. This was later modified to permit nonlinear geometric analysis.

In response to the growing movement to promote CAE at the design stage, C-MOLD developed some special products. The first was Quickfill, a 2.5D midplane analysis tool with a fast solver. Although it had a limited range of results, the product was intended to be used by non specialists. A later version called 3D Quickfill, released in 1998, used the dual domain technique introduced by Moldflow.

## Simcon

Simcon continued to develop their 2.5D software to encompass warpage. In 1998 Simcon introduced a product called Rapid Mesh that, like the Moldflow dual domain method discussed above, utilized an exterior mesh on a 3D geometry. Designed for quick evaluation of mold designs, Rapid Mesh had a limited set of results and was a competitor to similar products from Moldflow and C-MOLD. This technique, which was called Simcon Surface Model Method, was then introduced to the main 2.5D product line and marketed as Cadmould Pro.

## Sigma Engineering

Sigma Engineering was a joint venture of the IKV Aachen, Simcon and MAGMA GmbH. MAGMA had developed a 3D code for simulation of casting called MAGMASOFT. Initiated in 1998, Sigma produced a 3D injection molding simulation called SIGMASOFT. This was based on the code MAGMASOFT and provided a full 3D analysis using voxel meshing. Voxel meshing is a structured mesh generation technique in which the 3D part geometry is divided into a series of smaller and smaller hexahedra (voxels). Meshing is stopped when it is deemed that there are sufficient voxels to permit accurate analysis. Coming from the casting industry, SIGMASOFT solved the Navier Stokes equations using finite differences. SIGMASOFT incorporated inertia, gravity and a flow front propagation scheme that could predict jetting. That is, regions of the mold that were initially filled could be unfilled at a later time. Unlike most commercial plastics CAE companies, Sigma Engineering does not offer a 2.5D midplane analysis.

## Timon

Timon started in business in 1986 but did not move into injection molding until the mid nineties. A subsidiary of the Toray Corporation, Timon recognized the need to interface to 3D geometry and produced a pseudo 3D simulation in 1996 called 3D TIMON. Unlike other companies that solved the Navier stokes equations for their 3D simulation, Timon extended the Hele-Shaw approximation to 3D dimensions [122]. Given a pressure distribution  $p$ , they assumed the three velocity components could be obtained as

$$v_x = -\kappa \frac{\partial p}{\partial x}, \quad v_y = -\kappa \frac{\partial p}{\partial y}, \quad v_z = -\kappa \frac{\partial p}{\partial z} \quad (1.6)$$

where  $\kappa$  solves the equation

$$\nabla^2 \kappa = -\frac{1}{\eta} \quad (1.7)$$

and  $\eta$  is the viscosity. Hence, for an incompressible fluid, instead of solving the Navier Stokes equations for  $p$ , at each node, it is only necessary to calculate a pressure field from the Laplace equation:

$$\nabla^2 p = 0 \quad (1.8)$$

and the fluid conductance from eqn.(1.7). The velocities are then obtained from eqn (1.6). Compared to a Navier Stokes solution, the number of unknowns at each node is reduced from four to two, and computational effort is reduced considerably.

## Transvalor

Transvalor is the commercial arm of the CEMEF. They commercialize, sell and support software that is developed at the CEMEF. In the late 1990's they distributed a product called Rem3D that is designed for 3D analysis of injection molding. Like Sigma Engineering, Transvalor did not develop and market any products using 2.5D midplane analysis. Their injection molding simulation focuses on 3D only.

## CoreTech Systems

Research funded by the Taiwanese government and carried out at the National Tsing-Hua University (NTHU) in Taiwan investigated injection molding from 1989 – 1999. This led to the creation of a commercial entity called CoreTech System Co. Ltd. in 1995 [79]. Marketed under the name Moldex, their original products were based on 2.5D midplane technology and offered analysis of all phases of injection molding.

## 1.8 Simulation Science Since 2000

While most academic work utilized finite differences or finite element methods for solution of the governing equations, the finite volume method was widely used in some fields of Newtonian and non-Newtonian fluid mechanics. A finite volume formulation for simulation of injection molding was given by Chang and Wang [32] in 2001.

Despite this contribution, the numerical methods for injection molding simulation are relatively mature, at least for the case of generalized Newtonian fluids and the indirect use of viscoelastic models as proposed by Douven [46] and Baaijens [9]. Consequently, academic simulation has focused more on linking properties to processing.

Central to this work is the development of morphology in semi-crystalline materials. Much of this effort has been influenced by Janeschitz-Kriegl and Eder at the University of Linz [50], [49]. While much previous work had been done on crystal-

lization in injection molding, it focused on thermal affects only. Eder et al. demonstrated the profound affect of shear on both the crystallization kinetics and the resulting morphology. It is now well established that a short, high shear treatment greatly increases the number of nuclei and hence the crystallization rate, whereas the total shear experienced affects the morphology [103]. For low shear, spherulitic structures are formed, while higher shear leads to oriented structures. Eder proposed the following equation for the effect of flow on the nucleation rate  $\dot{N}_f$ ,

$$\dot{N}_f + \frac{1}{\lambda_N} N_f = f \quad (1.9)$$

where  $\lambda_N$  is a relaxation time which, according to Eder and Janeschitz-Kriegl [49], has a large value and varies with temperature and  $f$  is a function that takes into account the effect of flow. Eder set the right hand side to be a function of the shear rate squared,  $\dot{\gamma}^2$ .

Zuidema [198] produced the first simulation to predict morphology in injection molding. He used the Schneider equations [139] to explicitly determine the distribution of oriented and spherulitic structures. To account for flow-induced crystallization, Zuidema [198] and Zuidema et al. [199] used the recoverable strain in the right-hand side of eqn.(1.9), rather than  $\dot{\gamma}^2$  as originally proposed by Eder et al.

Kennedy and Zheng [97] presented an alternative method. The right-hand side of eqn.(1.9) is set equal to the change in free energy of the melt. Instead of using differential equations, they used the following integral equation for crystallinity  $\alpha_f$ ,

$$\alpha_f = g_m \int_0^t \dot{N}(s) \left[ \int_s^t G(u) du \right]^m ds \quad (1.10)$$

where  $g_m$  is a constant that depends on  $m$ , with  $m = 4 - 3 \langle \mathbf{u}\mathbf{u} \rangle : \langle \mathbf{u}\mathbf{u} \rangle$ . Here  $\mathbf{u}$  is a unit vector in the direction of the c-axis of the crystalline structure and is calculated according to the flow field. Hence,  $m$  will vary from 1 for linear structures to 3 for spherical semi-crystalline regions, thereby providing information on the morphology. This approach has the advantage that micromechanics theories can be used for determining properties. Further details are provided by Zheng and Kennedy [186] and a detailed discussion is provided in Chapter 5 of this thesis.

The development of morphology calculation is under rapid development. Pantani et al. [124] give a review of progress thus far. A major challenge is to determine material properties given a calculated morphology.

Explicit calculation of the crystallization kinetics and the resulting morphology has enabled some progress to be made in the area of solidification. We discuss this further in Chapter 5. Despite these attempts, there is no generally accepted model for solidification, and it remains an area of research.

We conclude this section with some comments on PVT property determination. In an



earlier section, we noted the availability of commercial apparatus from Gnomix and SWO. These devices are designed to measure PVT characteristics at high temperature and pressures. Due to their robust design, they have high thermal inertia, and so cannot make measurements at the high cooling rates seen in injection molding. This is a problem when trying to understand the crystallization process as it relates to injection molding, where cooling rates are very high. At the centre of a molding that is 3mm thick, the cooling rate is of the order of ten degrees per second, whereas closer to the mold wall, it will be higher. Han and Wang [70] presented a method to adjust PVT data obtained under slow cooling rates for use at high cooling rates using a crystallization model. They showed an improvement in linear shrinkage prediction of molded samples using the transformed data for both PA66 and fiber filled PBT. However their crystallization model did not include any flow induced effects.

Brucato et al. [25] presented an apparatus that permitted study of the density of solidified polymer under high pressure and high cooling rates. They concluded that, at high cooling rates, pressure effects tend to be insignificant. This is contrary to observations made with low cooling rate equipment.

Most recently a new PVT device has been designed in the Netherlands. It permits both high cooling rate, high pressure and shear effects. Using this apparatus and Wide Angle X-ray Diffraction (WAXD) Van der Beek et al. [39] studied the effect of shear and temperature on the specific volume and morphology of two isotactic polypropylene (iPP) samples. They concluded that flow effects on specific volume evolution increased with increased shear rate, pressure and average molecular weight. On the other hand, the sensitivity of specific volume to flow effects decreases with the temperature at which shear is applied. The authors further surmised that crystallization models that consider only one phase, for example the  $\beta$ -crystalline phase in iPP, may not be able to fully describe the crystallization kinetics due to flow.

### 1.8.1 Commercial Developments Since 2000

An important industrial trend is in-mold assembly. Essentially the idea is to create as much of a system in the mold as possible. This has led to development of insert molding and over-molding. The latter has become popular with soft-touch TPU's for improved grip on hand held appliances. Three-dimensional analysis is advantageous for these processes as the components have complex geometry that often cannot be represented by shell models. Most of the commercial suppliers of simulation software now offer a 3D code, with varying levels of support for these features.

Another trend is the move to thinner-walled moldings. This has been fuelled in part by the personal electronics industry, particularly laptop computers and mobile phones. In an effort to reduce weight and cost, wall thicknesses in these devices are often under 1mm. The desire to pack more functions into laptops and phones has led to miniaturization of electrical connectors. Wall thicknesses in these parts can be as low as 0.14mm. Successful analysis of such moldings requires accurate thermal boundary conditions at the part-mold interface. Unfortunately there has been little

fundamental work in this area. In-situ measurements of thermal contact resistance (TCR) and mold wall temperatures under molding conditions were described by Delaunay et al. [36]. This provided thermal contact resistance as a function of time for an iPP resin (Solvay PHV 252) in contact with 40CMD8 mold steel. The TCR varies considerably with time and differs from one side of the mold to the other. Other investigators [180] have noted that the default heat transfer coefficient values used in commercial simulation packages may have to be reduced in order to agree with experimental data on molding with very thin micro-features.

The current decade has seen major changes in the companies offering simulation codes. One significant commercial development was the initial public offering by Moldflow. In March 2000, Moldflow Corporation successfully listed itself on the NASDAQ stock exchange. It was the first plastic CAE company to reach this milestone.

A further milestone occurred in April 2000 when Moldflow acquired AC-Technology and the C-MOLD range of products. After the acquisition, Moldflow was by far the largest company involved in simulation of injection molding.

Further consolidation in the industry occurred with the acquisition of SDRC by EDS in 2001.

More recently, Plastics and Computer were acquired in 2005 by the VI Group, a publicly listed CAD/CAM supplier to the injection molding industry.

## **Moldflow**

Post acquisition, Moldflow retained the technical staff from C-MOLD and built new premises in Ithaca New York to house the existing staff, a new laboratory and facilitate growth. The first product from the post acquisition company was MPI 3. It was a combination of the best technologies from Moldflow and C-MOLD. Since then there have been a regular series of product releases – mostly aimed at improving analysis capabilities for midplane, dual domain and true 3D solvers.

The major advance in 3D simulation was the introduction of warpage analysis in 3D. Fan et al. [55] introduced a 3D warpage analysis which included calculation of mechanical properties from the calculated fiber orientation distribution.

Following the industrial trend toward in mold assembly, Moldflow 3D and dual domain analysis products have been extended to over-molding and insert analysis. It is now possible to consider the effect of an insert or an over-molded part on the flow of the encapsulating materials [54]. In the case of plastic over-molding, the temperature of the first shot, after packing and cooling, is used as a boundary condition for the injection of the second material. For inserts, an initial temperature is specified and heat transfer within the insert is calculated as a function of time.

Generally, simulation has considered that the mold cavity dimensions do not change during processing. Baaijens [9] considered the effect of mold elasticity on pressure



calculation by adding a term to the pressure equation. Such an approach is valid if the mold deformation is uniform. However, due to pressure gradients inside the mold, this is rarely the case. Mold elasticity effects are especially significant in thin-wall moldings where pressures are high. It is not unusual to see injection pressures of 250-300 MPa. Leo and Cuvelliez [109] showed the effect of mold elasticity on the pressure decay during packing - an important factor for shrinkage and warpage prediction. Further investigations including mold deformation were undertaken by Delaunay et al. [37]. In view of this work and the above mentioned industrial trend to thin-walled molding, Moldflow analysis has been extended to include mold deformation - either due to the structure of the mold and its elastic properties or, in particular, core shift. Such an analysis requires coupling of the flow and structural analyses [10]. For a given time step, the calculated pressure distribution is used to determine the mold deflection. The deflection is used to update the flow domain by deforming the mesh, (for 3D analysis), or changing the thickness, (for 2.5D midplane analysis). The flow in the next time step is then calculated using the updated domain and the process continues until the end of fill and packing. Using this technique it is possible to more accurately calculate the residual stress in the part and hence its deformation. Moreover, it is possible to determine the residual stresses in the mold during the molding cycle. These results can be interfaced to metal fatigue analysis so as to assess mold life - an important factor in mass produced items.

## **Timon**

Timon continued to develop its range of 3D products. Using the method discussed in the previous section, Timon developed a hybrid analysis [123] in which areas that were meshed with three or fewer elements across the thickness were solved using 2.5D analysis whereas those with more than four elements were analyzed using the generalized Hele-Shaw scheme described earlier. In 2003, Timon introduced a product for designing optical lenses using a prediction of birefringence. This was the first commercial program to predict optical properties.

## **Core Tech Systems**

Using the finite volume method proposed by Chang and Yang [32], Core Tech produced a 3D analysis in 2001 called Moldex3D/Solid. This product uses a variety of element shapes for analysis. For example, it is possible to create a mesh with several wedge elements near the mold wall, and tetrahedral elements in the centre. The idea is to improve the heat transfer calculations near the mold wall. While the approach may be effective for the filling phase, the location of the frozen layer during packing may not be predicted accurately. Moldex3D/Solid has since been extended to include filling, packing, cooling and warpage.

## 1.9 Outline of Thesis

The preceding sections demonstrate the complexity of injection molding and the huge effort that has been expended on modeling and simulation. Many simplifications must be made to create a practical simulation tool for industry. Moreover, in the absence of scientific understanding of some aspects of the process, an engineering approach needs to be adopted. Koen [100] elegantly defines the *engineering method* as, "the strategy for causing the best change in a poorly understood situation within the available resources". This captures the difficulty experienced by anyone wanting to simulate injection molding. Many aspects of the process and the materials used are poorly understood, there are limitations on computing power, and some known details of the actual process are difficult to model. This thesis identifies some problems in the simulation of injection molding, both practical and scientific, and offers solutions in the spirit of the engineering method.

Chapter 2 reviews the Hele-Shaw approximation and discusses material data that is relevant to simulation. Two problems are identified. The first concerns the geometry requirements imposed by the Hele-Shaw approximation. The second is the intrinsic error introduced by using material properties, obtained under laboratory conditions, in a simulation where conditions are very different from the laboratory conditions.

Chapter 3 proposes a solution to the geometry problem. We describe a method for analysis of 3D solid models known as Dual Domain Finite Element Analysis. Originally developed for flow analysis, the extension to structural analysis is described thereby enabling warpage analysis. The method has been extremely successful both technically and commercially.

Chapter 4 looks at a practical method that overcomes some aspects of the material data problem as it relates to prediction of shrinkage. The method is known as the Corrected Residual In-Mold Stress (CRIMS) method and is in commercial use.

Chapter 5 presents some current work to further improve warpage simulation by means of improved physical modeling of injection molding. This is accomplished by predicting crystallization kinetics and morphology of semi-crystalline materials.

Chapter 6 presents some models to predict material properties using crystallization kinetics and morphology predictions. This enables transformation of data obtained under laboratory conditions to the conditions experienced in simulation. We also provide some validation of an injection molding simulation that uses the models.

Chapter 7 summarizes the previous chapters and proposes some areas for future investigation.

## 1.10 Background of Candidate

During my period of candidature I have been employed as Director of Technology Development, Executive Vice President and Chief Technology Officer for Moldflow Corporation. In this capacity I was responsible for development of technology for either new products or improvement to existing products.

Specifically

- I managed and contributed to the development of dual domain finite element analysis for flow and structural analysis. I am a named inventor on a patent application for the latter. The details are presented in Chapter 3.
- I introduced the concept of the corrected residual in-mold stress technique.

I also initiated and managed a number of research projects with external groups to improve our understanding of the physics involved in simulation of injection molding. These projects are briefly described below.

- SWIM (Shrinkage Warpage in Injection Molding): A collaboration between Moldflow Pty. Ltd., Ecole Nationale Supérieure d'Artes et Métiers (ENSAM) Paris, Laboratoire de Thermocinétique at the University of Nantes (France), formerly known as ISITEM, University Claude Bernard (Lyon), and the industrial partners Solvay Central Research in Brussels, Belgium and Legrand in Limoges, France. This project was designed to investigate improvements in the modeling of warpage simulation. ENSAM were responsible for molding of samples and shrinkage and warpage measurements, ISITEM conducted modeling and experiments on the thermal contact resistance between polymer and mold in the molding process and University of Claude Bernard investigate the dependence of PVT measurement on rate of cooling. Solvay is a European material supplier and provided resin for the project, Legrand is a major French molding company and constructed the mold used in the project. Moldflow provided both standard and modified software to the project members. The project resulted in several publications, [112], [36], [37] and two Ph.D. theses [21], [111]. It also resulted in the development and commercialization of a viscous-elastic residual stress model for warpage in Moldflow software and a visco-elastic model for residual stress prediction.
- SCOOP (Shrinkage Crystallization and Orientation Of Polymers): A collaboration with the same participants as the previous project. The project aimed at understanding the development of crystallization and morphology and their affect on shrinkage. It resulted in a Ph.D. thesis [102] and a publication [103]. The project led to the development of a unique model for structure development in injection molded products.

- FISH: (Fibers in SHrinkage): A collaboration with the same participants as the previous project. The project aimed at investigating the effect of glass fibres on crystallization and morphology. It resulted in a thesis [47]. We do not discuss details here as we make no further reference to this work in the thesis.
- University of Sydney: A collaboration between Sydney University and Moldflow which was partly funded by Australian Research Council (ARC) grants and aimed at improving the prediction of fiber orientation in injection molding. Most commercial simulations of fiber orientation used, and still do, the Folgar Tucker model [60] and the orientation tensor approach of Advani and Tucker [3]. This approach utilized the so called "interaction coefficient" - a scalar quantity - the value of which was unable to be determined experimentally. One of our goals was determination of this quantity. The project resulted in some new results for simulations of concentrated fiber suspensions. Fan et al. introduced the Brownian Configuration Field method for fiber simulations [53]. This was compared to some analytical results by Zheng et al. in [183]. Of considerable importance was the direct simulation of a fiber suspension by Fan et al. [52]. This technique led to the determination of the interaction coefficient (in tensorial form). An error in the evolution equation for the orientation tensor in case of tensorial interaction coefficient in this paper was corrected by Zheng et al. [184]. The use of tensorial interaction coefficients has been implemented in Moldflow software but not commercially released. We make no further mention of this work in the thesis.
- CRC Polymers: A collaboration between Moldflow and the Cooperative Research Center for Polymers aimed at predicting properties of injection molded material and constitutive models with solidification, which may be applied in injection molding. This project has run for the past eight years and continues today. Research providers are University of Sydney (theoretical modeling), Monash University (experiments on properties of molded parts and synchrotron studies on morphology), the CRC for Polymers (experiment and characterization of materials for simulation) and the Australian Nuclear Science and Technology Organization (synchrotron studies). Moldflow is the only industrial participant - its role is theoretical modeling, implementation and validation of the developed models. It has led to the implementation of the model for morphology development and crystallization described in Chapter 5 of this thesis in Moldflow software. The following papers have been produced by the Monash team: [190], [191], [192], [193], [194]. The Sydney team have published the following papers: [152], [153]. Moldflow has published the following refereed papers and conference proceedings: [181], [94], [182], [97], [186], [187], [188], [68].

During this period I have been a named inventor on the following patents and patent applications:

- Apparatus and method for structural analysis [57]. This is discussed in Chapter 3.
- Apparatus and methods for predicting properties of processed material [185]. This is discussed in Chapters 5 and 6.

## CHAPTER TWO

# Simulation of Injection Molding

---

This chapter reviews the basic theory of simulation so as to introduce two significant problems that must be overcome to improve simulation. The first arises from approximations used to simplify the governing equations. These are historical in nature and reflect computing power limitations of the past and even today. Their effect is to require the need for a model based on the midplane of the injection molded part. The second problem arises from the need to use material data in the simulation that is not obtained under injection molding conditions. We will see that the material data available today falls short of what is required to model the process - particularly for semi-crystalline materials.

## 2.1 Introduction

A typical injection moulding process consists of four stages: (i) filling of the molten polymer into the mould; (ii) packing of more material into the mould under high pressure to compensate for volumetric shrinkage of the material as it cools; (iii) cooling during which the material solidifies while in the mould until it is sufficiently solid; (iv) ejection of the solidified product from the mould. During filling, packing and cooling, the material experiences a complex thermomechanical history which leads to changes in local specific volume. While the part is in the mould, it is constrained within the plane of the part and so stresses develop in the part during solidification. Upon ejection, the relaxation of these stresses causes instantaneous shrinkage that is usually anisotropic and non-uniform throughout the moulded part. Further shrinkage may also occur during cooling after ejection. The anisotropic and non-uniform shrinkage behavior will result in a degree of warpage. Whilst warpage is the main focus of this work, it depends on the simulation of the filling, packing and cooling phases. We first review the simulation of these phases and then consider the prediction of warpage at the end of the chapter.

## 2.2 Filling and Packing Analysis(2.5D)

Filling is the most thoroughly studied stage of the injection molding process. The basic requirement is to predict pressure and temperature distributions in the mold cavity and the advancement of the melt front. While early work used finite differences or analytical solutions in simple geometries, the seminal paper of Hieber and Shen [74] provided a breakthrough. This work introduced a hybrid analysis technique for the filling phase in which temperature and pressure equations were solved using finite differences and finite elements respectively. Frequently referred to as 2.5D analysis, this technique remained the cornerstone of commercial simulation until the mid 1990's and the appearance of three-dimensional analysis. In the remainder of this section we briefly review this approach and extend it to the packing phase.

In deriving the governing equations for a polymer melt, we assume that the fluid is a continuum. That is we ignore the molecular structure of the material and assume that it is possible to define physical variables such as density and velocity at a point in the fluid. Moreover, we assume that these quantities vary smoothly so that differentiation with respect to both position and time is possible.

The motion of the melt in injection molding is governed by the conservation laws of mass, momentum and energy, respectively.

As a polymer melt is compressible, the conservation of mass equation takes the form:

$$\frac{\partial \rho}{\partial t} + (\nabla \cdot \rho \mathbf{v}) = 0 \quad (2.1)$$

where  $\rho = \rho(\mathbf{x}, t)$  is the density of the fluid and  $\mathbf{v} = \mathbf{v}(\mathbf{x}, t)$  is the fluid velocity at a point.

The conservation of momentum equation may be written:

$$\frac{\partial (\rho \mathbf{v})}{\partial t} + \nabla \cdot \rho \mathbf{v} \mathbf{v} = \nabla \cdot \underline{\boldsymbol{\sigma}} + \rho \mathbf{g} \quad (2.2)$$

where  $\underline{\boldsymbol{\sigma}}$  is the stress tensor and  $\mathbf{g} = \mathbf{g}(\mathbf{x}, t)$  is the acceleration due to gravity. The above equation deals with conservation of linear momentum only. It is also necessary to consider the conservation of angular momentum. Indeed it turns out that a necessary and sufficient condition for conservation of angular momentum is that the stress tensor  $\underline{\boldsymbol{\sigma}}$  be symmetric [67]. That is  $\sigma_{ij} = \sigma_{ji}$ .

Finally the conservation of energy takes the form:

$$\rho c_p \left( \frac{\partial T}{\partial t} + \mathbf{v} \cdot \nabla T \right) = \beta T \left( \frac{\partial p}{\partial T} + \mathbf{v} \cdot \nabla p \right) + p \nabla \cdot \mathbf{v} + \underline{\boldsymbol{\sigma}} : \nabla \mathbf{v} + \nabla \cdot (k \nabla T) \quad (2.3)$$

where  $c_p$  is the specific heat, measured at constant pressure,  $T = T(\mathbf{x}, t)$  is the tem-

perature at a point in the fluid,  $\beta$  is the coefficient of volume expansion,  $p$  is the pressure at a point in the fluid and  $k$  is the thermal conductivity of the fluid.

The above equations are quite general. For simulating injection molding, some simplification is possible by considering:

- Material properties;
- Geometric considerations and
- Mathematical manipulation.

We consider each in turn.

### 2.2.1 Material Assumptions

The stress in a fluid may be written in the form

$$\underline{\sigma} = -p\underline{\mathbf{I}} + \underline{\tau}$$

where  $\underline{\mathbf{I}}$  is the identity tensor,  $p$  the pressure and  $\underline{\tau}$  is known as the viscous or extra stress tensor.

In order to make some progress in modeling using a continuum approach, we require a relationship between the stress and the kinematics of the fluid motion. A particularly simple relationship is the Newtonian fluid defined by setting

$$\underline{\sigma} = -p\underline{\mathbf{I}} - \frac{2}{3}\eta(\text{tr}\underline{\mathbf{D}})\underline{\mathbf{I}} + 2\eta\underline{\mathbf{D}}$$

where  $\eta$  is the viscosity of the fluid and  $\underline{\mathbf{D}} = (\nabla\mathbf{v} + \nabla\mathbf{v}^T)/2$  is the strain rate tensor. Hence the extra stress tensor has the form

$$\begin{aligned}\underline{\tau} &= -\frac{2}{3}\eta(\text{tr}\underline{\mathbf{D}})\underline{\mathbf{I}} + 2\eta\underline{\mathbf{D}} \\ &= \eta\dot{\underline{\gamma}}\end{aligned}$$

where  $\dot{\underline{\gamma}}$  is the deviatoric rate of strain tensor. In order to better capture the behavior of polymer melts we allow the viscosity to depend on the strain rate. This defines a class of fluids, called generalized Newtonian fluids, which are of use in describing flows dominated by shear forces [16] and so of particular interest for injection molding simulation. As we want the viscosity to be independent of the coordinate system, we make viscosity depend on an invariant of the rate of strain tensor. The



first invariant of the deviatoric strain rate  $\dot{\underline{\gamma}} \equiv \text{tr } \dot{\underline{\gamma}} = 0$ . Moreover, for shear flow, the third invariant may be shown to be zero [16]. We therefore allow the viscosity to depend on the second invariant of  $\underline{\dot{\gamma}}$  defined as

$$\begin{aligned} II_{\dot{\underline{\gamma}}} &= \sum_i \sum_j \dot{\gamma}_{ij} \dot{\gamma}_{ji} \\ &= \dot{\gamma} \end{aligned}$$

and often called the shear rate.

There are several possible choices for the viscosity function. We will consider the Cross model, which has the form:

$$\eta = \frac{\eta_0}{1 + (\eta_0 \dot{\gamma} / \tau^*)^{1-n}} \quad (2.4)$$

where  $\eta_0$  is the viscosity at zero shear and  $\tau^*$  is the shear stress at the transition between Newtonian and power law behavior. For molding simulation, it is usual to include the effect of temperature on the viscosity by means of an Arrhenius or WLF correction. In the case of the WLF function, the viscosity has the form

$$\eta = \frac{\eta_0}{1 + (\eta_0 \dot{\gamma} / \tau^*)^{1-n}} \quad (2.5)$$

with

$$\eta_0 = D_1 \exp \left[ \frac{-A_1 (T - D_2)}{A_2 + (T - D_2)} \right] \quad (2.6)$$

where  $A_1, A_2, D_1, D_2$  and  $n$  are constants to be determined from experimental data.

## 2.2.2 Geometric Considerations

The equations above are quite general and impose no constraint on flow geometry. However most injection molded components are thin walled by which we mean a local thickness  $2H$ , is much smaller than a typical length. Noting that the density is a state variable and so depends on pressure and temperature and adopting a Cartesian coordinate system in which the  $x - y$  plane is defined to be in the plane of the part and the local thickness is in the  $z$  direction, we can show [92] that equations (2.1-2.3) for a generalized Newtonian fluid take the form:

$$0 = \kappa \frac{Dp}{Dt} - \beta \frac{DT}{Dt} + \frac{\partial v_x}{\partial x} + \frac{\partial v_y}{\partial y} + \frac{\partial v_z}{\partial z} \quad (2.7)$$

$$\frac{\partial p}{\partial x} = \frac{\partial}{\partial z} \left( \eta \frac{\partial v_x}{\partial z} \right) \quad (2.8)$$

$$\frac{\partial p}{\partial y} = \frac{\partial}{\partial z} \left( \eta \frac{\partial v_y}{\partial z} \right) \quad (2.9)$$

$$\frac{\partial p}{\partial z} = 0 \quad (2.10)$$

$$\rho c_p \frac{DT}{Dt} = \beta T \frac{Dp}{Dt} + \eta \dot{\gamma}^2 + \frac{\partial}{\partial z} \left( k \frac{\partial T}{\partial z} \right) \quad (2.11)$$

where the specific volume  $V = 1/\rho$  and

$$\kappa = -\frac{1}{V} \left( \frac{\partial V}{\partial p} \right)_T \text{ and } \beta = \frac{1}{V} \left( \frac{\partial V}{\partial T} \right)_p$$

are the isothermal coefficients of expansion and expansivity of the material, respectively. Of particular importance is that the pressure has no dependence on the  $z$  coordinate. That is, the pressure is assumed constant through the thickness of the part. This is often referred to as the lubrication approximation.

### 2.2.3 Simplification by Mathematical Analysis

The momentum equations (2.8) and (2.9) may be integrated twice with respect to  $z$  across the cavity thickness. Carrying out the integration and assuming the fluid velocity is zero at the mold wall (no slip condition) we obtain from (2.8) and (2.9), respectively,

$$v_x(x, y, z) = \frac{\partial p}{\partial x} \left[ \int_{-H}^H \frac{z'}{\eta} dz' - C(x, y) \int_{-H}^H \frac{dz'}{\eta} \right] \quad (2.12)$$

$$v_y(x, y, z) = \frac{\partial p}{\partial y} \left[ \int_{-H}^H \frac{z'}{\eta} dz' - C(x, y) \int_{-H}^H \frac{dz'}{\eta} \right] \quad (2.13)$$

where

$$C(x, y) = \frac{\int_{-H}^H (z/\eta) dz}{\int_{-H}^H dz/\eta}.$$

We now define gapwise average velocities as follows:

$$\begin{aligned}\bar{v}_x(x, y) &= \frac{1}{2H} \int_{-H}^H v_x(x, y, z) dz \\ &= \frac{-S}{H} \frac{\partial p}{\partial x}\end{aligned}\quad (2.14)$$

$$\begin{aligned}\bar{v}_y(x, y) &= \frac{1}{2H} \int_{-H}^H v_y(x, y, z) dz \\ &= \frac{-S}{H} \frac{\partial p}{\partial y}\end{aligned}\quad (2.15)$$

where

$$S = \frac{1}{2} \left\{ \int_{-H}^H \frac{z^2}{\eta} dz - \frac{\left( \int_{-H}^H (z/\eta) dz \right)^2}{\int_{-H}^H dz/\eta} \right\} \quad (2.16)$$

and is known as the fluidity.

To establish an equation for the pressure involving only  $x$  and  $y$ , we substitute (2.11) into (2.7) and integrate across the cavity thickness to obtain:

$$\begin{aligned}0 &= \int_{-H}^H \left\{ \kappa \frac{Dp}{Dt} - \frac{\beta}{\rho c_p} \left[ \beta T \frac{Dp}{Dt} + \eta \dot{\gamma}^2 + \frac{\partial}{\partial z} \left( k \frac{\partial T}{\partial z} \right) \right] + \frac{\partial v_x}{\partial x} + \frac{\partial v_y}{\partial y} + \frac{\partial v_z}{\partial z} \right\} dz \\ &= \int_{-H}^H \left\{ \kappa \frac{Dp}{Dt} - \frac{\beta}{\rho c_p} \left[ \beta T \frac{Dp}{Dt} + \eta \dot{\gamma}^2 + \frac{\partial}{\partial z} \left( k \frac{\partial T}{\partial z} \right) \right] \right\} dz \\ &\quad + \int_{-H}^H \left( \frac{\partial v_x}{\partial x} + \frac{\partial v_y}{\partial y} \right) dz + [v_z]_{z=-H}^{z=H} \\ &= \int_{-H}^H \left\{ \kappa \frac{Dp}{Dt} - \frac{\beta}{\rho c_p} \left[ \beta T \frac{Dp}{Dt} + \eta \dot{\gamma}^2 + \frac{\partial}{\partial z} \left( k \frac{\partial T}{\partial z} \right) \right] \right\} dz \\ &\quad + \frac{\partial}{\partial x} \int_{-H}^H v_x dz + \frac{\partial}{\partial y} \int_{-H}^H v_y dz\end{aligned}$$

where in the last step we have used the no-slip condition.

The last two terms may be evaluated using equations (2.14) and (2.15) to give a final equation for pressure:

$$\frac{\partial}{\partial x} \left( S \frac{\partial p}{\partial x} \right) + \frac{\partial}{\partial y} \left( S \frac{\partial p}{\partial y} \right) = \quad (2.17)$$

$$\frac{1}{2} \int_{-H}^H \left\{ \kappa \frac{Dp}{Dt} - \frac{\beta}{\rho c_p} \left[ \beta T \frac{Dp}{Dt} + \eta \dot{\gamma}^2 + \frac{\partial}{\partial z} \left( k \frac{\partial T}{\partial z} \right) \right] \right\} dz \quad (2.18)$$

The left-hand side of eqn.(2.17) is immediately recognizable as a two-dimensional Hele-Shaw flow. We remark that mathematical studies of such flows were considered by Richardson [132] as a model for injection into a thin walled cavity well before any commercial programs were available. Such flows are related also to flow in a porous medium [134]. Indeed, this equation is used to model the resin transfer molding process in which molten resin impregnates a porous preform placed in the mold prior to injection. In this application the fluid conductance  $S$  represents the permeability of the preform.

## 2.2.4 Boundary Conditions and Solidification

At injection points it is common to assume a constant melt temperature and a constant flow rate. Boundary conditions at the plastic mold interface were either a fixed mold temperature and a corresponding value of heat transfer coefficient or a specified heat flux.

A major challenge in molding simulation is modeling the phase change. Extrapolation of existing viscosity models to low temperature introduces inaccuracies, particularly for semi-crystalline materials. The problem is that no model shows the rapid increase in viscosity that occurs when the material crystallizes. Commercial simulations typically use the concept of a "no-flow temperature" or "transition temperature" to deal with this. The no-flow temperature is determined using a capillary rheometer, with a die of length 20mm and diameter 1mm. A pressure of 21 MPa. is applied and the rate of extrusion measured while lowering the melt temperature at a rate of 2°C/min. The no-flow temperature is defined as the temperature at which the extrudate velocity is zero. Transition temperature is determined using a DSC in cooling at a rate of 20°C/min. The transition temperature is taken to be the temperature at the intersection of two straight lines that are fitted to the peak and the specific heat trace before the transition (see Figure 2.1). Whether a no-flow or a transition temperature is chosen, its use in software is the same. As soon as the calculated temperature falls below the no-flow or transition temperature, the melt's velocity is set to zero. Hence these temperatures determine the position of the frozen layer in the simulation. This is not so important for the filling phase in moldings of normal thickness (1.5 - 3mm).

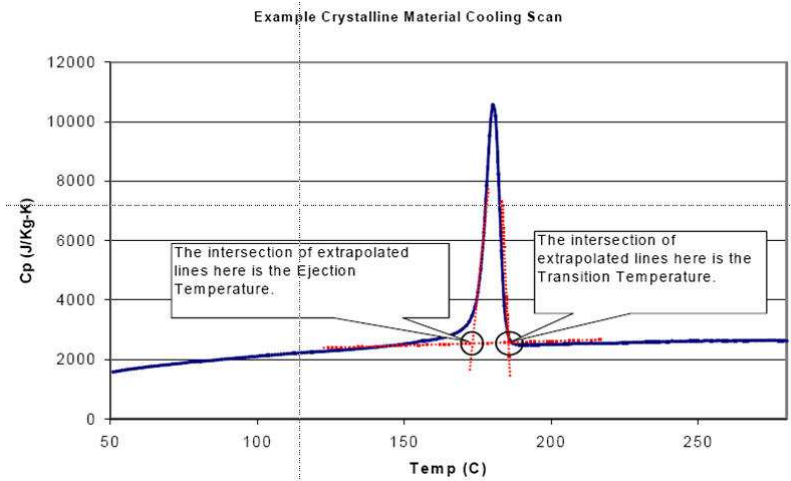


Figure 2.1: Determination of transition temperature from DSC data.

However in the packing phase, the frozen layer prediction has a significant effect on pressure distribution and pressure decay. Consequently, the frozen layer thickness is of importance when trying to calculate residual stresses in the molded part and hence shrinkage and warpage.

## 2.2.5 Solution of the Governing Equations

The equations used for simulation of injection molding are a single equation for pressure as a function of  $x$  and  $y$  (eqn.(2.17)) and an equation for temperature (eqn.(2.11)). With appropriate boundary conditions [92], these equations may be readily solved using a hybrid scheme introduced by Hieber and Shen [74] in which finite element and finite difference methods are used for the solution of the pressure and temperature fields respectively. Kennedy [92] provides details on the solution algorithms and methods.

As the pressure field varies only in  $x$  and  $y$ , the mesh required for the finite element scheme is a two-dimensional network of triangles or quadrilaterals embedded in three-dimensional space. The nodes forming the mesh are located at the midplane of the part. The grid for the temperature field, however, fills the domain occupied by the melt and so is fully three-dimensional. Similarly, despite the lack of a  $z$ -component of velocity, the velocity is calculated at each point of 3D space within the mold cavity. Prediction of pressure in two-dimensions and both temperature and velocity in three-dimensions has led to the use of the term 2.5D analysis for the injection molding simulation.

Further details on derivation and solution for the filling and packing phases may be found in Boshouwers and van der Werf [20], Chiang et al. [33] and Kennedy [95], [92].

## 2.3 Mold Cooling Analysis

Within the mold are channels through which coolant is circulated to extract heat. The location and proximity of cooling channels depends on the part geometry, cavity configuration and the location of ejection mechanisms and moving components of the mold. Frequently it is not possible to ideally locate the channels and as a result temperature variation occurs over both the mold surface and between the mold halves. Whilst it is common to simply assume a fixed mold temperature for simulation of filling and cooling, a better result may be obtained by performing a mold cooling analysis. This requires a 3D analysis of heat transfer throughout the mold. A detailed analysis using finite elements was given by Karjalainen [89]. However due to the difficulty of generating a 3D mesh for the mold, most commercial solutions use a boundary element method (BEM) similar to that proposed by Rezayat and Burton [130]. As mesh generation improves, there may be a swing to finite elements solutions for cooling because the BEM does involve non-sparse, non-symmetric matrices which tend to consume large amounts of computer memory.

Generally the results of cooling analysis are the mold surface temperatures or heat flux (averaged over the injection cycle). Either may be used to replace the mold temperature boundary condition required for flow analysis.

## 2.4 Warpage Analysis

Warpage is arguably the most important problem to be tackled by simulation. Early academic work on the problem sought to predict stresses developed in the material during processing. This was then input to a finite element structural analysis program to determine the actual deformation of the component after ejection from the mold. These methods, generally known as residual stress methods, are still under active development. The first commercial products for shrinkage and warpage prediction used a different approach [62]. Instead of stress they sought to determine strain directly and use this as input to the structural analysis. These techniques are part of the class of residual strain methods. We briefly describe both in the sequel.

### 2.4.1 Residual Strain Methods

The model introduced by Moldflow [62] has the form [165]:

$$S^{\parallel} = \sum_{i=1}^{i=5} b_i M_i \quad (2.19)$$

$$S^{\perp} = \sum_{i=6}^{i=10} b_i M_i \quad (2.20)$$

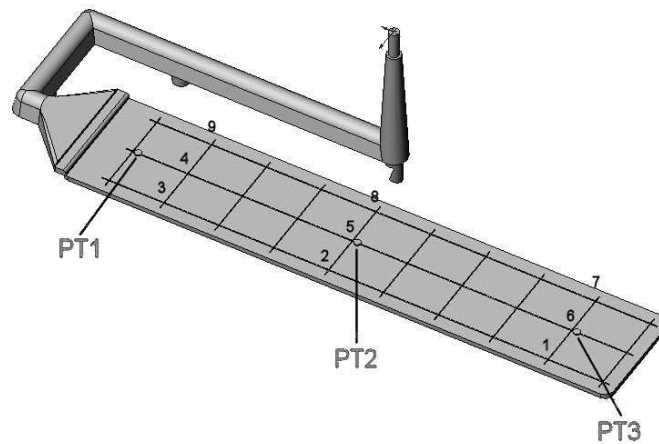


**Figure 2.2:** Schematic of tag die used for shrinkage measurements.

where  $S^{\parallel}$  and  $S^{\perp}$  are the calculated shrinkage strains parallel and perpendicular to the flow direction,  $b_i$  are material constants and the  $M_i$  are measures of the effects of processing and were calculated using results from filling and packing analyses.  $M_1 = M_6$  and is the volumetric shrinkage,  $M_2 = M_7$  are measures of the level of crystallinity,  $M_3 \neq M_8$  are measures of molecular orientation,  $M_4 = M_9$  are measures of the effect of relaxation and  $M_5 = M_{10}$  are constants and should be small if the model is valid for a given material. The material constants  $b_i$ , ( $i = 1, \dots, 10$ ), were obtained by the following procedure:

- Samples were molded at up to 28 different process conditions or thicknesses. The samples were made in an instrumented mold and on an instrumented molding machine. Measured data were used to determine the processing conditions used for each sample;
- The shrinkage of each sample was measured in directions parallel and perpendicular to the flow direction using a grid pattern etched on to the mold (see Figure 2.2). Four regions of the die are defined by the points 3254, 4589, 2165 and 6785. Measurements of shrinkage are made in each region.
- Simulations were run at the same conditions used for molding to determine values of  $M_i$ , ( $i = 1, \dots, 10$ ) and
- Measured shrinkages and the calculated values of  $M_i$  ( $i = 1, \dots, 10$ ) were substituted in equations (2.19) and (2.20) and the  $b_i$  ( $i = 1, \dots, 10$ ), were calculated by regression analysis.

The material constants,  $b_i$  ( $i = 1, \dots, 10$ ), were stored in a database. In use the customer would run an analysis to determine the  $M_i$ , ( $i = 1, \dots, 10$ ), then equations

(2.19) and (2.20) were used to calculate strains parallel and perpendicular to the flow direction for every element in the mesh. The direction of flow angle was also calculated elementally based on flow analysis results. The calculated strains were then input to a structural analysis to determine the deformed shape. It is well known that any difference in the temperature of the mold halves can have a dramatic affect on warpage. Typically such differences are determined by cooling analysis. In the residual strain model the effect of temperature differences between the mold halves was introduced by modifying the shrinkage strain on the top and bottom of the element so as to produce a bending moment.

This technique was used in Moldflow software until 1997. It was successfully applied to unfilled and short fiber reinforced amorphous and semi-crystalline materials.

The need to mold the samples to determine the shrinkage coefficients  $b_i$ , ( $i = 1, \dots, 10$ ) was a disadvantage of the method but necessary to obtain reasonable accuracy. For short-fiber reinforced thermoplastics, one may assume that the level of crystallization, molecular orientation and mold restraint are second order effects compared to volumetric shrinkage and the resulting fiber orientation distribution. In 1997, a model for calculation of shrinkage strains specifically for reinforced materials was introduced by Zheng et al. [189]. This model did not require the molding of samples and gave excellent predictions of deformed shape, but tended to underestimate the actual deflection.

## 2.4.2 Residual Stress Models

Two types of residual stresses arise in injection molding:

- Flow induced stresses, which arise from the effect of flow on the molecular configuration of the material;
- Pressure induced stresses, which arise due to a fluid core that exists within the frozen layers during the packing phase, and
- Thermal residual stresses, which arise from the thermal contraction of the material as it solidifies.

Baaijens [9] has shown that the flow induced stresses are an order of magnitude smaller than the pressure induced and thermal residual stresses. We note however that the flow induced stresses have an important effect on the development of anisotropic material properties and so are important in discussion of warpage. We return to this point in Chapter 5.

Early work on calculation of residual stresses was influenced by the literature on residual stresses in glass [108], and was concerned with the use of viscoelastic or elastic constitutive models ([86], [137]). However, an important difference exists between glass cooling and molding - namely, the effect of packing pressure. The



origin of stresses in a freely quenched material, as in glass making, is temperature change. The material cools from the outside, as in molding, and the resulting residual stress distribution is typically compressive at the surface and tensile in the core. In the case of injection molding, however, the residual thermal stress distribution is determined by the varying pressure history in the packing phase coupled with the frozen layer growth, and the stresses can become tensile at the surface layer. Baaijens [9], noted this effect and developed a thermo-viscoelastic model that was isotropic and accounted for both thermal stress and the stress induced by pressure applied in the packing phase for an amorphous material.

Residual stress models are generalizations of Hooke's law which, for an elastic solid, has the form,

$$\sigma_{ij} = c_{ijkl}^e \varepsilon_{kl} \quad (2.21)$$

where  $\sigma_{ij}$  and  $\varepsilon_{kl}$  are, respectively, the stress and total strain tensors and  $c_{ijkl}^e$  is the tensor of elastic constants or stiffness tensor. The strain tensor is determined by differentiating the components of the displacement vector  $\mathbf{u}$  and is defined to be

$$\varepsilon_{ij} = \frac{1}{2} \left( \frac{\partial u_i}{\partial x_j} + \frac{\partial u_j}{\partial x_i} \right). \quad (2.22)$$

Residual stress models are frequently formulated using a viscoelastic constitutive relationship [9], [131]. A general linear anisotropic thermoviscoelastic constitutive relationship may be written,

$$\sigma_{ij} = \int_0^t c_{ijkl} (\xi(t) - \xi(t')) \left( \frac{\partial \varepsilon_{kl}}{\partial t'} - \alpha_{kl} (\xi(t) - \xi(t')) \frac{\partial T}{\partial t'} \right) dt' \quad (2.23)$$

where  $c_{ijkl}$  is the viscoelastic relaxation modulus,  $t$  is time,  $T$  is temperature,  $\alpha_{kl}$  is the tensor of thermal coefficients of expansion and  $\xi(t)$  is a pseudo time scale defined as

$$\xi(t) = \int_0^t \frac{1}{a_T} dt' \quad (2.24)$$

where  $a_T$  is the time temperature shift factor that accounts for the effect of temperature on material response.

We encounter a problem when using eqn.(2.23) for non-isothermal systems. First, eqn.(2.23) assumes that the material is thermorheologically simple, by which we mean, the change in linear visco-elastic behavior of the material, as a function of temperature, corresponds to a shift in logarithmic timescale [141]. Unfortunately, to obtain material data for relaxation functions satisfying the assumption of thermorheological simplicity is not always possible, since a large number of real materials are actually thermorheologically complex. Secondly, the relaxation functions used

in eqn.(2.23) may depend on the internal structures which themselves are in turn affected by processing conditions - particularly for those systems involving semi-crystalline materials and phase change. The exact relation between the internal structures and the relaxation functions is largely unknown (either theoretically or experimentally). Because of the above-mentioned complexity related to the viscoelastic data, it is common to further approximate the problem with a viscous-elastic calculation in which the material is assumed to sustain no stress above a certain temperature and is elastic below that temperature. But what is this temperature to be? We discussed a similar problem in Section 2.2.4. There the problem was solved by introducing a transition or no-flow temperature. For warpage, we adopt the same approach and assume the transition temperature  $T_t$ , is the temperature above which no stress is sustained in the material. Below this temperature the material is assumed elastic. Under this assumption we have

$$\sigma_{ij} = \begin{cases} 0 & \text{for } T \geq T_t \\ \int_0^t c_{ijkl}^e \left( \frac{\partial \varepsilon_{kl}}{\partial t'} - \alpha_{kl}(t') \frac{\partial T}{\partial t'} \right) dt', & \text{for } T < T_t. \end{cases} \quad (2.25)$$

A more elaborate discussion of residual stress calculation, including the case of anisotropic materials such as short fiber reinforced thermoplastics is given by Zheng et al. [184].

Equation (2.25) is generally solved subject to the following assumptions:

1. With respect to the local coordinates in which the  $z$ -direction is normal to the local midplane, the shear strains  $\varepsilon_{13} = \varepsilon_{23} = 0$ .
2. The normal stress  $\sigma_{33}$  is constant across the thickness.
3. As long as  $\sigma_{33} < 0$ , the material sticks to the mold walls.
4. Before ejection, the part is fully constrained within the plane of the part such that the only non-zero component of strain is  $\varepsilon_{33}$ .
5. Mold elasticity is neglected.
6. The material behaves as an elastic solid after the part is ejected.

In practice, the residual stresses are calculated by finite element analysis. The discretization involved means that the residual stress is calculated for each element at grid points through the thickness. Hence, eqn.(2.25) may be written

$$\sigma_{ij(e)}(z_i) = \begin{cases} 0 & \text{for } T \geq T_t \\ \int_0^t c_{ijkl}^e \left( \frac{\partial \varepsilon_{kl}}{\partial t'} - \alpha_{kl}(t') \frac{\partial T}{\partial t'} \right) dt', & \text{for } T < T_t \end{cases} \quad (2.26)$$

where the subscript ( $e$ ) refers to the element number and the stress is calculated at each gridpoint  $z_i \in [-H, H]$ . In order to obtain the shrinkage of the part, the calculated residual stresses are used as the loading condition in a structural analysis. This requires an additional set of boundary conditions to prevent rigid body motion of the geometry. We achieve this by selecting three nodes on the part that are not co-linear. Denoting displacement degrees of freedom in the coordinate directions  $x$ ,  $y$  and  $z$  by  $u_x$ ,  $u_y$  and  $u_z$  respectively, we define the boundary conditions to be:

node 1:  $u_x = u_y = u_z = 0$

node 2:  $u_x = u_y = 0$

node 3:  $u_z = 0$ .

All rotational degrees of freedom are unconstrained. With these boundary conditions the part is free to shrink and deform, yet rigid body motion is prevented. Deformations may be calculated, and from these, warpage and shrinkage can be determined.

To illustrate the performance of the viscous-elastic model described above, we provide an example. Luye [111] measured pressure in an ISO mold of dimension 60mmx60mmx3mm for an iPP produced by Solvay (PHV 252). The following processing conditions were used for the molding:

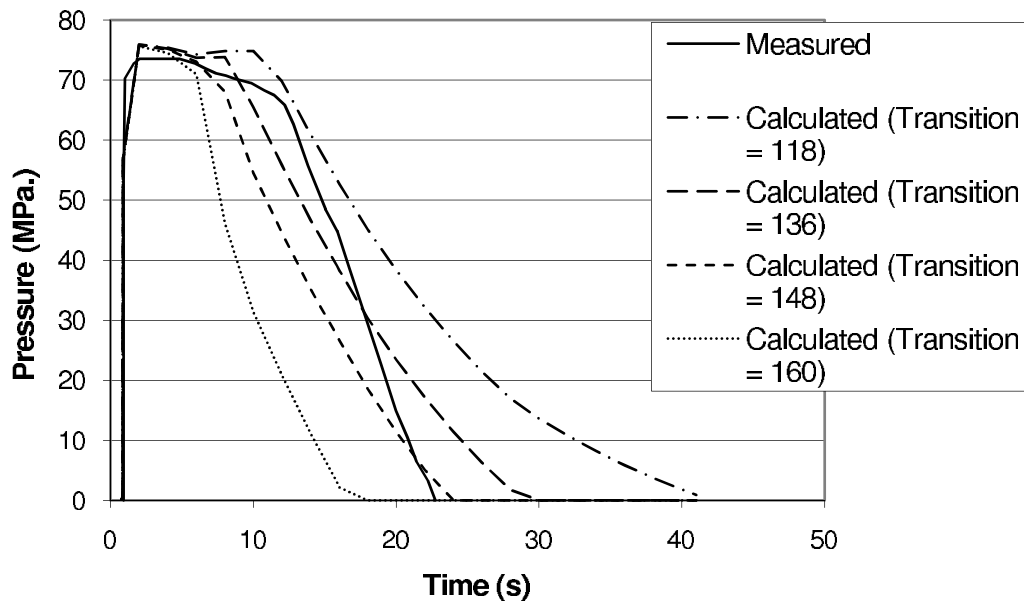
<b>Molding Parameter</b>	<b>Value</b>
Melt temperature	220°C
Injection time	1 s
Mold temperature	43°C
Coolant flow rate	7 l/min
Nozzle holding pressure	80 MPa.
Holding time	15s
Total cooling time (holding time + cooling time)	40s

Figure 2.3 shows pressure traces from simulations run using the same conditions as above, with fixed transition temperatures ranging from 118-160°C

These simulations had no crystallization kinetics and were based on the 2.5D mid-plane theory presented in this chapter. The actual transition temperature for the material was measured to be 118°C. Clearly the value of transition temperature chosen has a significant effect on the pressure decay in the packing phase. The measured trace in Figure 2.3 is from [111].

An obvious question is what effect does this have on shrinkage? In Figure 2.4 we calculate shrinkage in the flow direction using the transition temperatures of Figure 2.3 and the viscous-elastic model described above.

As expected, the effect is significant. Any attempt to improve warpage prediction for semi-crystalline materials will need to overcome the use of a fixed transition temperature.



**Figure 2.3:** Packing pressure for various values of no-flow or transition temperature. The measured data is from Luye [111].

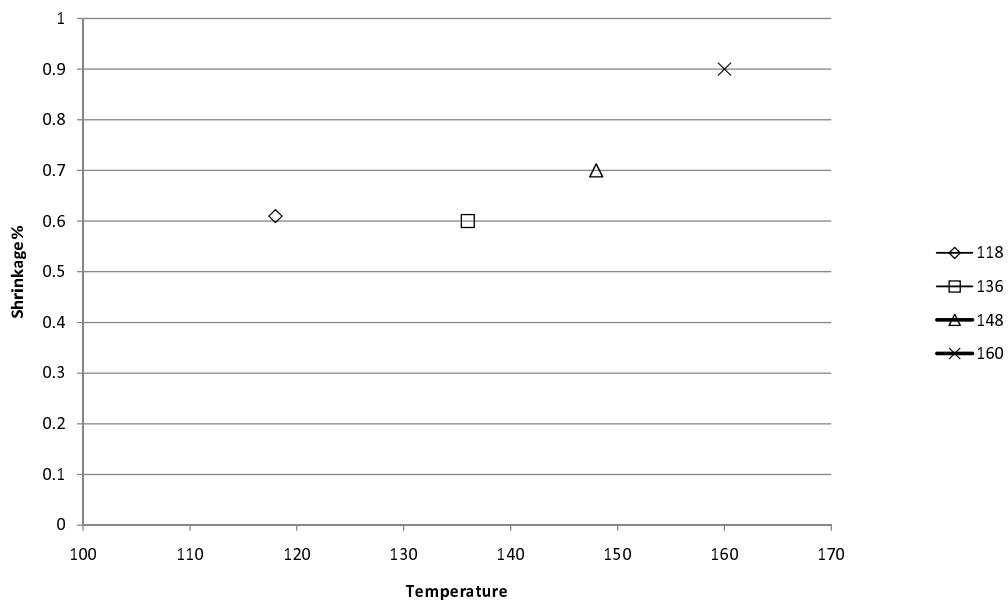


**Figure 2.4:** Calculated parallel shrinkage for various no-flow, or transition, temperatures. The measured value from Luye [111] is 0.8%.

## 2.5 Material Testing Techniques

Most material properties for injection molding simulation are obtained using laboratory tests under well controlled conditions. However, in the factory, injection molded material is subject to very extreme conditions often far outside of those used in laboratory characterization. This leads to intrinsic errors in simulation. We review some of these problems in this section. While some concerns apply to amorphous materials, we focus on semi-crystalline materials.

The essential problem relates to the high rate of cooling, high shear rate and high pressure seen in injection molding. Some areas of concern that we consider in later chapters are listed below:

- Specific heat can be measured as a function of temperature, but current instruments have a lower rate of cooling than rates in injection molding. Consequently, errors due to using a fixed transition temperature will be observed. Also latent heat of fusion will be absent from the simulation unless explicit calculation of crystallization kinetics are incorporated.
- Thermal conductivity may be determined as a function of temperature. However this is also at a relatively low cooling rate and leads to an error in the transition temperature between solid and melt. Current methods also ignore the effect of the microstructure that develops during processing on thermal conductivity. We note tests are done on static material, and so ignore any effects of flow on transition temperature. Van den Brule postulated that conductivity of an amorphous polymer may be anisotropic due to flow effects [26]. Experimental support for this claim has been provided by Venerus et al. [161], [162]. We surmise that the case for semi-crystalline materials may be similar.
- PVT data is generally measured in machines with high thermal inertia, and so leads to errors in transition temperature as cooling rates are so low. Moreover, flow induces different crystalline structures with different densities and (anisotropic) properties.
- Viscosity at low temperatures and/or high shear rates is very hard to determine, as viscous dissipation leads to inaccuracy in temperature measurement. Moreover, the rate of change of temperature in laboratory experiments is much lower than in the molding process. Commercial simulation software uses constitutive relationships such as the Cross - WLF model (see eqn.(2.5)). Low temperature data cannot be obtained to fit this relationship, and the suppression of solidification by supercooling effects that depend on cooling rate cannot be incorporated. Despite the fact that a transition from melt to solid is usually involved in a polymer forming process - not just injection molding - there does not exist a suitable constitutive equation to deal with this phenomenon.

- Thermo-mechanical properties that are required for warpage calculation can be anisotropic and depend strongly on the morphology of the material, and hence on the processing history.

## 2.6 Two Critical Issues

From the foregoing, two formidable problems arise.

The first is the Hele-Shaw approximation. It leads to a simple equation for pressure, eqn.(2.17), that may be readily solved using finite elements for pressure and a finite difference scheme for temperature and velocity. However, the modeling requirement of a midplane mesh is out of step with the CAD industry, which has embraced true 3D geometry. One solution is to move to full 3D simulation of the molding process. But this is not without problems. As injection molded parts have thin wall sections, it is necessary to have many elements across the thickness to capture the high thermal gradient in the thickness direction. Even today this leads to large models and long computation times. In Chapter 3 we describe a method for performing flow and warpage analysis on a 3D thin-walled geometry, making use of the Hele-Shaw approximation but using geometric data from a 3D solid CAD of the part.

The second problem relates to material data. How do we overcome the intrinsic error introduced by using data measured under laboratory conditions in simulation? More particularly, how do we dispense with the fixed transition temperature and the associated problems with material properties for semicrystalline materials? Chapter 4 proposes an engineering solution to this problem in which we adjust calculated properties, obtained with very simple models, with measured results on real injection molded samples. A scientifically more satisfying method is introduced in Chapters 5 and 6, where we calculate crystallinity explicitly and use this to vary material properties during processing.



## CHAPTER THREE

# The Geometry Problem

---

In this chapter we consider the requirements for creating models for analysis based on the mathematical model for simulation given in the previous chapter. It will be shown that the need to derive a special model for analysis is a major commercial problem for Moldflow. We then briefly discuss two solutions to this problem - automatic midplane generation and full 3D analysis and their limitations. Finally we describe the dual domain finite element analysis (DD/FEA) technique as a means to overcome these limitations.

### 3.1 Modeling for Analysis

In the last chapter we showed that the governing conservation equations may be reduced to a single equation for pressure as a function of  $x$  and  $y$ , eqn.(2.17), and an equation for temperature, eqn. (2.11), and mentioned their solution by a hybrid method which uses finite element analysis to determine the pressure field and finite differences to determine the temperature field. For a planar triangular element, Kennedy [92] has shown that the Galerkin finite element formulation for the pressure field gives rise to linear equations of the form:

$$[\mathbf{K}] \{\mathbf{p}\} = \{\mathbf{q}\} \quad (3.1)$$

where  $\{\mathbf{p}\}$  and  $\{\mathbf{q}\}$  are respectively, the pressure and flow rate vectors for the element and  $[\mathbf{K}]$  is the elemental stiffness matrix with

$$k_{ij} = \frac{S}{4A} f_{ij}(x, y) \quad (3.2)$$

where  $S$  is the fluidity defined by equation (2.16),  $A$  is the area of the triangular element and the  $f_{ij}$  are functions that depend only on the local coordinates of the



nodes forming the element.

Hence, the only information required to form the stiffness terms are the coordinates of the nodes, and the thickness of the component for analysis. The required mesh is therefore a lattice of triangles, defined by nodes located at the midplane of the component. To each element a local thickness is assigned. We refer to such a mesh as a *midplane mesh* or *midplane model*.

When flow analysis using the 2.5D approximation was introduced by Moldflow in 1981, the CAD industry was in its infancy. Component geometry was modelled using wire frame or surface models. This interfaced very well with the 2.5D analysis requirements. Given a surface, a mesh was generated and each of the elements was assigned the surface thickness.

During the 1990's a paradigm shift occurred in the CAD industry. Solid modeling, in which the outer component geometry was stored as B-spline surfaces in such a way that a photorealistic model was created, was introduced. Because such a model contained all information about the component, solid model geometry became the core of design, manufacturing and engineering databases. Given a solid model, a user of 2.5D molding simulation had to create a special model for analysis. Figure 3.1 shows a solid model of a complex molding. The time required to get a meshed model for simulation was estimated to be in excess of two weeks. Given that the task requires human interaction, this represents considerable expense in direct salary costs and lost opportunity. Thus we see that the need for the midplane model introduces a major commercial problem. Moreover, as solid modeling continues to become more widespread for design and engineering in the plastics industry it cannot be ignored.

We are therefore faced with the following problem: *How can we produce an analysis system that interfaces directly to solid geometry, thereby removing the need for the user to construct a special model for analysis?*

One possible solution is to try and reduce the time by providing tools to assist users to midplane a geometry. Another is to use 3D analysis rather than 2.5D. Both approaches have been tried and are discussed briefly below.

## 3.2 Midplane Generation

Automatic generation of a midplane from a 3D geometry is not a trivial task. Figure 3.2 shows the idea. The challenge is to automatically deduce the midplane mesh with thickness defined for all elements from the 3D geometry shown at left.

Much of the academic work in this area was focused on obtaining the medial axis of a 3D geometry and was driven by needs in the fields of image analysis and hexahedral mesh generation. Most approaches were drawn from the image processing field and attempted to find the medial axis of the object [40]. A drawback of these schemes was the time required to compute the midplane was in the order of hours. A more important problem was that the midplane mesh was often not as planar as the

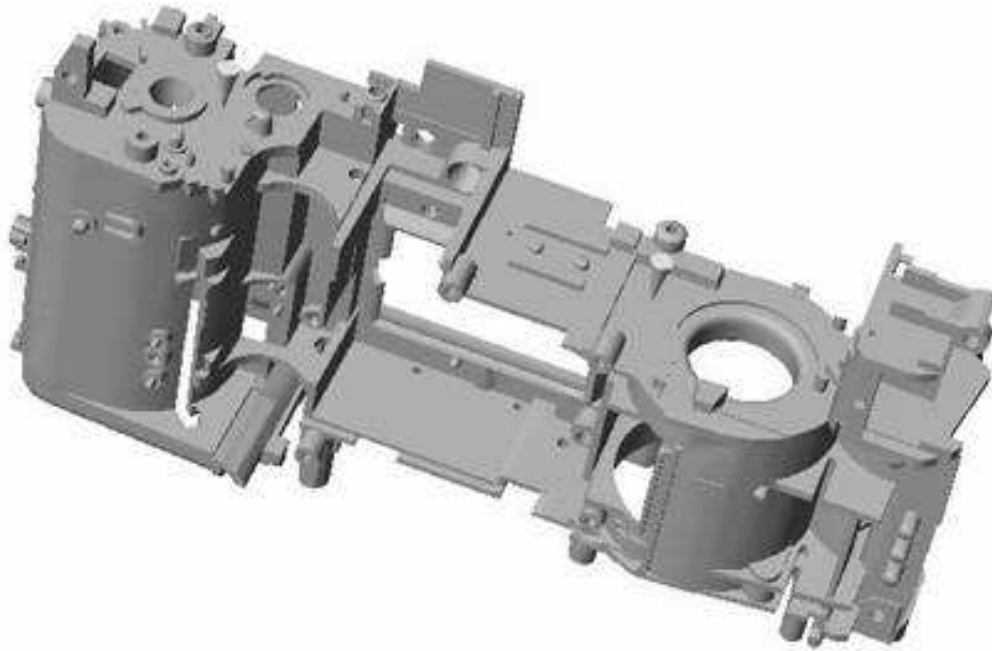


**Figure 3.1:** Kodak Advantix camera molding.

original geometry. While this had little effect on the flow analysis, it looked disturbing to users. Worse still was that the structural characteristics of the part were not preserved, and so this approach prevented structural analysis and hence warpage analysis on the part.

Kennedy and Yu [93] presented an automatic midplane generator using a different approach. Here the original starting point was the mesh used for stereolithography, which consisted of planar triangles often of very poor aspect ratio. These were remeshed to improve aspect ratio and then grouped into surfaces. Algorithms were developed to determine the direction that a surface should be collapsed in. During collapse, the thickness change from original to the midplane was assigned to the resulting midplane elements. This approach was effective for planar thin parts but had some difficulty with small features such as bosses. The generated mesh often had discontinuities which needed to be fixed manually.

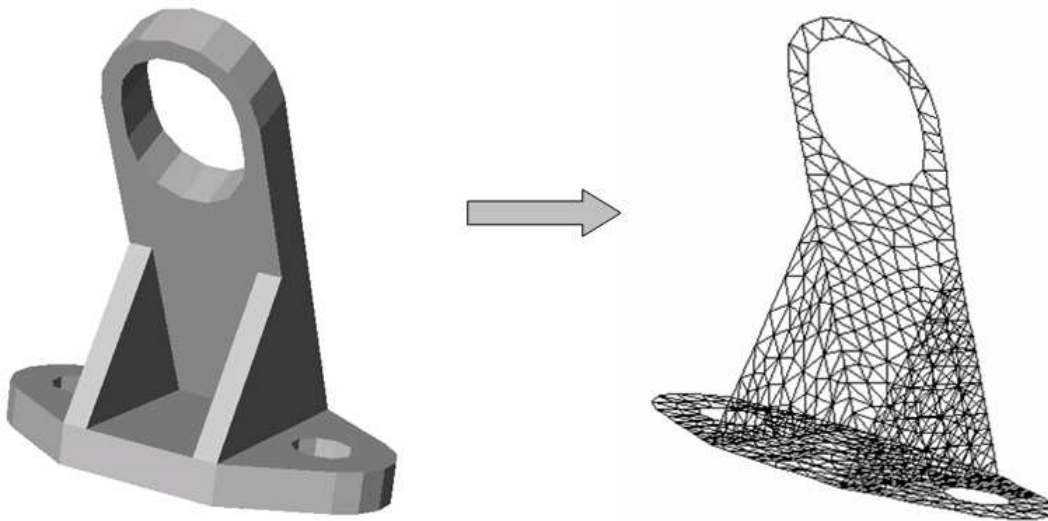


**Figure 3.2:** Automatic generation of a midplane mesh.

### 3.3 3D Analysis

To eliminate the need to create a midplane mesh, one approach is not to use the 2.5D approximation at all and instead solve the conservation equations in three dimensions. Hetû et al. [73] gave the earliest example of 3D injection molding analysis. Such analysis makes fewer assumptions but requires the computational domain to be meshed with tetrahedral or hexahedral elements. This approach is necessary for parts with thick sections for which the assumptions of 2.5D are not valid. However, due to the low thermal conductivity of plastics, injection molded parts tend to be thin-walled. In the thickness direction, temperature gradients in the order of hundreds of degrees per millimeter necessitate the use of many elements across the part thickness. Consequently, in thin-walled parts, the number of elements for 3D analysis increases dramatically and leads to excessive compute times and resources.

### 3.4 Dual Domain FEA

The limitations of automatic midplane generation and full 3D analysis discussed above spurred the development of other technologies to address the problem of interfacing to solid geometry. A very successful approach used the external mesh on a 3D geometry. Figure 3.3 shows the basic idea. Consider a cross-section of a rectangular plate injected at its centre, Figs. 3.3 a) and b). If we prescribed a thickness for the surface elements, it would be possible to perform a 2.5D analysis on the surface mesh.

However, such an analysis would not be physically consistent, as the material would

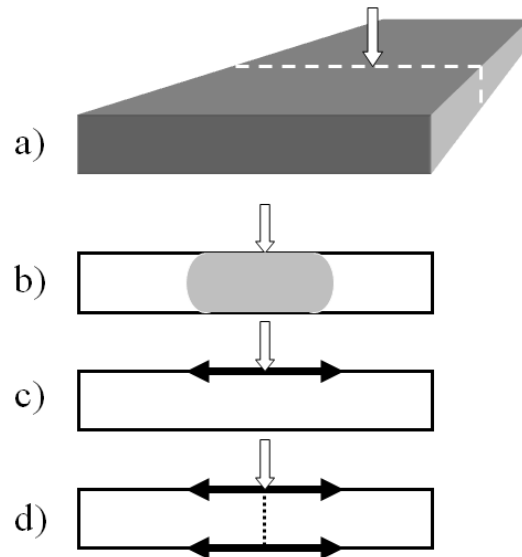


**Figure 3.3:** Dual domain flow analysis; a) depicts injection into a rectangular plate; b) shows the actual flow in a cross-section; c) shows the flow advancement on the surface mesh and d) shows the dual domain concept that ensures agreement with the physical reality as depicted in b).

flow over the top surface, around the edges and then along the lower surface forming a weld line under the injection point as in Fig.3.3 c). The solution is to link the top and bottom mesh at the injection point as shown in Fig. 3.3 d). Material then flows simultaneously along the top and bottom surfaces as expected. This gives rise to the name *Dual Domain* Finite Element Analysis (DD/FEA). In fact we perform two analyses, one on each side of the surface mesh. As we are in fact filling two domains, it is necessary to double the flow rate at the injection point to obtain the fill times calculated with a midplane mesh for a given geometry.

Real parts are always more complex than simple plates. Consider the cross-section of a plate with a rib as shown in Fig.3.4.

With the injection point linked to top and bottom surfaces, flow emanates and hits the rib, Fig.3.4a). At the rib it is necessary to again form a link to the opposite surface so that flow goes up the rib, and continues past the rib, in a sensible way as shown in Fig.3.4b). While the idea is simple, it is quite complex to implement. Nevertheless, a product based on this idea was released in 1997. Patents on the concept have been awarded in the United States [179] and Europe [178] and are pending in many other jurisdictions.

To summarize, dual domain flow analysis has three basic steps:

- Generation of a surface mesh;
- Establishing relationships between the elements on the top and bottom surfaces so that a thickness may be defined; and

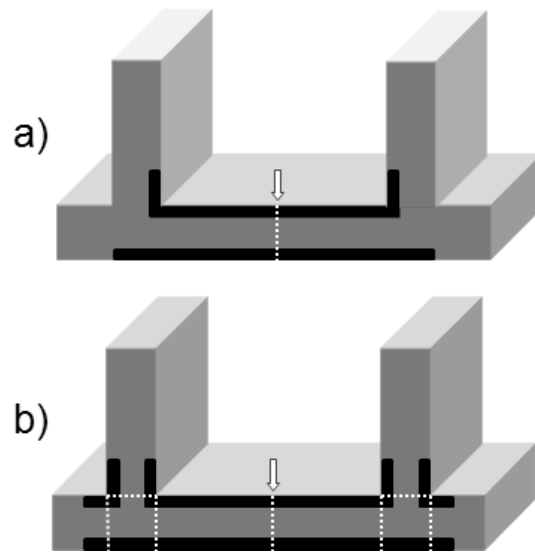


Figure 3.4: Dual domain flow analysis for a part with a rib.

- Adding in connector elements to maintain physically realistic flow patterns.

Full implementation details are disclosed in Yu and Thomas [179].

### 3.5 Dual Domain Structural Analysis

The Dual Domain concept was taken up very rapidly by Moldflow users, so much so that there was immediate pressure to extend the idea to mold cooling and warpage analysis. The mold cooling analysis was easily extended. The boundary element approach for the mold was retained, and coupled with a heat transfer analysis in the plastic material enclosed by the surface mesh.

In order to permit warpage analysis, a structural analysis capability was first required. The initial idea was due to Zhiliang Fan at Moldflow. The extension of the idea to structural analysis was a necessary pre-requisite for warpage analysis. Much of the following description was published in [56].

The method is best introduced by means of an example. The essential idea is to model the structural performance, that is the bending and membrane characteristics, of a plate using only a surface mesh defining the outer boundary of the plate. Consider the plate shown in Figure 3.5. parallel shrinkage vs noflow From the geometric point of view, the flat plate, of thickness  $h$ , can be seen as the perfect bonding of two plates each of thickness  $h/2$ . If we consider such an assembly, we can see that it could be modelled using two shells, each with their reference surface at the geometric center of the two plates. However, this is problematic, as the nodes defining the mid-surfaces are displaced from the outer surface. We want to use the mesh on

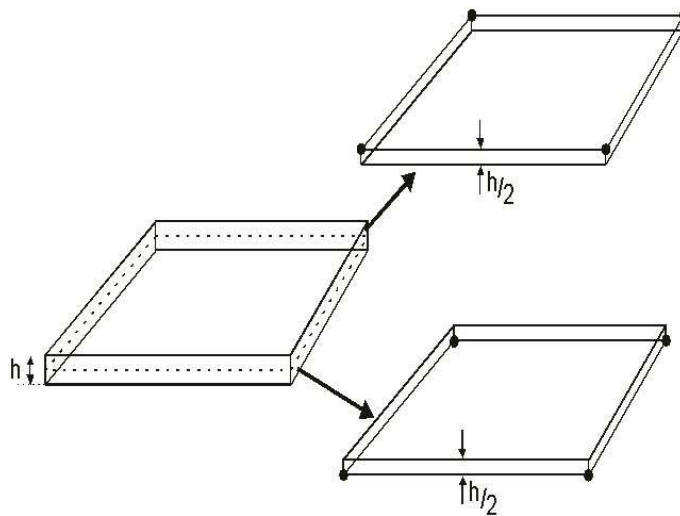


**Figure 3.5:** A simple plate may be decomposed into two plates; each of half the original thickness, and perfectly bonded together.

the outer surface *without* modification. This is accomplished by using eccentric shell elements.

A shell element may be defined such that its reference plane is located anywhere (Figure 3.6). The distance from which the reference plane is displaced from the mid-surface is called the eccentricity. Returning to the problem, we can see in Figure 3.5 the top plate can be modeled using eccentric shell elements with their top surfaces as reference surfaces. Similarly, the bottom plate can be modeled using eccentric shell elements with their bottom surfaces as reference surfaces. This solves the problem by allowing us to use existing nodes on the outer surfaces of the plate. In order to get the correct structural response, however, the two plates of thickness  $h/2$  must be “bonded together” in some way. The bonding of the top and bottom plates involves imposing the Love-Kirchhoff assumption of classical plate or shell theory (see, for example, [41]) and requires that a normal to the plate or shell remains straight after deformation and be unchanged in length. This is accomplished by the use of multi-point constraints.

In summary, for structural analysis, the dual domain method involves the following steps:

- Meshing of the outer surface of the structure and establishing relationships between elements on the top and bottom surfaces to define local thickness;
- Use of shell elements with their reference surfaces at the surfaces defining the outer boundary of the three dimensional object and
- The use of multi-point constraints to ensure that normals to the top and bottom surfaces remain straight after deformation.

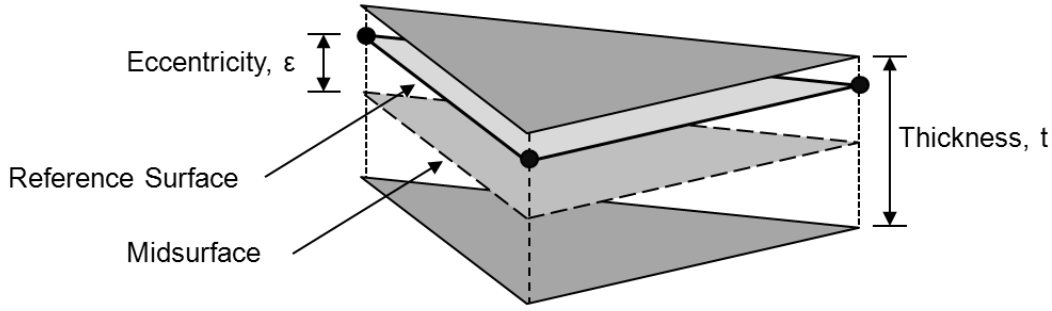


Figure 3.6: Eccentric shell element.

The constraints used depend on the type of element chosen. In our implementation we use a plane triangular facet shell element. This is a three node element with 18 degrees of freedom (six at each node - three displacements and three rotations). The element is constructed by superimposing the local membrane formulation due to Bergan and Felippa [13] with the bending formulation due to Batoz and Lardeur [12] and transforming the combined equations to the global coordinate system. The drilling rotation degree of freedom about a local reference surface normal is used in the membrane formulation, and is defined in the local element system by

$$\theta_z = \frac{1}{2} \left( \frac{\partial u_y}{\partial x} - \frac{\partial u_x}{\partial y} \right). \quad (3.3)$$

To define the relationship between the degrees of freedoms of node  $n$  and those of its matching node  $p$  (see Figure 3.7) we require that the normals to the midsurface before deformation remain straight after deformation. Adopting the local coordinate system of the element, we denote the three displacement DOF and the three rotational DOF at node  $n$  by  $u_{x_n}, u_{y_n}, u_{z_n}$  and  $\theta_{x_n}, \theta_{y_n}, \theta_{z_n}$  respectively. There are then the following relationships between the degrees of freedom of node  $n$  and displacements and rotations of its matching point  $p$ :

$$u_{x_n} = u_{x_p} - \theta_{y_p} h \quad (3.4)$$

$$u_{y_n} = u_{y_p} + \theta_{x_p} h \quad (3.5)$$

$$u_{z_n} = u_{z_p} \quad (3.6)$$

$$\theta_{x_n} = \theta_{x_p} \quad (3.7)$$

$$\theta_{y_n} = \theta_{y_p} \quad (3.8)$$

$$\theta_{z_n} = \theta_{z_p} + \frac{h}{2} \left[ \frac{\partial \theta_{x_p}}{\partial x} + \frac{\partial \theta_{y_p}}{\partial y} \right] \quad (3.9)$$

where  $h$  is the distance between node  $n$  and its matching point  $p$ . Note that the relationship in equation (3.9) is obtained using equation (3.3) and so is particular to the element type chosen.

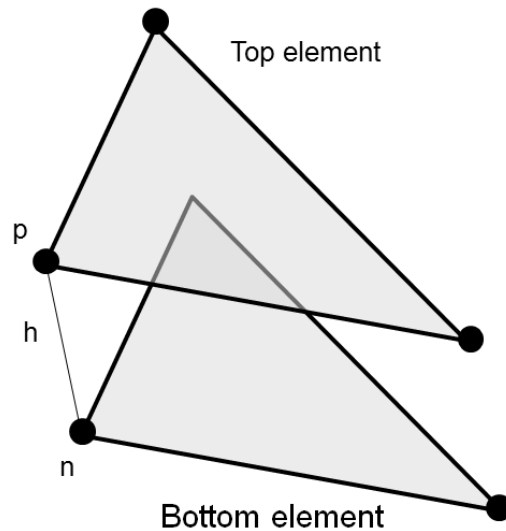


**Figure 3.7:** Elements matched for dual domain structural analysis.

This system of constraints is imposed at all nodes on the bottom (or top) surface of the model with the exception of those at the edges. Elements forming the edge of the plate are assigned one sixth of the thickness of the adjacent elements on the top and bottom surfaces.

With these constraints the structural performance of the composite structure is identical to the original plate. The composite model may now have appropriate boundary conditions and loading applied for structural analysis and so be used for warpage analysis of the 3D geometry.

In general, the mesh on the top surface is not coincident with the bottom mesh. Hence, a normal from a node  $n$  on the bottom surface will not generally coincide with a node on the top surface. Instead, it is more likely that the normal will intersect the top element at a point  $p$ , say (see Figure 3.8). In this case we interpolate the required constraints using the three nodes defining the top element.



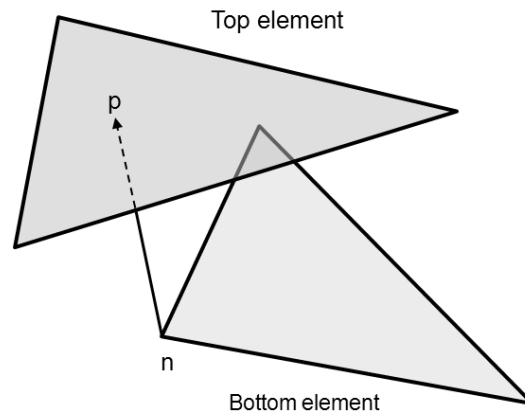


**Figure 3.8:** Elements generally are not simply separated by a distance  $h$ . Usually the normal from node  $n$  intersects the top element at some point within the element. In this case interpolation is required.

### 3.6 Warpage Analysis Using the Dual Domain FEM

In order to use the dual domain approach for warpage analysis, we load the finite element model with shrinkage strains or membrane stresses derived from the analysis of the filling, packing and cooling stages of the molding process as discussed in Chapter 2.

An analysis comparing warpage analysis results for dual domain and the conventional midplane model is presented for the part models shown in Figure 3.9 and Figure 3.10, respectively.

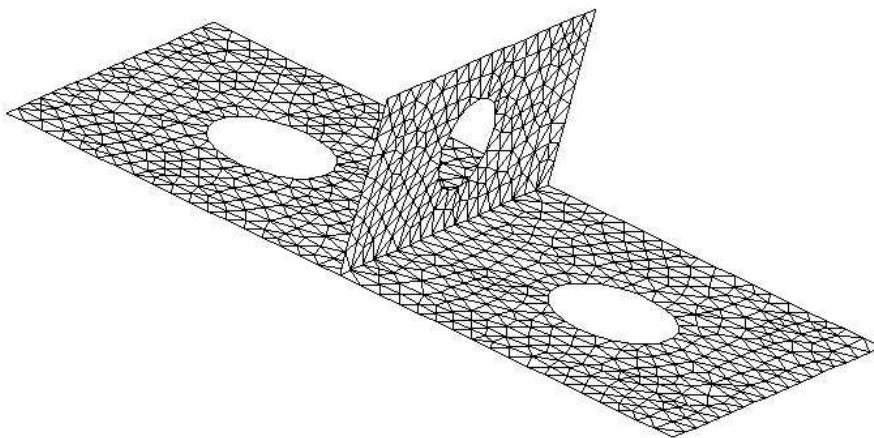


**Figure 3.9:** Midplane mesh of the model

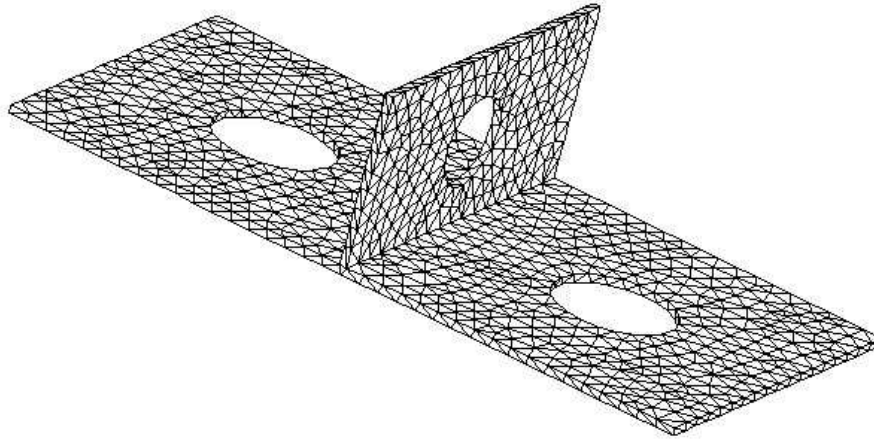


**Figure 3.10:** Dual domain mesh of the model.

The part has a base of 180x90mm. The holes in the plate are each 30mm diameter. The rib has dimensions 90x50mm. Wall thickness of the base and the ribs is 2mm.

The material used for analysis was an unfilled PA66 manufactured by BASF under the name ULTRAMID A3W. Each model was injected at the two corners along the shorter dimension of the base. For each model, filling, packing, cooling and residual stress analyses were performed. The part, in-situ with the mold and cooling line configuration is shown in Figure 3.11.

Process conditions used for the analyses are given below:

<b>Parameter</b>	<b>Value</b>
Melt temperature	290°C
Injection time	1.00 sec
Total Part Volume	37.12 cm <sup>3</sup>
Flow rate	37.12 cm <sup>3</sup> /s
Packing profile	50 MPa. for 10 s
Total Cooling Time	10 s
Environment Temperature and Pressure	25 °C and 0 MPa.
Line 1 coolant temperature	31°C
Line 2 coolant temperature	31°C
Line 1 coolant flow rate	9.5 l/min.
Line 2 coolant flow rate	3.8 l/min.
Target Mold temperature	60°C

Results for the analysis are shown in Figures 3.12 and 3.13. In interpreting these

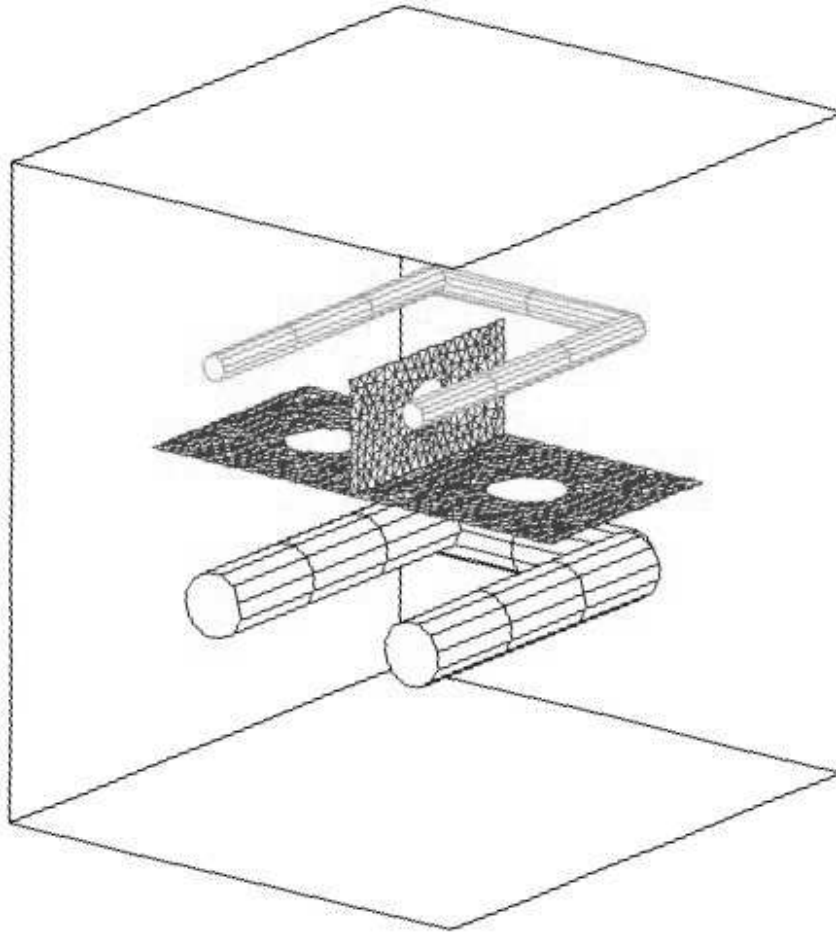
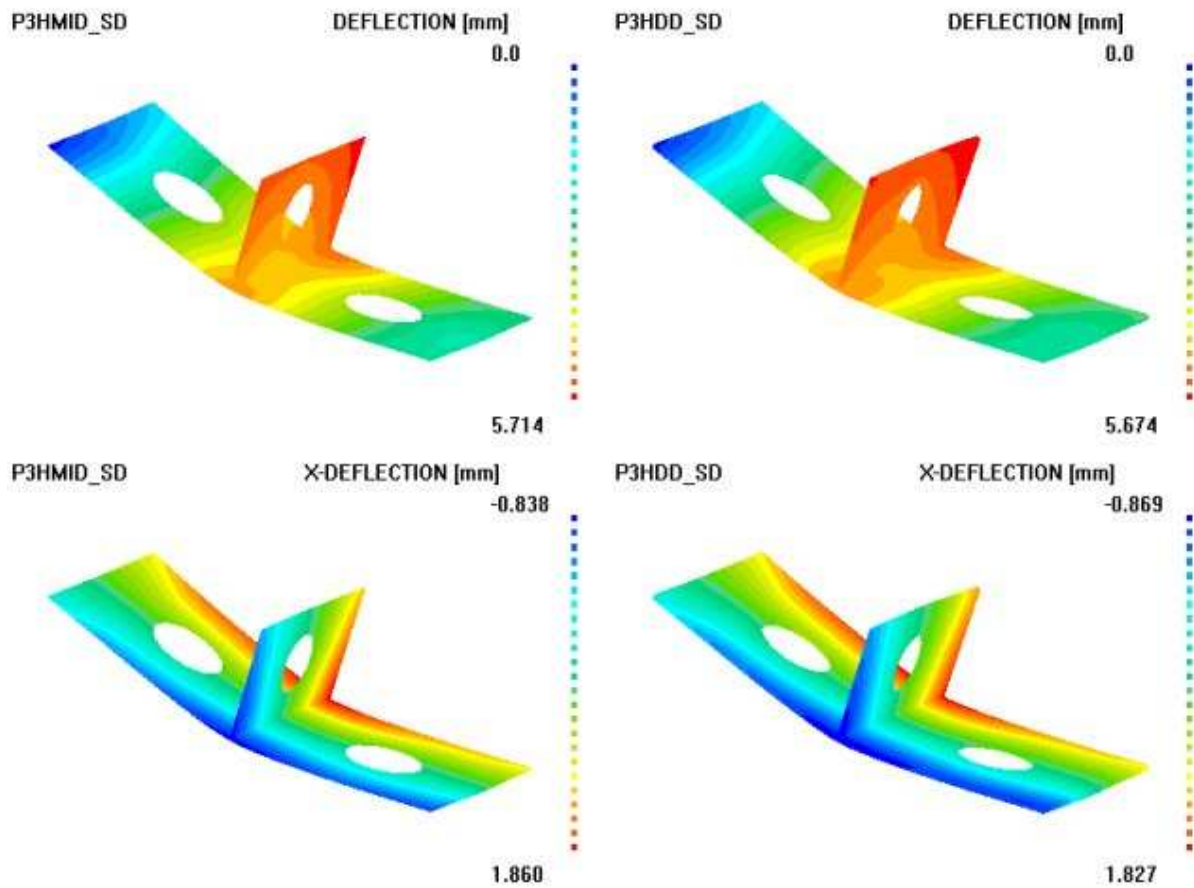


**Figure 3.11:** The part shown in-situ within the mold with cooling lines.

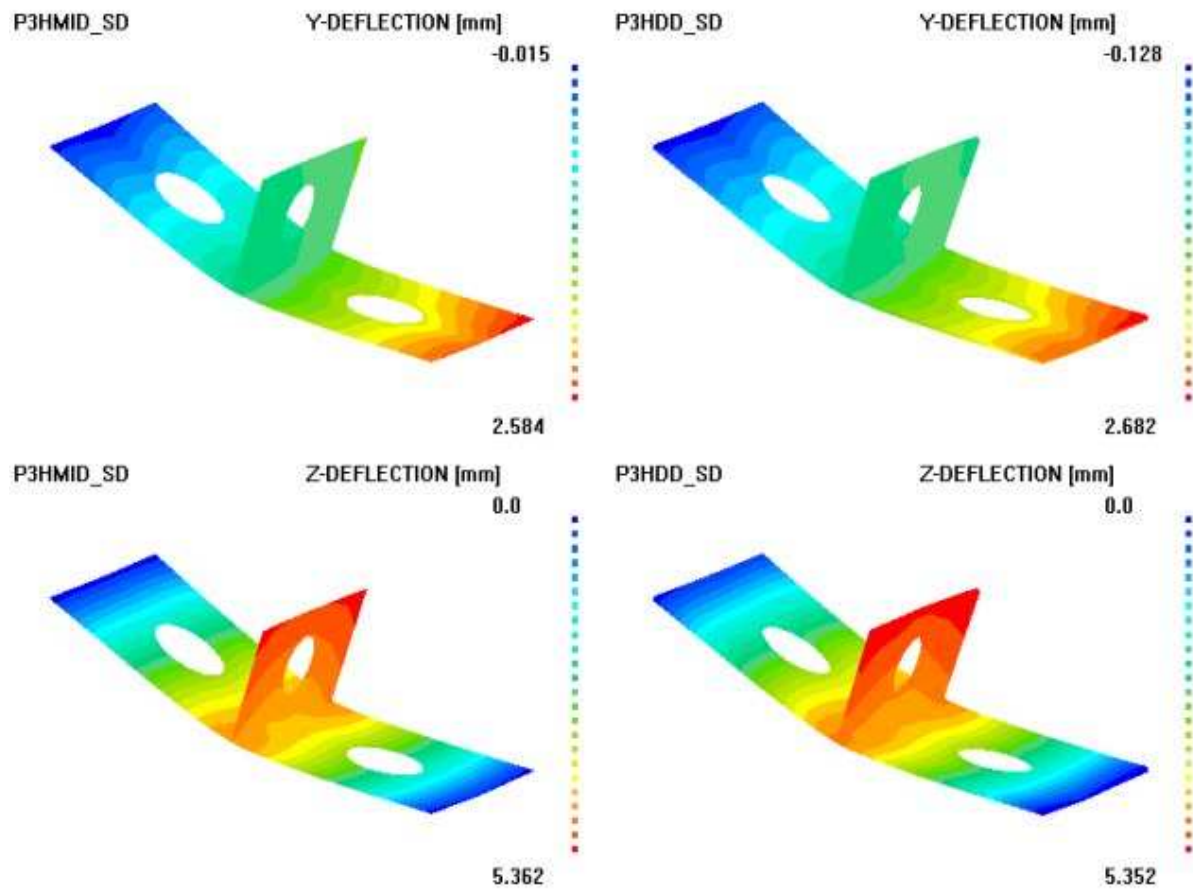
results, the lowest corner of the part represents the origin. The  $x$  axis extends in the width direction of the part (NE of origin), the  $y$  axis extends along the longest dimension of the part (NW) and  $z$  is normal to the  $x - y$  plane in a right orthogonal system. It can be seen that in terms of both total magnitude of predicted deflection and distribution of deformation in the global  $x$  direction, results from the midplane model and the dual domain model are virtually identical.

Figure 3.13 compares midplane and dual domain results in the  $y$  and  $z$  directions. Good agreement between midplane and dual domain results are observed.

There is a slight computational overhead incurred in using the dual domain approach. The time to perform a linear static analysis on the midplane model, which comprised 898 nodes, was 7 seconds while the time to perform a similar analysis on the dual domain model, with 1810 nodes, was 28 seconds. Considering the time required to create a midplane model, this increased solution time is inconsequential. Hence, the method is extremely efficient when judged by the total time taken to



**Figure 3.12:** Midplane results for total deformation and deformation in  $x$  directions are at left. Dual domain results for the same deflections are at right.



**Figure 3.13:** Comparison of midplane results (left) and dual domain results (right) for  $y$  and  $z$  deflections.

obtain a result.

Patents for the dual domain structural analysis have been granted in the USA [57] and several other jurisdictions. Details of the implementation of the method are provided in the patent.



# Overcoming Material Data Limitations

---

This chapter introduces a method that uses measured shrinkage on test samples to determine correction factors for residual stresses calculated using conventional material data. The method overcomes some of the problems highlighted in Chapter 2 and leads to improved accuracy for shrinkage prediction.

Much of this chapter has been published recently by Kennedy and Zheng [98].

## 4.1 The Material Data Problem

In Chapter 2 we introduced the basic equations of residual stress calculation. These equations involve considerable simplification in order to use readily available material data. Of these assumptions, the most serious one is the assumption of viscoelastic material behavior. Whilst ignoring the viscoelastic nature of the material, the simulation assumes that the material suddenly becomes elastic when the temperature falls below the transition temperature,  $T_t$ . The problem is that  $T_t$  is not a well defined material property. For semi-crystalline materials  $T_t$  depends on the rate of cooling as well as the shear treatment given to the material [50]. Despite this complexity,  $T_t$  is considered constant in most commercial simulations, and is measured using a DSC at cooling rates much lower than those encountered in injection molding. Moreover, such a measurement ignores any flow-induced crystallization effects. Unfortunately, the residual stress calculation is quite sensitive to the value of  $T_t$  used.

Apart from the difficulty of dealing with the transition temperature, there are other problems associated with obtaining material data for use in simulation. While modulus and thermal coefficient of expansion values for materials are available, they are typically measured on dogbone specimens. When these specimens are molded, the flow of the material is dissimilar to the flow in molding of real parts. Consequently, the values obtained are valid for a particular set of process conditions and



flow regime. For semi-crystalline materials the problem is very complex. For example, usually polypropylene displays anisotropy in shrinkage such that shrinkage along the flow direction is greater than that measured transverse to flow. However, under some conditions, this anisotropy is reversed [111]. One method of introducing this anisotropy is to “build it into” the mechanical properties for the analysis. But reversed anisotropy, as observed by Luye [111], is not possible for constant values of mechanical properties. On the other hand, the current state of the art is well short of being able to predict properties as a function of processing. Indeed, we note that this remains one of the outstanding problems of polymer science [116]. In the following sections, we introduce a commercially viable solution to the problem of obtaining suitable material data for warpage simulation.

## 4.2 Hybrid Model

The model proposed is hybrid in that it utilizes measured shrinkage data to improve the prediction of shrinkage from theoretical models such as equations (2.23) or (2.25). The model may be used for filled and unfilled materials, and appears to perform well for polymer blends. We discuss here the model for unfilled materials.

The model presented has been developed for midplane implementation and so uses the results from a finite element, Hele-Shaw flow analysis as described in Chapter 2. Consider a cavity divided into elements of local thickness  $2H$ . We propose a model of the form:

$$\bar{\varepsilon}_{11}^{(c)} = b_1 \bar{\varepsilon}_{11}^{(p)} + b_2 \bar{\varepsilon}^o + b_3 \quad (4.1)$$

$$\bar{\varepsilon}_{22}^{(c)} = b_4 \bar{\varepsilon}_{22}^{(p)} + b_5 \bar{\varepsilon}^o + b_6 \quad (4.2)$$

where  $\bar{\varepsilon}_{11}^{(c)}$  and  $\bar{\varepsilon}_{22}^{(c)}$  are the corrected principal shrinkage strains in the directions parallel and transverse to flow respectively,  $\bar{\varepsilon}_{11}^{(p)} = \bar{\varepsilon}_{22}^{(p)}$  are the predicted principal shrinkage strains,  $b_i (i = 1, \dots, 6)$ , are constants to be determined and  $\bar{\varepsilon}^o$  is a strain measure of the effects of orientation in the material.

Note that the predicted strains are considered isotropic for the unfilled case. Consequently the thermomechanical properties used in their determination may also be isotropic. This simplifies the required material data significantly. Although this simplification ignores the observed anisotropy in measured samples, the model introduces anisotropy in the corrected strains.

For unfilled amorphous materials the observed shrinkage anisotropy parallel and transverse to flow is usually small. However, even small variations can significantly affect warpage of parts with low torsional stiffness. For these materials the degree of anisotropy may be related to the orientation of molecules in the material.

Semi-crystalline polymers develop a complex layered morphology [50] that governs the thermomechanical properties of the material and influences shrinkage

anisotropy. The relationship between processing and morphology is an area of current research (see for example, [198], [50], [181], [42], [80], [147]) and will be explored further in Chapters 5 and 6. While general relationships have not yet been developed, it does appear that the resulting morphology is related to the molecular orientation of the material prior to solidification. In this work we assume that the orientation state may be measured by a function,  $\Theta_{11}(z, t)$ . We allow this function to depend on cooling rate  $dT/dt$ , the second invariant of the deformation rate tensor  $II_{\mathbf{D}}$  and relaxation time  $\lambda$ . Consequently, we set

$$\Theta_{11}(z, t) = f(dT/dt, II_{\mathbf{D}}, \lambda) \quad (4.3)$$

We note that  $\Theta_{11}(z, t)$  may be readily calculated by a conventional, filling, packing and cooling phase simulation, and define an average value  $\bar{\Theta}$  by integrating  $\Theta_{11}(z, t)$  over the thickness of the cavity. i.e.

$$\bar{\Theta} = \frac{1}{2H} \int_{-H}^{+H} \Theta_{11}(z, t) dz. \quad (4.4)$$

We then define

$$\bar{\varepsilon}^o = C \bar{\Theta} \quad (4.5)$$

where  $C$  is a constant.

### 4.2.1 The Contracted Notation

To simplify the notation in the sequel, we digress from discussion of the model to introduce a contracted form of eqn.(2.21). We define a mapping from contracted notation to tensor notation as follows [169]:

Contracted Notation	Tensor Notation
1	11
2	22
3	33
4	23
5	13
6	12

Equation (2.21) may then be written:

$$\sigma_m = c_{mn}^e \varepsilon_n, \quad (4.6)$$

where  $m \in \{1, 2, 3, 4, 5, 6\}$  and  $n \in \{1, 2, 3, 4, 5, 6\}$ . Assuming a transversely isotropic

material model, with axis of material symmetry in the 1 direction, equation (4.6) may be written in the matrix form:

$$\begin{pmatrix} \sigma_1 \\ \sigma_2 \\ \sigma_3 \\ \sigma_4 \\ \sigma_5 \\ \sigma_6 \end{pmatrix} = \begin{pmatrix} c_{11}^{(e)} & c_{12}^{(e)} & c_{12}^{(e)} & 0 & 0 & 0 \\ c_{12}^{(e)} & c_{22}^{(e)} & c_{23}^{(e)} & 0 & 0 & 0 \\ c_{12}^{(e)} & c_{23}^{(e)} & c_{22}^{(e)} & 0 & 0 & 0 \\ 0 & 0 & 0 & c_{44}^{(e)} & 0 & 0 \\ 0 & 0 & 0 & 0 & c_{55}^{(e)} & 0 \\ 0 & 0 & 0 & 0 & 0 & c_{66}^{(e)} \end{pmatrix} \begin{pmatrix} \varepsilon_1 \\ \varepsilon_2 \\ \varepsilon_3 \\ \varepsilon_4 \\ \varepsilon_5 \\ \varepsilon_6 \end{pmatrix} \quad (4.7)$$

in which  $c_{44}^{(e)} = \frac{1}{2} (c_{22}^{(e)} - c_{23}^{(e)})$  and  $c_{55}^{(e)} = c_{66}^{(e)}$ . Also, in the contracted notation,  $\varepsilon_1 = \varepsilon_{11}$ ,  $\varepsilon_2 = \varepsilon_{22}$  and  $\varepsilon_3 = \varepsilon_{33}$  while  $\varepsilon_4 = 2\varepsilon_{23}$ ,  $\varepsilon_5 = 2\varepsilon_{13}$  and  $\varepsilon_6 = 2\varepsilon_{12}$ . The stiffness matrix components may be expressed in terms of engineering quantities as,

$$\begin{aligned} c_{11}^{(e)} &= \frac{(1 - \nu_{23})E_{11}}{1 - \nu_{23} - 2\nu_{12}\nu_{21}}, \\ c_{12}^{(e)} &= \frac{\nu_{21}E_{11}}{1 - \nu_{23} - 2\nu_{12}\nu_{21}}, \\ c_{22}^{(e)} &= \frac{E_{22}}{2(1 - \nu_{23} - 2\nu_{12}\nu_{21})} + G_{23}, \\ c_{23}^{(e)} &= \frac{E_{22}}{2(1 - \nu_{23} - 2\nu_{12}\nu_{21})} - G_{23}, \\ c_{55}^{(e)} &= G_{12}. \end{aligned}$$

It is possible to invert eqn.(4.6) to obtain

$$\varepsilon_n = s_{mn}^e \sigma_m \quad (4.8)$$

where the  $s_{mn}^e$  are the compliances which may be obtained by inverting the stiffness matrix.

Assuming isotropic material behavior and using the contracted notation we have:

$$\begin{aligned}
c_{11}^{(e)} &= \frac{(1-\nu)E}{1-\nu-2\nu^2}, \\
c_{12}^{(e)} &= \frac{\nu E}{1-\nu-2\nu^2}, \\
c_{22}^{(e)} &= \frac{E}{2(1-\nu-2\nu^2)} + G, \\
c_{23}^{(e)} &= \frac{E}{2(1-\nu-2\nu^2)} - G, \\
c_{55}^{(e)} &= c_{66}^{(e)} = G = \frac{E}{2(1+\nu)}.
\end{aligned}$$

That is,

$$\begin{pmatrix} \sigma_1 \\ \sigma_2 \\ \sigma_3 \\ \sigma_4 \\ \sigma_5 \\ \sigma_6 \end{pmatrix} = \frac{2G}{(1-2\nu)} \begin{pmatrix} A & \nu & \nu & 0 & 0 & 0 \\ \nu & A & \nu & 0 & 0 & 0 \\ \nu & \nu & A & 0 & 0 & 0 \\ 0 & 0 & 0 & B/2 & 0 & 0 \\ 0 & 0 & 0 & 0 & B/2 & 0 \\ 0 & 0 & 0 & 0 & 0 & B/2 \end{pmatrix} \begin{pmatrix} \varepsilon_1 \\ \varepsilon_2 \\ \varepsilon_3 \\ \varepsilon_4 \\ \varepsilon_5 \\ \varepsilon_6 \end{pmatrix} \quad (4.9)$$

where  $A = 1 - \nu$  and  $B = 1 - 2\nu$  or, in compliance form,

$$\begin{pmatrix} \varepsilon_1 \\ \varepsilon_2 \\ \varepsilon_3 \\ \varepsilon_4 \\ \varepsilon_5 \\ \varepsilon_6 \end{pmatrix} = \frac{1}{E} \begin{pmatrix} 1 & -\nu & -\nu & 0 & 0 & 0 \\ -\nu & 1 & -\nu & 0 & 0 & 0 \\ -\nu & -\nu & 1 & 0 & 0 & 0 \\ 0 & 0 & 0 & 2F & 0 & 0 \\ 0 & 0 & 0 & 0 & 2F & 0 \\ 0 & 0 & 0 & 0 & 0 & 2F \end{pmatrix} \begin{pmatrix} \sigma_1 \\ \sigma_2 \\ \sigma_3 \\ \sigma_4 \\ \sigma_5 \\ \sigma_6 \end{pmatrix} \quad (4.10)$$

where  $F = 1 + \nu$ .

### 4.2.2 Prediction of the $b_i$

We now return to the discussion of the model. Using the notation introduced above, the essential idea is to determine the left-hand side of equations (4.1) and (4.2) from experiments and then use simulation to determine the corresponding values of  $\bar{\varepsilon}_1^{(p)}$ ,  $\bar{\varepsilon}_2^{(p)}$  and  $\bar{\varepsilon}^0$ . The  $b_i$  are then found using linear regression analysis.

We first consider the experimental data required. The experimental sample is shown in Figure 4.1. Thickness of the sample may be adjusted to 1.7mm, 2mm, 3mm and 5mm. Typically, 28 processing condition sets are used to form the samples. Pro-

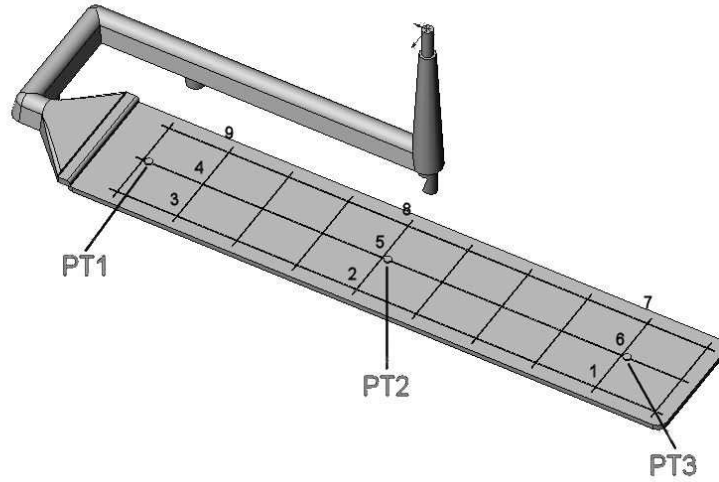


Figure 4.1: Schematic of tag die used for experimental samples.

cessing condition sets are created by varying sample thickness, injection time and holding pressure. The mold has an etched grid to facilitate shrinkage measurement; it is also fitted with three pressure transducers along the flow length as shown in Figure 4.1. After molding, samples are stored for 10 days in a controlled atmosphere to account for any relaxation or post molding crystallization. After this time, the length of the molded sample in the direction parallel to flow  $l_1^{(m)}$ , is measured on the sample from point 4 to 6 in Figure 4.1. Denoting the length of the mold from point 4 to 6 as  $l_1$ , we define the shrinkage in the direction parallel to flow,  $\bar{\varepsilon}_1^{(m)}$ , as

$$\bar{\varepsilon}_1^{(m)} = \frac{l_1 - l_1^{(m)}}{l_1}.$$

Similarly, denoting the measured length of the sample from points 2 to 8 in Figure 4.1 by  $l_2^{(m)}$ , we define the shrinkage in the direction perpendicular to flow  $\bar{\varepsilon}_2^{(m)}$ , as

$$\bar{\varepsilon}_2^{(m)} = \frac{l_2 - l_2^{(m)}}{l_2},$$

where  $l_2$  is the length of the mold from points 2 to 8 in Figure 4.3.

The predicted strains  $\bar{\varepsilon}_1^{(p)}$  and  $\bar{\varepsilon}_2^{(p)}$  are determined by first calculating the residual stress using eqn.(2.26) and the appropriate boundary conditions discussed in Section 2.4.2. For each set of processing conditions used to produce a sample, a simulation is run and values of  $\sigma_{1(e)}^{(p)}(z)$  and  $\sigma_{2(e)}^{(p)}(z)$  are calculated over the thickness, for each element in the model, with eqn.(2.26). We now define an average elemental stress,

$\bar{\sigma}_{1(e)}^{(p)}$  and  $\bar{\sigma}_{2(e)}^{(p)}$  as follows:

$$\bar{\sigma}_{1(e)}^{(p)} = \frac{1}{2H} \int_{-H}^{+H} \sigma_1^{(p)}(z) dz$$

$$\bar{\sigma}_{2(e)}^{(p)} = \frac{1}{2H} \int_{-H}^{+H} \sigma_2^{(p)}(z) dz$$

These stresses are then averaged for the  $n$  elements that comprise the grid area defined by points 1, 7, 9 and 3 in Figure 4.1 to give:

$$\bar{\sigma}_1^{(p)} = \frac{1}{n} \sum_{e=1}^{e=n} \bar{\sigma}_{1(e)}^{(p)}$$

$$\bar{\sigma}_2^{(p)} = \frac{1}{n} \sum_{e=1}^{e=n} \bar{\sigma}_{2(e)}^{(p)}$$

Finally, we calculate the strains  $\bar{\varepsilon}_{1e}^{(p)}$  and  $\bar{\varepsilon}_{2e}^{(p)}$  for the grid area using eqn.(4.10). In addition, for each set of conditions, we compute values of  $\bar{\varepsilon}^o(z)$  according to equations (4.3) to (4.5). Hence, all the strains in equations (4.1) and (4.2) are known. The constants  $b_i, i \in \{1, 2, \dots, 6\}$  are then determined using linear regression and are stored in a database.

### 4.2.3 Using the Model

For prediction of shrinkage and warpage we use a similar procedure. An analysis is run under the desired conditions to get  $\sigma_{1(e)}^{(p)}(z_i)$  and  $\sigma_{2(e)}^{(p)}(z)$  using eqn.(2.26) and  $\tau_{11}(z, t)$  from eqn.(4.3). These quantities are then averaged and converted to strains for each element. As values of  $b_i, i \in \{1, 2, \dots, 6\}$  and  $E, \nu$  are known from the database for a given material, the right-hand sides of equations (4.1) and (4.2) may be calculated to give the corrected strains  $\bar{\varepsilon}_{1(e)}^{(c)}$  and  $\bar{\varepsilon}_{2(e)}^{(c)}$ . Equation (4.9) may be used to transform the corrected strains to corrected stresses  $\bar{\sigma}_{1(e)}^{(c)}$  and  $\bar{\sigma}_{2(e)}^{(c)}$ . We then define membrane forces per unit length,  $N_1$  and  $N_2$ , in the principal stress directions using

$$N_{i(e)} = \int_{z=-H}^{z=H} \bar{\sigma}_{i(e)}^{(c)} dz \quad (4.11)$$

$$= 2H \bar{\sigma}_{i(e)}^{(c)}, \quad i = 1, 2 \quad (4.12)$$

These forces can be passed to the structural analysis program to determine shrinkage.

So far all the corrections have involved averaged quantities and any asymmetry in the residual stress distribution has been lost. Any practitioner of injection molding knows that temperature differences between the mold halves are a major source of warpage problems and must be accounted for. To do this, we return to the (uncorrected) predicted residual stresses  $\sigma_{1(e)}^{(p)}(z_i)$  and  $\sigma_{2(e)}^{(p)}(z_i)$ . Elemental bending moments per unit length,  $M_{1(e)}$  and  $M_{2(e)}$ , in the principal stress directions are defined by:

$$M_{1(e)} = \int_{z=-H}^{z=H} \sigma_{1(e)}^{(p)}(z_i) z dz \quad (4.13)$$

$$M_{2(e)} = \int_{z=-H}^{z=H} \sigma_{2(e)}^{(p)}(z_i) z dz. \quad (4.14)$$

The quantities  $N_{1(e)}$ ,  $N_{2(e)}$ ,  $M_{1(e)}$  and  $M_{2(e)}$  are passed to a structural analysis program which calculates the deformation of the part and hence shrinkage and warpage.

The correction process described above is known as the Corrected Residual In-Mold Stress (CRIMS) model.

### 4.3 Results for Unfilled Polypropylene

To demonstrate the performance of the CRIMS model we present some results for an unfilled iPP homopolymer (Solvay Eltex PHV252). The procedure described in the previous section was performed for the set of conditions listed in Figure 4.2. All calculations were performed with Moldflow Plastics Insight software V4.1 (build 03104).

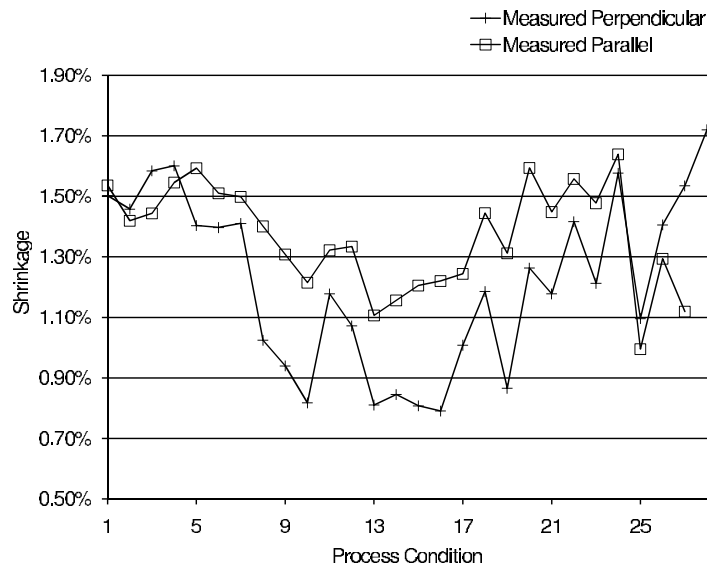
Measured shrinkages, parallel and perpendicular (i.e. transverse), to flow are shown in Figure 4.3. It is important to note that the feed system is such that the pressure variation along the sample is negligible for thickness of 2mm or more. While it is possible to measure shrinkages along the length, and so obtain more data per sample for regression analysis, we have not done this here. It can be argued that for thin samples it is more appropriate to measure along the flow path but our measurements illustrate the basic idea. Consequently the parallel and perpendicular shrinkages are measured along the lines from points 4 to 6 and points 2 to 8 respectively, as indicated in Figure 4.1. Of particular note is the high degree of orthotropy exhibited by the material. Also of interest is the fact that, while the parallel shrinkage is usually higher than perpendicular, there exist some conditions under which this trend is reversed.

Figure 4.4 shows measured shrinkages, calculated shrinkages using the uncorrected residual stress distribution and calculated shrinkages obtained with the CRIMS model in the direction parallel to flow. Each point on the graph represents a different set of processing conditions used to produce the sample. The actual conditions used to produce each molded sample are provided in Figure 4.2. Similarly, Figure 4.5 shows shrinkage results for the perpendicular direction.

Expt No.	Melt Temp °C	Mold Temp °C	Flow Rate cm <sup>3</sup> /s	Sample Thickness mm	Hold Pressure MPa.	Hold Time s	Cooling Time s
1	225.5	46.8	20.6	2	27.2	15	20
2	225.2	48	24.6	2	27.3	15	20
3	225.6	47.4	33.3	2	27.3	15	20
4	225.3	47.4	15.7	2	27.1	15	20
5	225.3	47.5	9.8	2	27.1	15	20
6	225.8	47.2	20.3	2	27.2	15	30
7	225.2	46.6	19.7	2	27.2	15	40
8	225.5	47.4	20.3	2	40.9	15	20
9	225.6	47.7	20	2	50.3	15	20
10	225.5	48.3	20.6	2	59.5	15	20
11	225.5	48.6	24.7	2	50.4	15	20
12	225.6	48.7	31.8	2	46.6	15	20
13	225.3	49.1	9.5	2	78	15	20
14	225.3	48.7	15.2	2	68.8	15	20
15	225.6	48.7	21	2	59.6	15	30
16	225.6	48.2	20	2	59.7	15	40
17	243.8	45.8	20.3	2	50.1	15	20
18	243.4	46.4	20.5	2	27.2	15	20
19	212	43.1	19.9	2	59.6	15	20
20	212.4	43.2	19.6	2	27.4	15	20
21	225.6	60.8	20.4	2	41	15	20
22	225.6	62	19.9	2	27.4	15	20
23	225.5	49.9	19.1	1.7	50.4	15	20
24	225.2	49.9	18.5	1.7	27.6	15	20
25	225.7	47.9	26.1	3.0/0	59.2	35	15
26	225.6	47.9	26	3.0/0	27.4	35	15
27	228	51.4	31.5	5	68.1	50	10
28	227.7	51.6	32.1	5	27.1	50	20

Figure 4.2: Conditions used to mold the samples of polypropylene (Eltex PHV252).





**Figure 4.3:** Measured parallel and perpendicular shrinkages of polypropylene.

Considering Figure 4.4, as expected, the measured shrinkages vary according to the conditions used to mold the samples. It is clear from Figure 4.2 that hold pressure is the dominant variable. The uncorrected model displays many of the same features as the experimental data; however, it results in significant overprediction. This may be attributed to the use of a viscous elastic model in which no stress relaxation is permitted whilst the material is in the mold. The shrinkages produced with corrected stress distributions show excellent agreement with the experimental data.

Figure 4.5 shows similar trends to those in Figure 4.4. The match between the experimental and calculated shrinkages using the corrected model is not as good as in the parallel direction, but nonetheless matches trends and in most cases magnitude. Although this argument is circular, in that the model has been generated with the same data it then reproduces, the agreement of the shrinkages obtained with the corrected stresses is reasonable. Indeed, given that the model uses just three parameters for each direction, and that the uncorrected values are so far off, the agreement between measured and corrected values is remarkably good.

## 4.4 Results on Other Materials

The applicability of the model to other materials is now considered. Using the same geometry as above we present results for the following materials:

- ABS
- PC

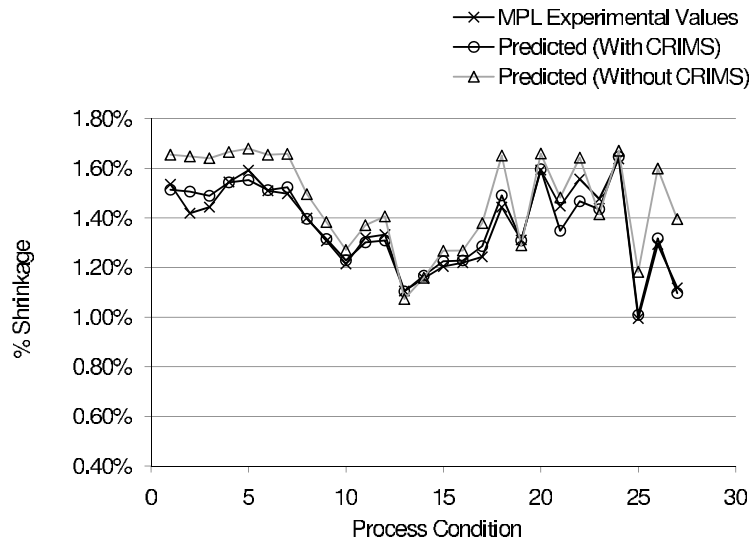


Figure 4.4: Parallel shrinkage of PP showing the effect of correction.

- PC+ABS Blend
- PBT

As above, all calculations were performed with Moldflow Plastics Insight software V4.1 (build 03104).

#### 4.4.1 ABS

The material is an ABS copolymer resin supplied by BASF under the tradename Terluran GP35 weiss P 10013. Figure 4.6 shows the measured parallel shrinkage and the shrinkage calculated with uncorrected and corrected stress. For the first eight processing conditions, the uncorrected model gives reasonable prediction. However the error then becomes significant for conditions 9 to 17. This demonstrates that a simple shifting of the results in the vertical axis is not sufficient to improve the prediction. The corrected values are in excellent agreement over most conditions.

Figure 4.7 shows the results for the perpendicular shrinkage. Not surprisingly, ABS shows little anisotropy, and similar comments as for the parallel direction apply.

#### 4.4.2 PC

We now consider a polycarbonate resin supplied by Bayer AG under the tradename Makrolon AL 2443. Figure 4.8 shows the parallel shrinkage. The uncorrected calculation shows excellent agreement in trend; however, the magnitude is too high. The

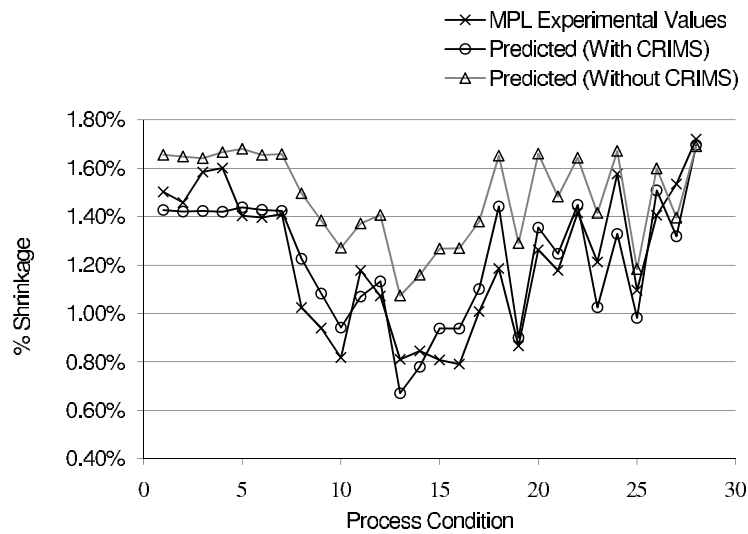


**Figure 4.5:** Perpendicular shrinkage of PP showing effects of correction.

corrected shrinkages are in excellent agreement with the experimental values. Figure 4.9 gives the results for the perpendicular direction. While the trends are almost the same as the parallel case, we see some slight anisotropy in this material. Depending on conditions, the perpendicular shrinkage is around 10-20% higher than parallel. The corrected model captures the experimental results very well.

#### 4.4.3 PC+ABS Blend

We now turn to a blend of PC and PBT supplied by DOW Chemical USA under the tradename Pulse 1725. Figure 4.10 shows the parallel shrinkages. The uncorrected results show a similar trend to the experimental values but dramatically underpredict shrinkage at condition 2. The corrected curve overcomes this problem and shows very good agreement with the experiment. Figure 4.11 shows the perpendicular shrinkage for this blend. As for the parallel case the corrected prediction is in very good agreement with the experimental values.

#### 4.4.4 PBT

We conclude this section with some results for another semicrystalline resin, namely, PBT. Figure 4.12 shows the parallel shrinkages. Unlike the previous cases we see the uncorrected shrinkage is in very good agreement with the experimental data, except for condition 20 where there is significant overprediction. For this material the

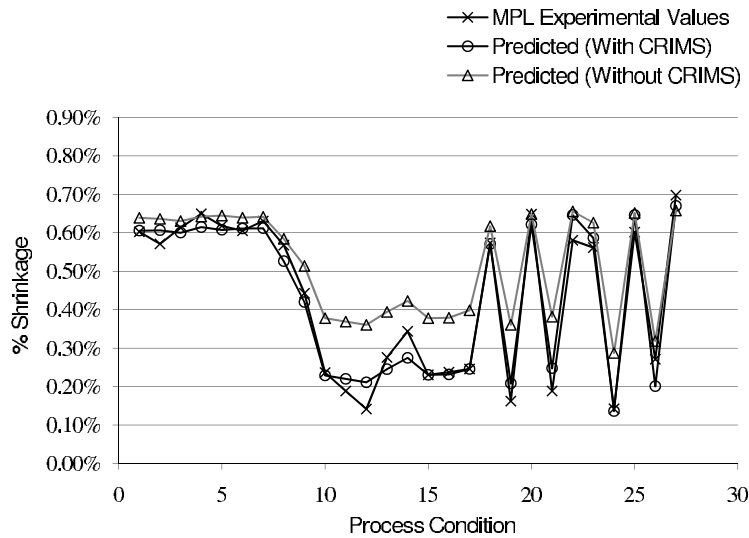


**Figure 4.6:** Parallel shrinkage of an ABS resin.

corrected values are slightly better than uncorrected. Figure 4.13 shows the perpendicular results. Here the uncorrected data underpredicts shrinkage significantly for conditions 1-7 and overpredicts slightly from 10-16. Then a series of alternate underprediction and slight overprediction is seen in conditions 17-23. Once again the corrected results are in very good agreement with the experimental values.

## 4.5 Filled Materials

In our introduction, we mentioned that the CRIMS model can also be applied to filled polymers. Filled polymers, in particular short glass fiber filled thermoplastics, may be analyzed to determine the orientation of the filler and then properties may be determined using micromechanics or some other technique. A review of the former has been given by Liang and Tucker [158]. Since the properties will in general be anisotropic, the predicted stresses given by eqn.(2.26) will not be isotropic. Consequently the correction procedure needs to be modified. Despite this apparent complexity, we can model short fiber reinforced polymers using only three parameters per direction, as for the unfilled case. Space does not allow a detailed treatment here, for the prediction of fiber orientation is a major issue, and itself deserves a thesis. Nevertheless we present below some results on two very different filled systems.

### 4.5.1 Glass Reinforced PA66

The material is a PA66 with 30% by weight of glass fibers. Figure 4.14 shows the parallel shrinkage. Uncorrected predictions dramatically overpredict the shrinkage;

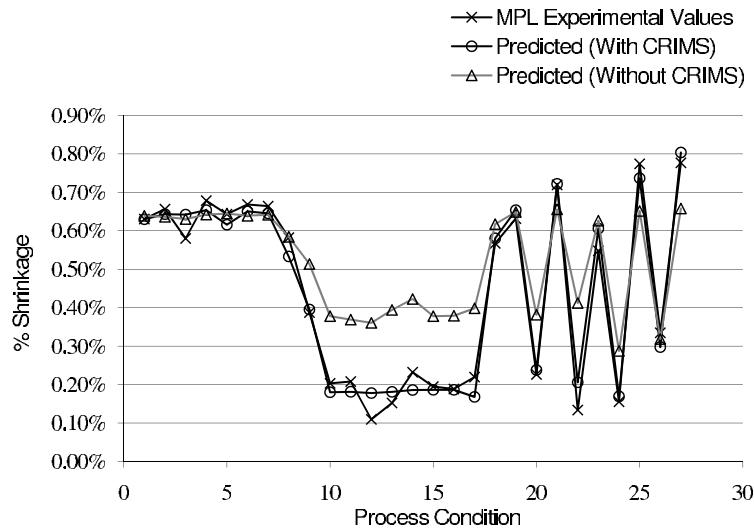


Figure 4.7: Perpendicular shrinkage of an ABS resin.

however, the agreement with trends is quite good. Note also the general lack of sensitivity of the uncorrected, corrected and experimental results to the changed conditions. This is typical of shrinkage in the parallel direction, as the glass reinforcement masks the effect of processing conditions on the matrix. The corrected value is quite good. Figure 4.15 shows the perpendicular results.

Due to the lack of reinforcement in the perpendicular direction, we see a marked effect on the actual shrinkage as conditions are changed. Uncorrected predictions are relatively insensitive to the changes in process conditions, and underpredict or overpredict depending on the condition used. The corrected results show correct magnitude as well as sensitivity to process change.

#### 4.5.2 Talc Filled PBT

Our final material is a PBT reinforced with 35% by weight of talc. Figure 4.16 shows the parallel results. We note a lack of sensitivity in the uncorrected predictions to changes in the process conditions, but generally the trends are well captured. The corrected results restore the sensitivity and show close agreement with the experimental values. Results for the perpendicular direction are shown in Figure 4.17. The shrinkage of the material is surprisingly anisotropic, and the uncorrected results lack sensitivity to process conditions. While this was not captured in the uncorrected analysis, the corrected values are in very good agreement with the experimental results.

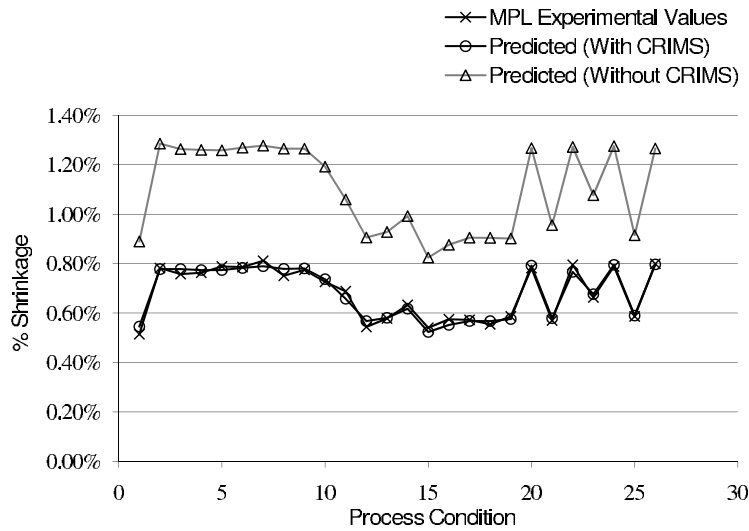


Figure 4.8: Parallel shrinkage of a PC resin.

## 4.6 Conclusion

We have described a method and model for overcoming inaccuracy due to the assumptions commonly used in shrinkage and warpage models. These assumptions stem from the lack of fundamental models for predicting the properties of molded materials. While the pursuit of such models is of great interest scientifically, the state of modeling today is far from ideal. Consequently we believe the use of experimental data to correct limited theoretical models is a useful engineering approach to the problem of shrinkage prediction.

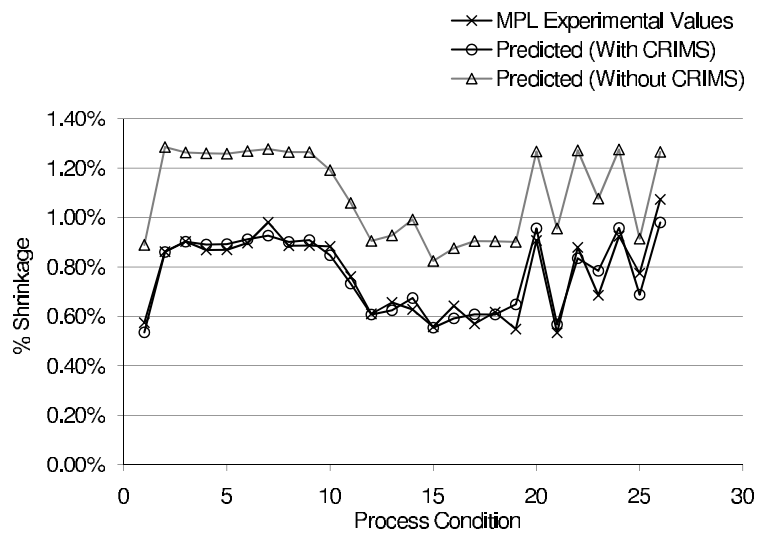


Figure 4.9: Perpendicular shrinkage of a PC resin.

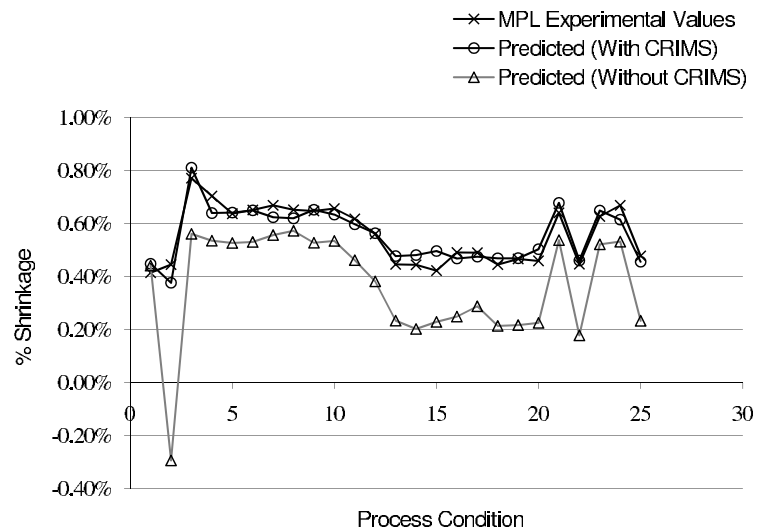


Figure 4.10: Parallel shrinkage of a PC+ABS blend.

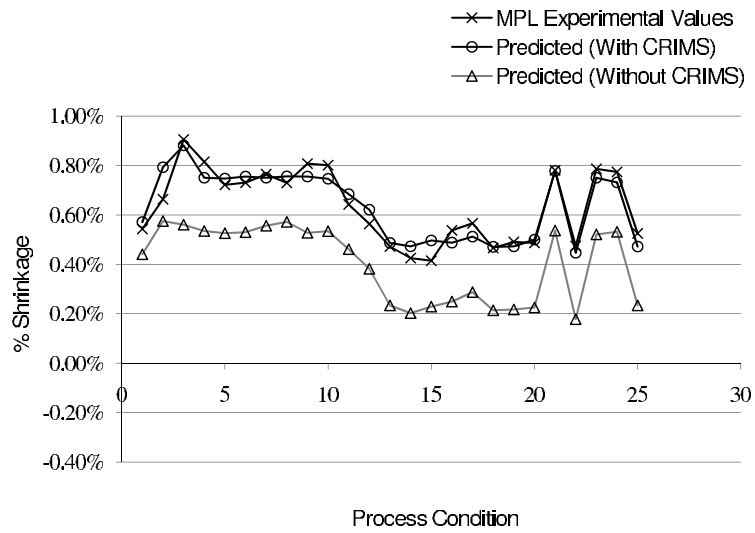


Figure 4.11: Perpendicular shrinkage of a PC+ABS blend.

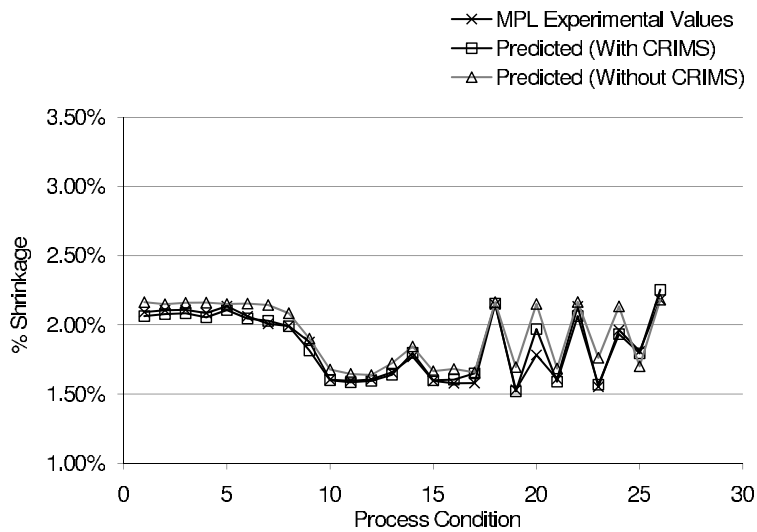


Figure 4.12: Parallel shrinkage of a PBT resin.



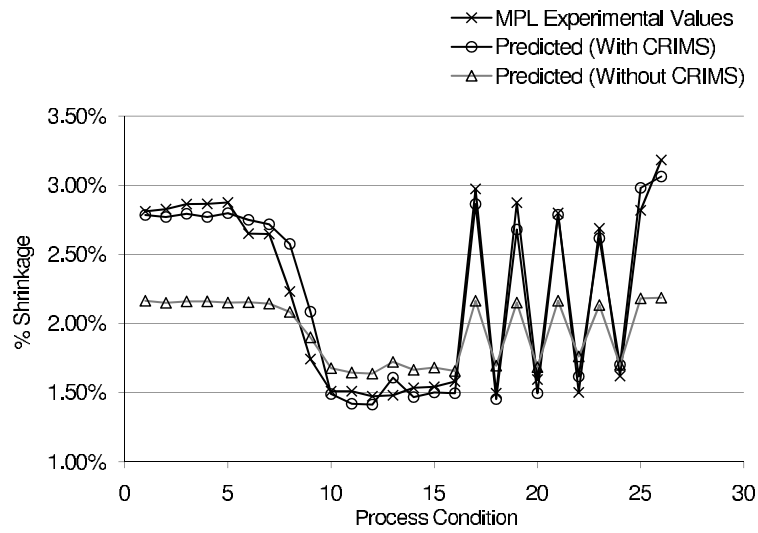


Figure 4.13: Perpendicular shrinkage of a PBT resin.

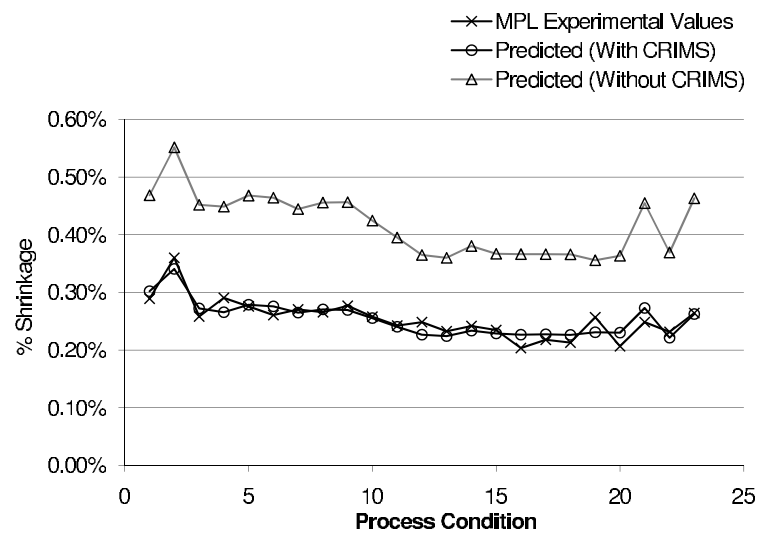
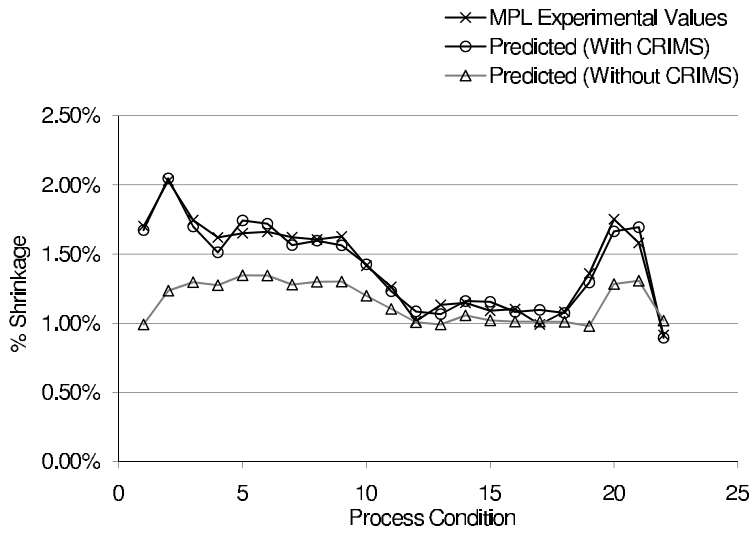
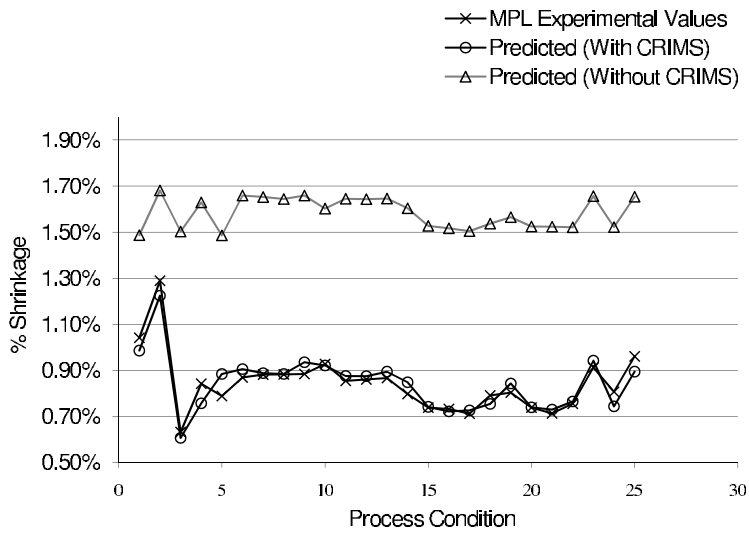


Figure 4.14: Parallel shrinkage of a 30% by weight short glass fiber reinforced PA66.



**Figure 4.15:** Perpendicular shrinkage of a 30% by weight short glass fiber reinforced PA66.



**Figure 4.16:** Parallel shrinkage of a 35% by weight, talc reinforced PBT.

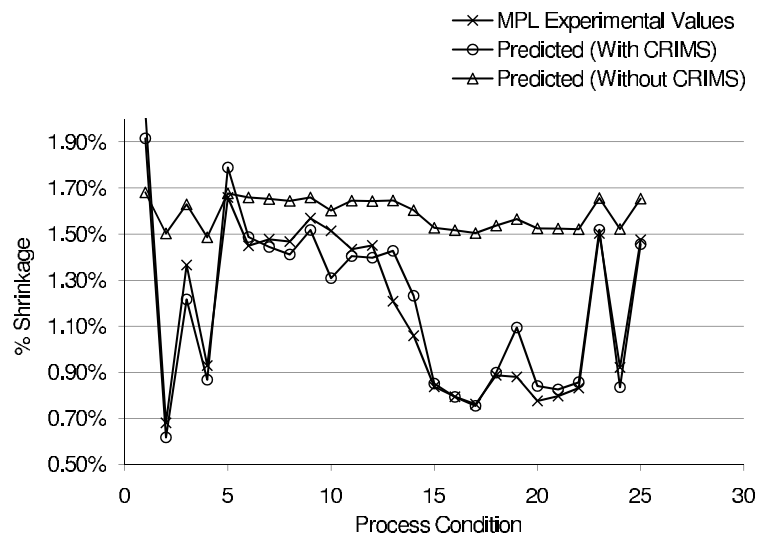


Figure 4.17: Perpendicular shrinkage of a 35% by weight, talc reinforced PBT.

## CHAPTER FIVE

# Improving Simulation Models

---

In this chapter we consider improved modeling of the injection molding process with a view to improving warpage prediction accuracy. Simulating warpage requires calculation of residual stress and requires knowledge of the thermal and mechanical properties of the material. It is the prediction of these properties that we consider here.

All problems discussed in this chapter are scientifically difficult, so much so that the facilities and skills required to address them are not all available within Moldflow. For this reason collaborations with various institutions were employed in these problem areas.

The problem of determining the properties of injection molded material has been in collaboration with the Cooperative Research Centre (CRC) for Polymers. The CRC concept is an initiative of the Australian Government and involves bringing industry and research providers together to tackle problems of scientific and commercial importance. Academic providers in our project are the University of Sydney (R.I. Tanner, X.J. Fan, S. Dai), Monash University (G. Edward, G. Liu, P. Zhu, C. Hadinata), and the Australian Nuclear Science and Technology Organization (Robert Knott). Moldflow staff involved with the work are the author and R. Zheng.

We also owe a great deal to the SCOOP (Shrinkage Crystallization and Orientation Of Polymers) consortium. This is a mixture of industrial and academic partners. Industrial partners are Legrand (France), Solvay Central Research (Belgium) and Moldflow. Academic partners are G. Regnier (ENSAM, Paris), R. Fulchiron and E. Boucher (University Claude Bernard, Lyon) and D. Delaunay (University of Nantes).

For amorphous polymers, properties are influenced by molecular orientation that results from processing [170]. However semi-crystalline materials are more complex. While much work has been done on crystallization of polymers, until recently, most efforts aimed at identifying kinetics in a quiescent state. In polymer processing there are non-isothermal effects as well as significant effects of flow. Polymer proper-

ties are determined by the morphology of the material, which in turn is determined by processing history. Our approach is to first model the injection molding process and predict the morphology of the material. The second stage involves determining properties for a given morphology. Here we discuss progress on the first stage.

## 5.1 Crystallization in Flowing Melts

The development of structure in a flowing melt has been extensively reviewed by Keller and Kolnaar [90]. Of particular importance is the work of the Linz group on the difference between crystallization under quiescent conditions and after a shearing treatment [50].

We begin with an experiment of Koscher and Fulchiron [103] in which a sample of isotactic polypropylene (Solvay Eltex PHV252) was initially melted in a Linkam shearing device, and the subsequent crystallization is observed using polarized light microscopy.

Figure 5.1a) shows the progress of crystallization at various times for quiescent conditions with the material at a temperature of  $140^{\circ}\text{C}$ . We see that the number of nuclei remains constant but the nuclei grow with time and form spherulitic structures.

Consider now the case where the material is sheared at various shear rates for a period of 10s while kept at  $140^{\circ}\text{C}$ . The results [103] for shear rates of  $0.5\text{s}^{-1}$  and  $5\text{s}^{-1}$  are shown in Figures 5.1b) and 5.1c) respectively. Figure 5.1b) shows that the low shear increases nucleation slightly, whereas the stronger shear of  $5\text{s}^{-1}$  has a profound effect on nucleation density. Note also the changed time scale in Figure 5.1c). It appears that the increase in shear rate has a dramatic effect on both the number of nuclei and hence on the rate of crystallization. Similar results were reported for isotactic polypropylene by Eder et al. [50] and Vleeshouwers and Meijer [164].

Finally we consider the case in which the shear rate is constant but the shearing time, and hence the total shear is varied [103] in Figures 5.1d) and 5.1e). For the shearing time of 10s, Figure 5.1d), we note the usual increase in crystallization whereas at the longer time, Figure 5.1e), we see a change in structure with the formation of row nuclei. Similar results were reported for iPP by Issaian et al. [104] and for isotactic poly (1-butene) by Acierno et al. [2]. So, in summary, the shear rate affects the number of nuclei and the rate of crystallization whereas the subsequent morphology development is determined by the shearing time.

It has also been established that the molecular weight (MW) and molecular weight distribution (MWD) of the polymer will affect the crystallization of the polymer after shearing. Using fiber pulling experiments, Jay et al. [85] and Duplay et al. [48] showed that, for a given shear rate, higher molecular weight isotactic polypropylene (iPP) showed faster crystallization. The effect of MWD and MW was also investigated by Vleeshouwers and Meijer [164] using cone and plate rheometry. They concluded an increase in crystallization rate depended on the presence of long

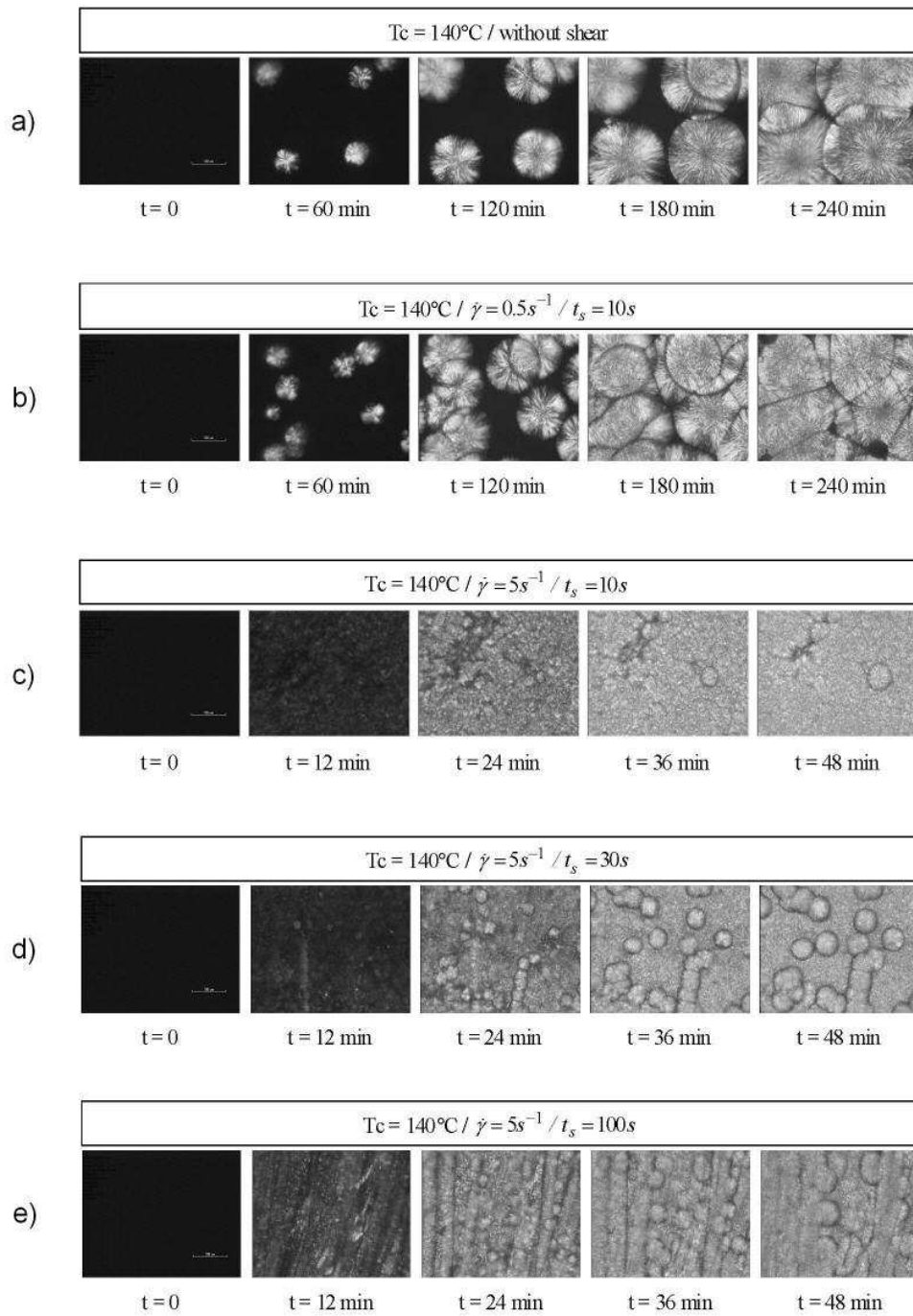


Figure 5.1: Crystallization of iPP for differing shear treatments.

molecules. Seti et al. [142] performed rheo-optical experiments in which an iPP of very high MW and narrow MWD was used to dope an iPP of lower MW. They showed that even at low concentrations, the doping had a significant effect on enhancing shear induced crystallization. They concluded that long chain overlap was a factor in shear induced crystallization.

Although flow-induced crystallization (FIC) has been considered by many investigators, there is a lack of a fundamental theory that explains exactly how FIC occurs and how to link it to the crystallization kinetics of the material. Nevertheless, various approaches have been proposed. Eder and co-workers ([50], [49], [24]), have used shear rate as the means by which nucleation is enhanced. Ziabicki [195], in his work on fiber spinning, introduced an exponential function called the "molecular orientation factor" into a Nakamura equation for the rate of crystallization, and so considered molecular orientation. Doufas et al. ([42], [43], [44], [45]) while interested in melt spinning, used a similar exponential enhancement factor in terms of the trace of the extra stress tensor. There are several variants of this approach. Zheng and Kennedy [181] proposed using the principal stress while Koscher and Fulchiron [103] used the first normal stress difference. Guo et al. [66] introduced flow-induced effects using a molecular deformation factor. This was obtained from a phenomenological equation involving the deformation intensity  $E$ , defined as  $E = \sqrt{2\text{tr}(\mathbf{D} \cdot \mathbf{D})}$  where  $\mathbf{D}$  is the deformation rate tensor. Zuidema et al. [199] replaced the strain rate in Eder and Janeschitz-Kriegl's work with recoverable strain. In an effort to introduce the effect of the high molecular weight tail, Peters et al. [127] used the recoverable strain with the highest relaxation time to drive the flow-induced crystallization. Other approaches that rely on molecular modeling and non-equilibrium thermodynamics have been proposed by Bushman and McHugh [28] and Coppola et al. [35].

## 5.2 A FIC Crystallization Model

Following the work of Kolmogoroff [101] we consider first crystallization under quiescent conditions. Let the rate of growth of the spherulite radius as a function of time be  $G$ . We assume that the spherulite begins growing from an initially small nucleus at time  $s$ . The radius at time  $t$  is then given by

$$\int_s^t G(u) du.$$

The spherulite volume,  $V_s$  at time  $t$  is

$$V_s(t) = \frac{4\pi}{3} \left[ \int_s^t G(u) du \right]^3$$

and this may be generalized to the case of non-spherical growth as follows

$$V_m(t) = g_m \left[ \int_s^t G(u) du \right]^m$$

where  $m$  is a constant and  $g_m$  a constant that depends on  $m$ . We note that this will be used later to introduce morphology prediction into the model. Denoting the rate of creation of nuclei per unit volume at time  $s$  by  $\dot{N}(s)$  the volume of semi-crystalline material at time  $t$  is given by

$$\alpha_f = g_m \int_0^t \dot{N}(s) \left[ \int_s^t G(u) du \right]^m ds. \quad (5.1)$$

This expression is unrealistic, as it assumes no impingement of spherulites, however, following Avrami [8], we can relate this volume to the relative crystallinity  $\alpha$ , as follows

$$\alpha = 1 - \exp(-\alpha_f).$$

Koscher and Fulchiron [103] have observed that the nucleation is strongly affected by shearing and that the growth rate is insensitive to short-term shear treatments. We therefore assume that the growth rate  $G(u)$  depends only on temperature and that it follows the Hoffman-Lauritzen theory [76]. That is

$$G(T) = G_0 \exp \left[ -\frac{U^*}{R_g(T - T_\infty)} \right] \exp \left( -\frac{K_g}{T\Delta T} \right), \quad (5.2)$$

where  $G_0$  and  $K_g$  are constants that can be determined by experiment under quiescent conditions,  $U^*$  is the activation energy of motion,  $R_g$  is the gas constant,  $T_\infty = T_g - 30$  where  $T_g$  is the glass transition temperature and  $\Delta T = T_m^0 - T$  in  $^\circ\text{C}$  is the degree of supercooling.  $T_m^0$  is the equilibrium melting temperature, which is assumed to depend on pressure only. The pressure dependence is represented by a polynomial function [63] so that

$$T_m^0 = a_{p0} + a_{p1}P + a_{p2}P^2 \quad (5.3)$$

where  $a_{p_i}, i \in \{0, 1, 2\}$  are constants.

The number of active nuclei  $N$ , is expressed as the sum of the number of growing nuclei in the quiescent state  $N_q$  and the number of growing nuclei created by the flow  $N_f$ . That is,

$$N = N_q + N_f. \quad (5.4)$$

The number of nuclei in the quiescent state has been investigated by several authors



( [4], [147], [103]) and has been found to be a linear function of the supercooling temperature  $\Delta T$  described by

$$\ln N_q = a_{q_0} + a_{q_1} \Delta T \quad (5.5)$$

where  $a_{q_0}$  and  $a_{q_1}$  are constants.

The number of flow-induced nuclei  $N_f$  is given by the differential equation [49]

$$\dot{N}_f + \frac{1}{\lambda_N} N_f = f \quad (5.6)$$

where  $\lambda_N$  is a relaxation time which, according to Eder and Janeschitz-Kriegl [49], has a large value and varies with temperature and  $f$  is a function that takes into account the effect of flow. Eder et al. [50], [49], and Braun et al. [24] have used  $f = (\dot{\gamma}/\dot{\gamma}_n)^2 g_n$  where  $\dot{\gamma}$  is the shear rate,  $\dot{\gamma}_n$  is the critical shear rate of activation and  $g_n$  is a factor with units  $[m^{-3}s^{-1}]$ . In such a model, at the cessation of flow the shear rate is zero and there is no contribution of flow to crystallization. This does not agree with the findings of Vleeshouvers and Meijer [164], who noted that the effect of flow on crystallization did not disappear when the shear rate was zero. In an effort to introduce a time dependent effect and so counter this problem, Zuidema et al. [199] replaced the  $(\dot{\gamma}/\dot{\gamma}_n)^2$  term by a function of the second invariant of the deviatoric elastic Finger tensor. All these approaches purport flow as the important driver of flow-induced crystallization. However, from the discussion above it is clear that the polymer itself (by way of MWD and MW) needs to be considered also. In an attempt to introduce this aspect of the problem, Peters et al. [127] have replaced the  $(\dot{\gamma}/\dot{\gamma}_n)^2$  term by a function of the second invariant of the deviatoric elastic Finger tensor associated with the highest relaxation time. In this way, the high molecular tail is given prominence in the flow-induced affects.

Here a slightly different view is proposed. Despite the lack of general agreement on the exact physics of flow-induced crystallization, it does appear that shear somehow induces a predilection for crystallization to occur. It seems then that a reasonable theory could be based on the free energy of the melt. Moreover, noting that the right hand side of equation (5.6)  $f$  is really the rate of nucleation at time  $t = 0$ , we start with Ziabicki's expression [196] for the nucleation rate under quiescent conditions and then, following a similar approach to Coppola et al. [35], add the flow-induced free energy change to the expression. Therefore  $f$  becomes a function of temperature, the change in free energy associated with quiescent conditions  $\Delta F_q$ , and the change in free energy associated with flow  $\Delta F_f$ .

We write

$$f(T, \Delta F_f) = C_0 k_B T \exp\left(-\frac{U^*}{R_g(T - T_g)}\right) \times \quad (5.7)$$

$$\left\{ (\Delta F_q + \Delta F_f) \exp\left[-\frac{K_g}{T[(1 + \vartheta \Delta F_f) T_m^0 - T]}\right] - \Delta F_q \exp\left[-\frac{K_g}{T \Delta T}\right] \right\}$$

where  $C_0$  is a constant that can be determined from experiment,  $\Delta F_q = \Delta H_0 \Delta T / T_m^0$  where  $\Delta H_0$  is the latent heat of crystallization and the factor  $\vartheta = T_m^0 / (\Delta H_0 T)$ .

Having decided on our crystallization model, we now turn to other aspects of the model and the determination of free energy change in the flowing melt.

### 5.2.1 Rheological Aspects

In the crystallizing system, the stress should have contributions from both the amorphous and the semi-crystalline phases, and the amorphous-contributed stress should vanish in the limit  $\alpha \rightarrow 1$ . We assume that the effects of the two phases on the extra stresses are given by the additive rule, i.e.,

$$\boldsymbol{\tau} = \boldsymbol{\tau}_a + \boldsymbol{\tau}_c \quad (5.8)$$

where  $\boldsymbol{\tau}_a$  and  $\boldsymbol{\tau}_c$  are the contributions of the amorphous phase and the semi-crystalline phase, respectively. This model conceives an intimate mixture on the molecular scale of the two component's phases at each point. Tanner [153] pointed out that this concept is at odds with the photographs of Boutahar et al. [23]. Figures 5.1a) and 5.1b) illustrate Tanner's point. There appear to be macroscopic crystallites within an amorphous matrix and so eqn.(5.8) does not apply. We accept this criticism but point out that the relation

$$\boldsymbol{\tau} = (1 - \alpha)\boldsymbol{\tau}_a + \alpha\boldsymbol{\tau}_c \quad (5.9)$$

is correct for  $\alpha = 0$  and  $\alpha = 1$ ; the problem is the region where  $\alpha \in (0, 1)$ . In injection molding, where solidification is rapid, we propose that this problem is not of concern and the prediction of properties is relevant only at the extremes  $\alpha = 0$  and  $\alpha = 1$ .

Calculation of the stresses  $\boldsymbol{\tau}_a$  and  $\boldsymbol{\tau}_c$  requires constitutive equations. Recent progress in this area suggests using the latest model for the amorphous phase. For example, the POM-POM model proposed by McLeish and Larson [115], or the extended POM-POM model ([163], [127]). However, our objective is a commercially realizable model. Computational speed is important. In fact, it is doubtful that any given constitutive model is going to be ideal. The crystallization process is so complex that at best we can capture the basic physics in the foreseeable future. While this should

yield qualitative predictions, some appeal to empirical relationships, or model calibration as undertaken in Chapter 4 for shrinkage, is likely in the near term. Consequently we make use of the extensive literature on constitutive equations derived from micromechanical models, ([14], [81], [151]). We choose to use dumbbell models in this work because of their computational simplicity. The amorphous phase will be described by FENE-P dumbbells (i.e. the finite extensible non-linear elastic model with a Peterlin closure approximation), while the semi-crystalline phase is modeled as rigid dumbbells. Despite its simplicity, the FENE dumbbell is still in the rheological literature [15].

## 5.2.2 Amorphous Phase

Booij [19] has shown that the flow-induced change of free energy for a system of elastic dumbbells is given by

$$\begin{aligned}\Delta F_f &= n_0 k_B T \int \psi \left( \ln \frac{\psi}{\psi_0} \right) d\mathbf{Q} \\ &= n_0 k_B T \langle \ln \frac{\psi}{\psi_0} \rangle.\end{aligned}\quad (5.10)$$

where  $\psi$  is the distribution function for the system,  $\psi_0$  is the equilibrium distribution and  $\mathbf{Q}$  is the bead-to-bead position vector. The distribution function satisfies the equation of continuity in the configuration space. That is

$$\frac{\partial \psi}{\partial t} + \frac{\partial}{\partial \dot{\mathbf{Q}}} \cdot (\dot{\mathbf{Q}} \psi) = 0 \quad (5.11)$$

where  $\dot{\mathbf{Q}}$  is determined by a force balance on the beads (see p.60 of Bird et al. [14]).

The stress tensor for the FENE elastic dumbbell is given by (see p.88 of Bird et al. [14])

$$\boldsymbol{\tau}_a = nH \left\langle \frac{\mathbf{Q}\mathbf{Q}}{1 - (Q^2/Q_0^2)} \right\rangle - nk_B T \mathbf{I} \quad (5.12)$$

where  $H$  is a spring constant that is independent of  $\mathbf{Q}$ , and  $Q_0$  is the maximum extension of the beads. In general it is not possible to solve eqn.(5.11) analytically and so evaluation of eqn.(5.12) is difficult. Peterlin [126] suggested an approximation (called the FENE-P approximation) to eqn.(5.12) in which the configuration-space average of the ratio is replaced by the ratio of the configuration space averages to give

$$\boldsymbol{\tau}_a = nH \frac{\langle \mathbf{Q}\mathbf{Q} \rangle}{1 - \langle (Q^2/Q_0^2) \rangle} - nk_B T \mathbf{I} \quad (5.13)$$

For the FENE-P model the distribution function satisfies the following diffusion

equation [172]:

$$\frac{\partial \psi}{\partial t} = - \left\{ \nabla \mathbf{v} - \frac{2H}{\zeta_a} f(\langle Q^2 \rangle) \mathbf{I} \right\} : \frac{\partial}{\partial \mathbf{Q}} \mathbf{Q} \psi + \left\{ \frac{2k_B T}{\zeta_a} \mathbf{I} \right\} : \frac{\partial}{\partial \mathbf{Q}} \frac{\partial}{\partial \mathbf{Q}} \psi \quad (5.14)$$

where

$$f(\langle Q^2 \rangle) = \frac{H}{1 - \langle (Q/Q_0)^2 \rangle}, \quad (5.15)$$

and  $\zeta_a$  is a friction constant. According to Wedgewood and Bird [172], the diffusion equation admits the solution:

$$\psi(\mathbf{Q}, t) = \left[ \left( \frac{2\pi k_B T}{H} \right)^3 \det \mathbf{c} \right]^{-1/2} \exp \left\{ -\frac{H}{2k_B T} (\mathbf{c}^{-1} : \mathbf{Q}\mathbf{Q}) \right\} \quad (5.16)$$

where the tensor  $\mathbf{c}$  satisfies the differential equation

$$\lambda_a \left( \frac{D\mathbf{c}}{Dt} - [(\nabla \mathbf{v})^T \cdot \mathbf{c} + \mathbf{c} \cdot \nabla \mathbf{v}] \right) + \left( 1 - \frac{\text{tr}(\mathbf{c})}{b} \right)^{-1} \mathbf{c} = \mathbf{I}. \quad (5.17)$$

and  $\lambda_a = \zeta_a/4H$  is the relaxation time of the fluid.

The fluid contribution to the stress  $\boldsymbol{\tau}_a$  is of the form (see p.69 of Bird et al. [14])

$$\boldsymbol{\tau}_a = n \langle \mathbf{Q}\mathbf{F}^{(c)} \rangle - nk_B T \mathbf{I} \quad (5.18)$$

where  $\mathbf{F}^{(c)} = f(\langle Q^2 \rangle) \mathbf{Q}$  is the FENE-P connector force. Equating eqn.(5.13) and eqn.(5.18) we obtain:

$$\langle \mathbf{Q}\mathbf{F}^{(c)} \rangle = f(\langle Q^2 \rangle) \langle \mathbf{Q}\mathbf{Q} \rangle. \quad (5.19)$$

Since the Peterlin approximation leads to an explicit distribution function, we can use eqn.(5.16) to carry out the integration associated with the configuration space average. That is,

$$\begin{aligned} \langle \mathbf{Q}\mathbf{Q} \rangle &= \int \mathbf{Q}\mathbf{Q} \psi(\mathbf{Q}, t) d\mathbf{Q} \\ &= \int \mathbf{Q}\mathbf{Q} \left[ \left( \frac{2\pi k_B T}{H} \right)^3 \det \mathbf{c} \right]^{-1/2} \exp \left\{ -\frac{H}{2k_B T} (\mathbf{c}^{-1} : \mathbf{Q}\mathbf{Q}) \right\} d\mathbf{Q} \end{aligned}$$

As  $\det \mathbf{c}$  is a scalar, it may be taken outside the integral. Setting  $\boldsymbol{\beta} = (H/2k_B T)\mathbf{c}^{-1}$

we have  $\det \mathbf{c} = (H/2k_B T)^3 \det \boldsymbol{\beta}^{-1}$  and substituting in the equation above we get:

$$\begin{aligned}
 \langle \mathbf{Q}\mathbf{Q} \rangle &= \left( \pi^3 \det \boldsymbol{\beta}^{-1} \right)^{-1/2} \int \mathbf{Q}\mathbf{Q} \exp(-\boldsymbol{\beta} : \mathbf{Q}\mathbf{Q}) d\mathbf{Q} \\
 &= \frac{1}{\pi^{3/2}} \frac{1}{\left( \det \boldsymbol{\beta}^{-1} \right)^{1/2}} \frac{\pi^{3/2} \boldsymbol{\beta}^{-1}}{2 \left( \det \boldsymbol{\beta} \right)^{1/2}} \\
 &= \frac{\boldsymbol{\beta}^{-1}}{2} \\
 &= \frac{k_B T}{H} \mathbf{c}
 \end{aligned} \tag{5.20}$$

where, in evaluating the integral on the RHS, we have used formula E.3-5 from Appendix E of Bird et al. [14].

Consider now the force

$$f \left( \langle Q^2 \rangle \right) = \frac{H}{1 - \langle (Q/Q_0)^2 \rangle}. \tag{5.21}$$

From Wedgwood and Bird [172] we see that

$$\begin{aligned}
 \langle (Q/Q_0)^2 \rangle &= (1/Q_0)^2 \text{tr} \langle \mathbf{Q}\mathbf{Q} \rangle \\
 &= \frac{k_B T}{H Q_0^2} \text{tr} \mathbf{c} \quad \text{using eqn.(5.20)} \\
 &= \frac{\text{tr} \mathbf{c}}{b}
 \end{aligned} \tag{5.22}$$

where  $b = Q_0^2 H / (k_B T)$  and represents a nonlinear spring constant. Hence

$$\begin{aligned}
 f \left( \langle Q^2 \rangle \right) &= \frac{H}{1 - \langle (Q/Q_0)^2 \rangle} \\
 &= \frac{H}{1 - (\text{tr} \mathbf{c}) / b}
 \end{aligned} \tag{5.23}$$

and from eqn.(5.19) we have

$$\langle \mathbf{Q}\mathbf{F}^{(c)} \rangle = k_B T \left[ 1 - \frac{(\text{tr} \mathbf{c})}{b} \right]^{-1} \mathbf{c}. \tag{5.24}$$

Returning to eqn.(5.18) we substitute eqn.(5.24) to obtain:

$$\boldsymbol{\tau}_a = n_0 k_B T \left( \left[ 1 - \frac{(\text{tr} \mathbf{c})}{b} \right]^{-1} \mathbf{c} - \mathbf{I} \right). \tag{5.25}$$

The model constants  $\lambda_a = \zeta_a/4H$  and  $b$  do have a physical interpretation, but in reality  $\zeta_a$ ,  $H$  and  $Q_0^2$  are difficult to determine. We obtain  $\lambda_a$  from rheological data. Fan [51] has also determined the non linear parameter  $b$  from rheological data but here we allow it to be an adjustable parameter. It affects the growth and magnitude of  $\tau_c$ . Although the parameter does not explicitly appear in the equation for  $\tau_c$ . It affects  $\tau_c$  through its influence on the free energy and hence on crystallinity. Zheng and Kennedy [186] showed the increase in a shear component of  $\tau_c$  for  $b = 5, 50$  and  $1000$  in the start up of a shear flow. In all cases, the qualitative trends of the transient response remained the same for different values of  $b$ , however, the stresses increased earlier with increasing  $b$ . For all calculations presented in this thesis we set  $b = 5$ .

In order to deal with nonisothermal conditions, we assume the amorphous phase is thermorheologically simple and use time-temperature superposition to account for the temperature dependence of  $\lambda_a$ . We write

$$\lambda_a(T) = a_T(T)\lambda_a(T_0), \quad (5.26)$$

where  $a_T(T)$  is a shift factor expressed in Arrhenius form as

$$\ln a_T(T) = \frac{E_a}{R_g} \left( \frac{1}{T} - \frac{1}{T_0} \right) \quad (5.27)$$

and  $T_0$  is a reference temperature. The constant  $E_a/R_g$  is determined from experimental data.

To complete this section we now consider the free energy due to flow. Substituting eqn.(5.16) into Booi's expression eqn.(5.10) and carrying out the integration gives:

$$\Delta F_f = \frac{1}{2}n_0k_B T \left\{ b \ln \left[ \frac{1 - \text{tr}(\mathbf{c}_0)/b}{1 - \text{tr}(\mathbf{c})/b} \right] - \ln \left[ \frac{\det(\mathbf{c})}{\det(\mathbf{c}_0)} \right] \right\} \quad (5.28)$$

where  $\Delta F_f$  is the flow-induced change in free energy in units  $\text{J}/\text{m}^3$ ,  $b = HQ_0^2/k_B T$  is the nonlinear spring constant and  $\mathbf{c}_0 = [b/(b+3)\mathbf{I}]$ .

### 5.2.3 The Semi-Crystalline Phase

The semi-crystalline phase is described by a rigid dumbbell model in which the polymer chain is represented by two beads spaced a distance  $R$  apart and connected by a rigid rod. When subjected to a flow field the rigid dumbbell may tumble and orient itself. Interaction of the dumbbell with the fluid is localized to the two beads, each of which has a frictional factor  $\zeta_c$  and a negligible mass. While the dumbbell model cannot represent the morphological details of the semi-crystalline phase its orientation distribution can be used to determine the degree of anisotropy in the semi-crystalline phase. To represent the dumbbell we describe its orientation with a single unit vector  $\mathbf{u}$  directed along its length.

The evolution of  $\mathbf{u}$  is given by [14]

$$\dot{\mathbf{u}} = \mathbf{L}_e \cdot \mathbf{u} - \mathbf{L}_e : \mathbf{u}\mathbf{u}\mathbf{u} + \frac{1}{\zeta_c R} (\mathbf{I} - \mathbf{u}\mathbf{u}) \cdot \mathbf{F}^{(b)} \quad (5.29)$$

where  $\mathbf{L}_e$  is an effective gradient operator defined as  $\mathbf{L}_e = \mathbf{L} - \xi \mathbf{D}$  with  $\mathbf{L} = (\nabla \mathbf{v})^T$  the velocity gradient,  $\xi$  is a parameter ranging from 0 to 2 and represents "non affine" motion,  $\mathbf{F}^{(b)}$  is a random force representing Brownian effects and  $\zeta_c$  is a friction term arising from hydrodynamic interaction. Increasing  $\xi$  reduces the strength of the strain rate relative to the vorticity. We set  $\xi = 2$  for our calculations.

Equation (5.29) may be substituted in eqn.(5.11), replacing  $\mathbf{u}$  and  $\dot{\mathbf{u}}$  by  $\mathbf{Q}$  and  $\dot{\mathbf{Q}}$  respectively, to give:

$$\frac{\partial \psi}{\partial t} + \frac{\partial}{\partial \mathbf{u}} (\dot{\mathbf{u}} \psi) = 0. \quad (5.30)$$

Equation 5.30 is a Fokker-Planck type equation that may be solved for the configurational distribution function  $\psi(\mathbf{u}, t)$ . We then define a second-order orientation tensor

$$\langle \mathbf{u}\mathbf{u} \rangle = \int \mathbf{u}\mathbf{u} \psi(\mathbf{u}, t) d\mathbf{u}.$$

An evolution equation for  $\langle \mathbf{u}\mathbf{u} \rangle$  may be written (see pg. 117 Bird et al. [14]).

$$\lambda_c \left( \frac{\Delta \langle \mathbf{u}\mathbf{u} \rangle}{\Delta t} + 2\mathbf{L}_e : \langle \mathbf{u}\mathbf{u}\mathbf{u}\mathbf{u} \rangle \right) + \langle \mathbf{u}\mathbf{u} \rangle = \frac{1}{3} \mathbf{I} \quad (5.31)$$

where  $\Delta/\Delta t$  denotes the upper-convected derivative defined with the effective velocity gradient tensor  $\mathbf{L}_e$  and  $\lambda_c$  is the time constant of the rigid dumbbell given by  $\lambda_c = \zeta R^2 / 12k_b T$ . In this work we disregard that definition of  $\lambda_c$  and allow it to depend on the relative crystallinity in the following empirical way:

$$\frac{\lambda_c}{\lambda_a} = \frac{(\alpha/A)^{\beta_1}}{(1 - \alpha/A)^{\beta-1}}, \quad \alpha < A \quad (5.32)$$

where  $A, \beta_1$  and  $\beta$  are parameters to be determined. This choice is explained in Zheng and Kennedy [182] and we note that as  $\alpha \rightarrow A$ ,  $\lambda_c \rightarrow \infty$ .

To calculate the second-order tensor  $\langle \mathbf{u}\mathbf{u} \rangle$  from eqn.(5.31) it is necessary to use a closure approximation for the term  $\langle \mathbf{u}\mathbf{u}\mathbf{u}\mathbf{u} \rangle$ . Many choices are available and the topic continues to be discussed in the literature (see [58], [34]). We choose the hybrid approximation proposed by Advani and Tucker [3], which is exact for the cases of random orientation and full alignment where  $\langle \mathbf{u}\mathbf{u} \rangle_{11} = \langle \mathbf{u}\mathbf{u} \rangle_{22} = \langle \mathbf{u}\mathbf{u} \rangle_{33} = 1/3$  and  $\langle \mathbf{u}\mathbf{u} \rangle_{11} = 1$  respectively.

The contribution of the semi-crystalline phase to the extra stress is given by (see page

118 Bird et al. [14]):

$$\boldsymbol{\tau}_c = \mu(\alpha) [3 \langle \mathbf{uu} \rangle - \mathbf{I} + 6\lambda_c \mathbf{D} : \langle \mathbf{uuuu} \rangle], \text{ with } \mu(\alpha) = \frac{\eta_a/\lambda_a}{1 - \alpha/A}. \quad (5.33)$$

The first term on the right hand side is an entropic term that has a relaxation time of the order  $\lambda_c$ , and the third term is the viscous term. In a usual rigid dumbbell system with a constant relaxation time, the viscous stress is instantaneous in the strain rate; the moment the flow stops, the stress disappears instantly. However, in a semi-crystalline system,  $\lambda_c \rightarrow \infty$  as  $\alpha \rightarrow A$ . Thus, no matter how small the rate of deformation tensor is, the viscous stress increases toward infinity, indicating a "stiff" region in which melt flow is not possible. This determines a "frozen" region in which the stress is locked-in.

Note the particular form of the shear modulus  $\mu(\alpha)$  in eqn.(5.33). In Doufas et al. [44], the proposed model has a constant shear modulus, regardless of the level of crystallinity. Tanner [153] pointed out that, in the case of small amplitude oscillatory shear, their model predicts a constant storage modulus  $G'$  in the high frequency limit, and so fails to describe the experimental data of Boutahar et al. [23]. This problem is overcome here by allowing the shear modulus to depend on the crystallization as in eqn.(5.33).

Equations (5.30) and (5.31) may be solved to determine the orientation tensor  $\langle \mathbf{uu} \rangle$ . We can then form the product  $\langle \mathbf{uu} \rangle : \langle \mathbf{uu} \rangle$ , which ranges in value from 1/3 to 1 corresponding to spherulitic and linear structures, respectively. In order to link the orientation of the crystalline material to the crystallization kinetics we allow the value of  $m$  in eqn.(5.1) to be a function of this product as follows:

$$m = 4 - 3 \langle \mathbf{uu} \rangle : \langle \mathbf{uu} \rangle. \quad (5.34)$$

This idea was introduced by Zheng and Kennedy [181], and couples the kinetics and morphology of the semi-crystalline material. For spherulitic structures  $m = 3$ , while for linear oriented structures  $m < 3$ . One difficulty associated with this approach is choosing the value of  $g_m$  to be used in eqn.(5.1) for non-integer values of  $m$ . In this work we simply set  $g_m = 4\pi/3, \forall m$ .

## 5.3 Viscosity Modeling

Figures 5.1a-c) suggest that the crystallizing melt be treated as a suspension of spheres in an amorphous liquid medium. In our approach we keep the physical properties of the amorphous phase independent of the crystallinity, but allow the properties of the suspension to change as crystallinity increases. Metzner [117] investigated suspensions of various shaped particles in Newtonian fluid and found



the viscosity function was well represented by

$$\frac{\eta}{\eta_a} = \left(1 - \frac{\phi}{A}\right)^{-2}$$

where  $\eta$  is the suspension viscosity,  $\eta_a$  is the solute viscosity,  $\phi$  is the volume fraction and  $A$  is an empirical parameter that varies with particle shape. According to Tanner [152], for smooth spheres  $A \sim 0.68$ , while for rough compact crystals  $A \sim 0.44$ . For a crystallizing system the spherulites will in fact be mixtures of amorphous and crystalline material. Moreover they are poorly represented by smooth spheres. Identifying  $\phi$  with  $\alpha$  we take the viscosity function to be

$$\frac{\eta}{\eta_a} = 1 + \frac{(\alpha/A)^{\beta_1}}{(1 - \alpha/A)^\beta}, \quad \alpha < A \quad (5.35)$$

where  $\eta$  is the viscosity of the suspension,  $\eta_a$  is the viscosity of the amorphous phase,  $A = 0.44$ , and  $\beta$  and  $\beta_1$  are empirical parameters. Boutahar et al. [23] consider the relationship between  $\phi$  and  $\alpha$  in more detail for a polypropylene but here we use a direct correspondence. The viscosity equation makes sense only if  $\alpha < A$ ; however, it is reasonable to use the relative crystallinity  $\alpha$ , despite the fact it can reach the value 1. Here we use the relative crystallinity instead of the absolute value since in our suspension-like model we are dealing with microstructures at the spherulite level, not at the lamellae level. That is, the suspending "crystals" are actually complex aggregates of both the crystalline phase and the amorphous phase rather than purely crystalline structures and the suspension will "jam" when  $\alpha = A$ .

The applicability of a suspension model for the viscosity of different classes of polymers has not been considered in the literature. Nevertheless the concept of a suspension has been discussed by Khanna [99] in the context of the effect of nucleating agents on polyamide-6. Boutahar et al. [22] also discusses the use of a suspension-type model for polypropylene. However Boutahar et al. [23] investigated polyolefins - namely polypropylene and polyethylene - and found that, although both materials form spherulites when crystallizing, the suspension model while appropriate for PP, was not applicable to PE which behaved more like a gel. We do not concern ourselves with this issue further but note that it is an area to be investigated in the future.

## 5.4 Crystallization Model Performance

A commercial polymer supplied by Solvay (PHV252) was used for this study. The material is an isotactic polypropylene homopolymer with tacticity 0.96,  $M_w=181\text{k/mol}$  and  $M_w/M_n=7.3$ .

## The Effect of Shear

In this section we focus on flow-induced nucleation enhancement and assume three-dimensional spherulitic growth. We consider different shear rates, shearing times and crystallization temperatures for the Solvay iPP PHV252. The FENE-P nonlinear spring parameter  $b$  is set to 5 in all cases and, to allow comparison with experimental results, the pressure is set to zero.

Figure 5.2 shows the predicted effect of shear rate on crystallization. Increasing shear rate has a marked effect on the rate of crystallization.

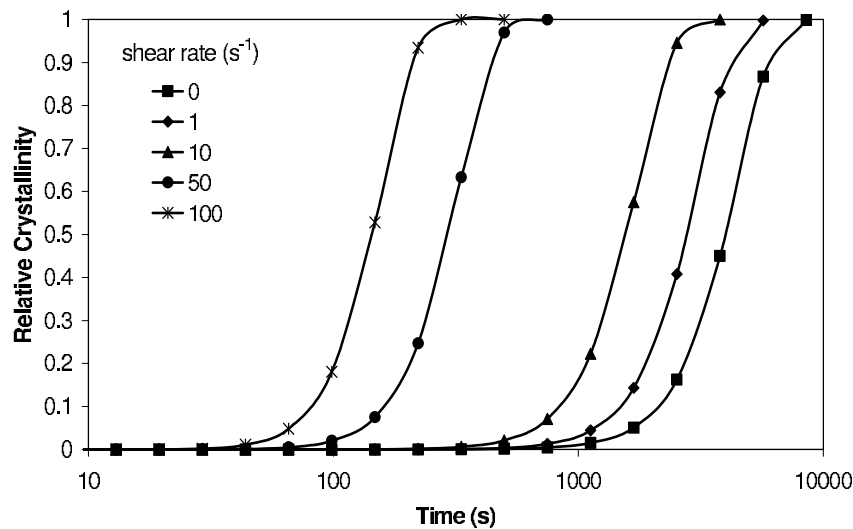


**Figure 5.2:** Relative crystallinity as a function of time at 140°C for different shear rates and a constant shearing time of 10 s.

The effect of shearing time on crystallization is shown in Figure 5.3. In the calculation a constant shear rate of  $50 \text{ s}^{-1}$  is applied for shear time  $t_s$  equal to 5s, 10s and 50s at 140°C. It is seen that crystallization is enhanced as the shearing time increases although the rate of crystallization is not as sensitive to time as to shear rate.

Figures 5.2 and 5.3 imply that the rate of crystallization increases with the applied total shear. In Figure 5.4 we show the results at combinations of shear rates and shearing time for which the total shear is a constant 500. It can be noticed that high shear rates with short shearing times are most effective in enhancing crystallization. This is in agreement with experimental observations reported by Vleeshouwers and Meijer [164] on a different iPP.

We also calculate the number of activated nuclei per unit volume  $N$  (scaled by  $N_0$ ) as a function of time for different combinations of shear rates and shearing times, at 140°C. Results are given in Figure 5.5 and several features are noticeable.

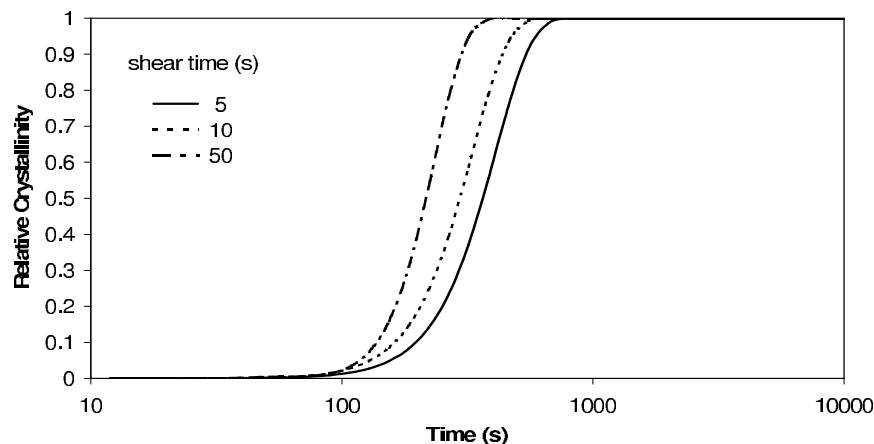


**Figure 5.3:** Relative crystallinity as a function of time at 140°C for different shearing times at constant shear rate of  $50 \text{ s}^{-1}$

First, the number of nuclei activated by the shear is significantly enhanced as the shear rate increases. Secondly, for all cases, after the cessation of flow the influence of the shear treatment remains for a long time before it starts to decay. The time for the decay to start depends on the relaxation time  $\lambda_N$ , which is set to  $10^6$  in the calculation. Thirdly, the number of nuclei also increases with increasing shearing time. Again, we can compare the influence of shear rate and shear time for the same total shear. For example, we can compare  $\dot{\gamma} = 10 \text{ s}^{-1}$ ,  $t_s = 50 \text{ s}$  with  $\dot{\gamma} = 50 \text{ s}^{-1}$ ,  $t_s = 10 \text{ s}$  (both combinations give  $\gamma = 500$ ), or  $\dot{\gamma} = 10 \text{ s}^{-1}$ ,  $t_s = 100 \text{ s}$  with  $\dot{\gamma} = 100 \text{ s}^{-1}$ ,  $t_s = 10 \text{ s}$  (both combinations give  $\gamma = 1000$ ), or  $\dot{\gamma} = 50 \text{ s}^{-1}$ ,  $t_s = 100 \text{ s}$  with  $\dot{\gamma} = 100 \text{ s}^{-1}$ ,  $t_s = 50 \text{ s}$  (both combinations give  $\gamma = 5000$ ). We again see that high shear rates with short shearing times are more effective in enhancing nucleation.

Of course, the performance of the model under these conditions is determined by the relaxation time value  $\lambda_N$ . The results of varying  $\lambda_N$  are reported in Zheng and Kennedy [186] and will not be discussed further.

Thus far, the model can be seen to capture some important qualitative aspects reported in the literature. To further examine its performance we plot in Figure 5.6 the half-crystallization time versus shear rate, for a shearing time of 10 s and temperatures of 130°C, 135°C and 140°C. The half-crystallization time is defined as the time required for the relative crystallinity to reach a value of 0.5. It is seen that the influence of shear rate on the half-crystallization time is low in the low shear rate range. Above a critical shear rate, (about  $1 \text{ s}^{-1}$  in this case), the half-crystallization time reduces dramatically. Experimental data of Koscher and Fulchiron [103] are plotted in the same figure for comparison, and reasonable agreement can be observed. The behavior of the model predictions is also in qualitative agreement with the predictions of Doufas et al. [42].

The influence of the shearing time on the half-crystallization time at a shear rate of

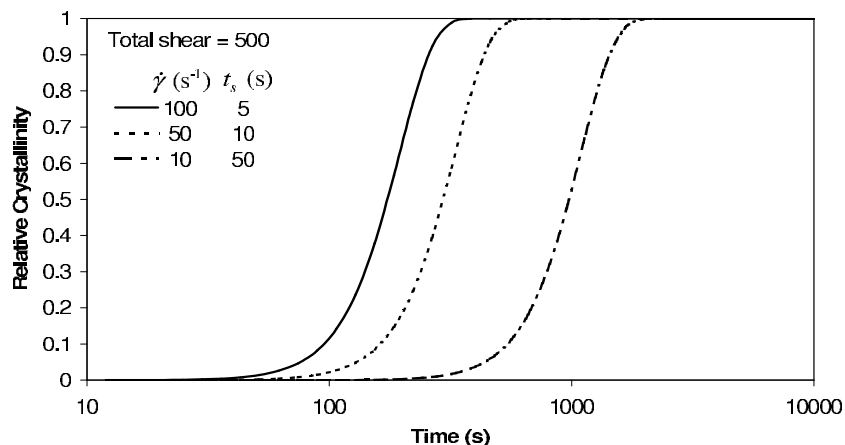


**Figure 5.4:** Relative crystallinity of an iPP as a function of time at  $140^{\circ}\text{C}$ , for combinations of different shear rates and shearing times, that produce the same total shear of 500.

$5\text{s}^{-1}$  and two crystallization temperatures is displayed in Figure 5.7. It shows that the effect of shearing time is more efficient in the range of small shearing time; that is, the half-crystallization time becomes less sensitive to the shearing time as the shearing time increases. This trend is confirmed by the experimental data of Koscher and Fulchiron [103].

Figure 5.8 displays the growth of spherulites after a 10s shear treatment for different shear rates at a temperature of  $140^{\circ}\text{C}$  and shows that higher shear rates lead to smaller spherulite sizes. This prediction is in agreement with experimental observations [49], [103].

From the discussion above, we conclude that the model described here captures many of the important features of polymer crystallization – particularly flow-induced effects.

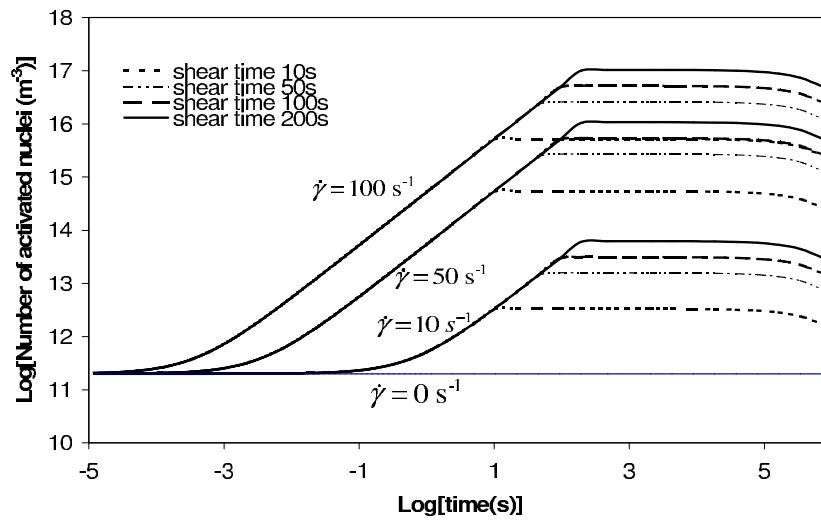


Figure 5.5: Activated nuclei number per unit volume, for iPP, as a function of time at 140°C, for different shear rates and shearing times.

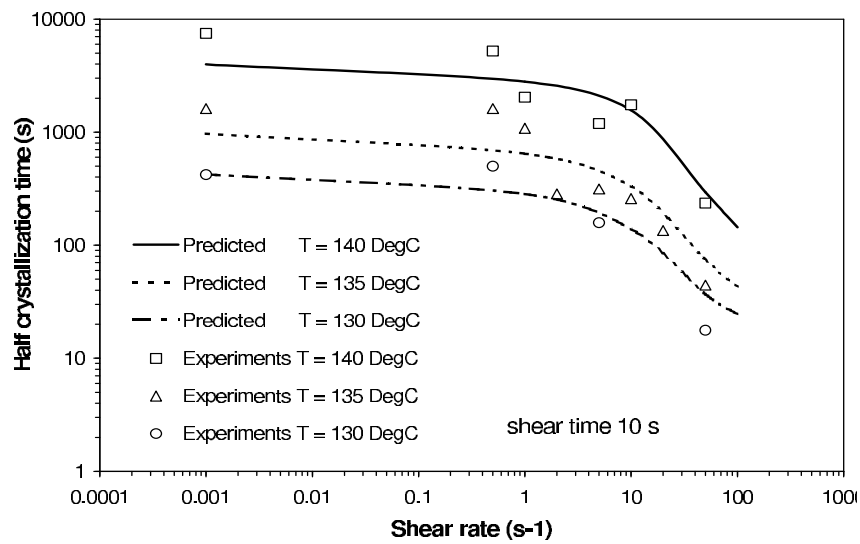


Figure 5.6: Predicted and experimental half crystallization time versus shear rate for iPP at three crystallization temperatures.

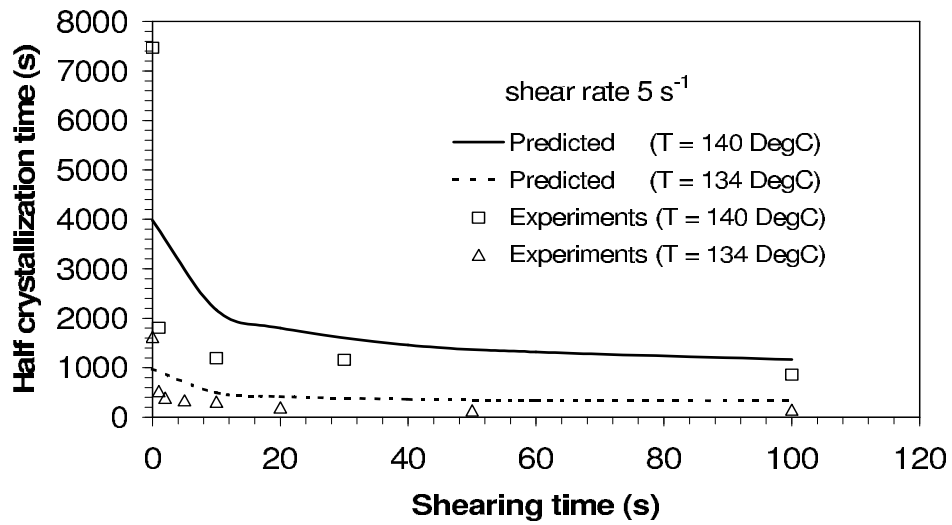


Figure 5.7: Predicted and experimental half crystallization time versus shearing time for iPP at a shear rate of 5 s<sup>-1</sup> and two crystallization temperatures.

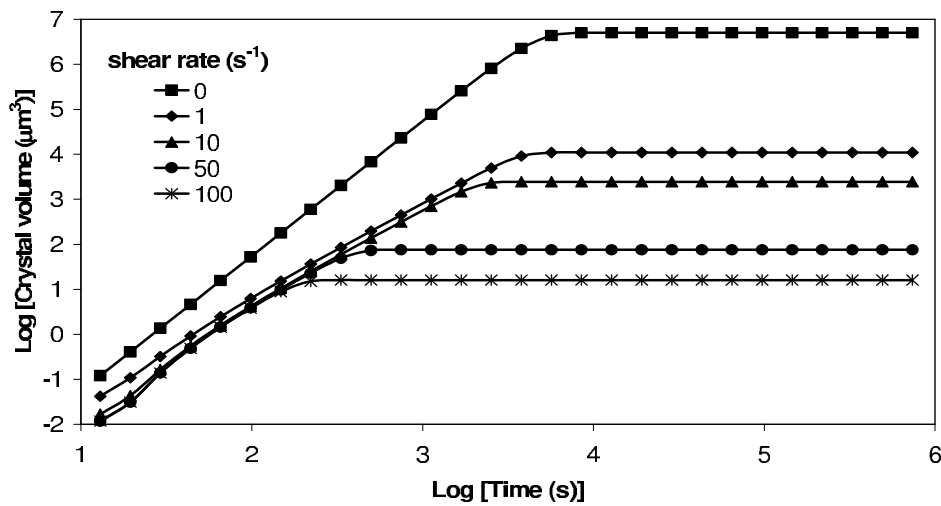


Figure 5.8: Crystal volume of iPP versus time at 140°C, after 10s shear treatments at different shear rates.



# Implementation in Molding Simulation

---

In this chapter, we implement the crystallization model discussed in Chapter 5 in a molding simulation. We discuss the use of crystallization modeling to predict properties of semi-crystalline materials "on the fly" during simulation. Finally we provide some validation of the molding simulation using these models.

## 6.1 Governing Equations

The crystallization model of Chapter 5 has been implemented in a special version of a commercial simulation package (Moldflow Plastics Insight Version 4 Revision 1).

The flow kinematics generated by the injection molding process are calculated using the equations discussed in Chapter 2 with the appropriate changes to account for the crystallization kinetics.

The pressure equation is

$$\nabla_{xy} \cdot (S_\rho \nabla_{xy} p) = \int_{-h}^h \left\{ \left( \frac{\partial \rho}{\partial T} \right)_{p,\alpha} \frac{\partial T}{\partial t} + \left( \frac{\partial \rho}{\partial p} \right)_{T,\alpha} \frac{\partial p}{\partial t} + \left( \frac{\partial \rho}{\partial \alpha} \right)_{p,T} \frac{\partial \alpha}{\partial t} \right\} dz \quad (6.1)$$

where



$$S_\rho = \int_{-h}^h \left( \rho(p, T, \alpha) \int_{-h}^z \frac{z'}{\eta(\dot{\gamma}, T, \alpha)} dz' \right) dz$$

and  $\nabla_{xy}$  denotes the gradient operator with respect to the  $xy$  plane in a Cartesian coordinate system in which the  $x - y$  plane is located at the midplane of the component to be analyzed and the  $z$  direction is in the local thickness direction. The viscosity  $\eta(\dot{\gamma}, T, \alpha)$  is of the form in eqn.(5.35) with  $\eta_a$  described by a WLF-Cross model involving shear and temperature dependence (see eqn.(2.5) of Chapter 2).

In addition to eqn.(6.1) we also need to solve the modified energy equation:

$$\begin{aligned} \rho c_p \frac{DT}{Dt} &= \nabla_{xy} \cdot (k \nabla T) + \boldsymbol{\tau} : \mathbf{D} \\ &+ \rho_c \Delta H_0 \chi_\infty \frac{D\alpha}{Dt} - \frac{T}{\rho} \frac{\partial \rho}{\partial T} \frac{Dp}{Dt} \end{aligned} \quad (6.2)$$

where  $\rho_c$  is the crystal density,  $\Delta H_0$  the latent heat of fusion and  $\chi_\infty$  the final level of crystallinity. The equation can be simplified by neglecting the in-plane thermal conduction terms and the gap-wise convection terms.

We now consider determination of the required material properties by using the results from the crystallization model.

## 6.2 Effect of Crystallization on Rheology

As discussed in Chapter 5, we regard the crystallizing polymer with growing crystalline structures as a suspension of semicrystalline material in an amorphous matrix. The relation between the system viscosity and the relative crystallinity is given by eqn.(5.35). Fitting experimental data of Pantani et al. [125] to eqn.(5.35) gives  $\beta_1 = 0.05$  and  $\beta = 9.2$  for a chosen value of  $A = 0.44$ . In using the data of Pantani et al. [125], we have converted the absolute crystallinity used in their paper to the corresponding relative crystallinity. The value of  $\beta$  so obtained is much higher than the usual value ( $\beta \approx 2$ ) in suspension theories [117]. This means that in a crystallizing system the increase of viscosity is much faster than in particulate suspensions, as if the crystalline structure plays a role akin to crosslinking.

Figure 6.1 compares results from our suspension model, eqn.(5.35) with  $A = 0.44$ ,  $\beta = 9.2$  and  $\beta_1 = 0.05$  with the data of Pantani et al. [125]. There is reasonable agreement, until the viscosity ratio reaches about 20, beyond which the two models behave differently. Our model shows that the viscosity turns up sharply and goes to infinity. Similar behavior has been reported in the work of Wassner and Maier [171], whereas Pantani et al. [125] showed that the viscosity levels off after an initial rapid

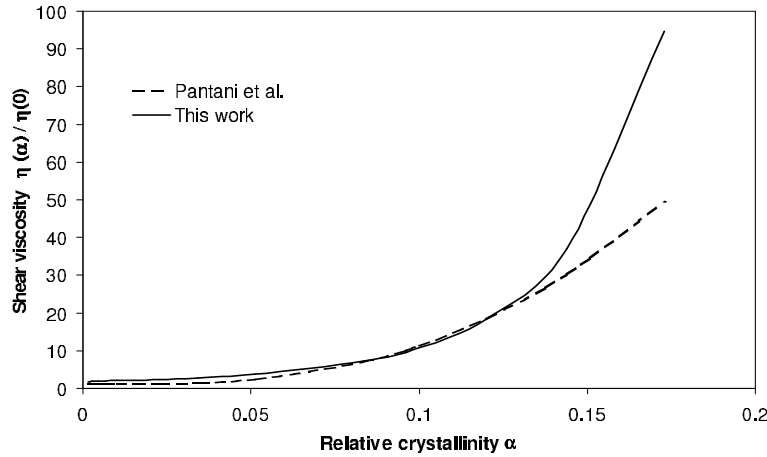


**Figure 6.1:** Comparison of the suspension model with the model of Pantani et al. [125].

increase. From a practical viewpoint, in injection molding an increase of viscosity by one order of magnitude from the melt viscosity effectively suppresses flow, and the stress becomes locked in the frozen material. Moreover, after cessation of flow the concept of viscosity is irrelevant in injection molding simulation.

### 6.3 Crystallization and Thermal Properties

We assume certain relationships for the effect of crystallization on thermal properties. For the Solvay PHV 252 iPP, specific heat  $c_p$ , and the thermal conductivity  $k$ , are assumed to vary with the relative crystallinity  $\alpha \in [0, 1]$ , in the following way:

$$c_p(\alpha, T) = \alpha c_{p_s}(T) + (1 - \alpha) c_{p_a}(T) \quad (6.3)$$

$$k(\alpha, T) = \alpha k_s(T) + (1 - \alpha) k_a(T) \quad (6.4)$$

where the values of  $c_{p_s}$ ,  $c_{p_a}$ ,  $\lambda_s$  and  $\lambda_a$  were determined by Le Bot [21] and Delaunay et al. [36] with

$$c_{p_s}(T) = 1451 + 10.68T$$

$$c_{p_a}(T) = 2124 + 3.10T$$

$$k_s(T) = 0.31 - (4.69 \times 10^{-4}) T$$

$$k_a(T) = 0.189 - (6.25 \times 10^{-5}) T$$

where  $T$  is in °C. Here the subscripts  $a$  and  $s$  refer to the amorphous (i.e., melt) and solidified phases, respectively.

For specific heat the assumption seems reasonable. However, experimental techniques developed by Schieber et al. [138] will allow investigation of the possibility that specific heat also depends on polymer orientation. We ignore this possibility here and accept eqn.(6.3).

Undoubtedly, questions remain on the validity of eqn.(6.4) as a model for thermal conductivity. Van den Brule described a theoretical argument for anisotropic thermal conductivity in a sheared amorphous polymer melt [26]. He proposed that the conductivity along the backbone of the polymer was higher than that transverse to this direction. Though conceptually reasonable, there has been no experimental evidence to validate the idea. In 1999, Venerus et al. [162] described an experiment for the determination of anisotropic thermal diffusivity in a melt after a shear treatment and later showed [161] that the diffusivity was indeed tensorial in nature for a polyisobutylene (PIB) melt. The diffusivity in the flow direction was significantly higher than that transverse to flow. In a later paper, Venerus et al. [160] provide evidence that there exists a stress-thermal law akin to the stress-optical law. By studying two different polymers with very different chemistry, the authors further conclude that the conductivity along the backbone is not important, in apparent contradiction to the theory proposed by van den Brule [26]. These assertions, that there exists a stress thermal law and that backbone conduction is not important, require further experiments on a wider range of polymers. Thermal conductivity is undoubtedly a complex property. The discussion above relates only to amorphous materials. Conductivity clearly depends on temperature, but also on molecular orientation and morphology in semi-crystalline materials. It is likely that the conductivity in the solid phase  $k_s$ , will depend not only on temperature as we assume, but also the morphology. Nevertheless, for now we use eqn.(6.4) above.

## 6.4 Crystallization and the Equation of State

The Pressure-Volume-Temperature (PVT) relationship which describes the specific volume as a function of pressure and temperature, plays an important role in injection molding simulations, including analyses of filling, packing and subsequent shrinkage and warpage (see, e.g., Walsh [165]; Zheng et al. [189]; Zheng et al. [184]). PVT measurements are usually conducted under quiescent and isothermal conditions, or at low cooling and heating rates [71] that are irrelevant to injection molding. The crystallinity-dependent specific volume is assumed to follow the mixture law

$$v = \alpha v_s + (1 - \alpha) v_a \quad (6.5)$$

where  $v_s$  and  $v_a$  are, respectively, the specific volumes of the solid and melt phases and  $\alpha \in [0, 1]$  denotes the relative crystallinity.

While eqn.(6.5) is not new [21], it has not been possible to determine its effectiveness due to the lack of experimental data. Brucato et al. [25] presented an apparatus that permitted study of the density of solidified polymer under high pressure and high cooling rates. They concluded that at high cooling rates, pressure effects tend to be insignificant. This is contrary to observations made with low cooling rate equipment. More recently a new PVT device has been developed in the Netherlands. It permits both high cooling rate, high pressure and shear effects [38]. Using this apparatus and Wide Angle X-ray Diffraction (WAXD), Van der Beek et al. [39] studied the effect of shear and temperature on the specific volume and morphology of two iPP samples. They concluded that flow effects on specific volume evolution increased with increased shear rate, pressure and average molecular weight. On the other hand, the sensitivity of specific volume to flow effects decreases with the temperature at which shear is applied. The authors further surmised that crystallization models that consider only one phase, for example the  $\beta$ -crystalline phase in iPP, may not be able to fully describe the crystallization kinetics due to flow. Despite this consideration, experimental results in [39] suggest that eqn.(6.5) is a reasonable model.

## 6.5 Numerical Scheme

The governing equations and material models provided in this chapter have been implemented in a simulation code based on Moldflow Plastics Insight, Version 4, Revision 1. We summarize the computation steps as follows:

1. Perform flow analysis, calculating pressure, velocity and temperature fields using equations (6.1) and (6.2) respectively;
2. Using the flow kinematics calculated in step 1, calculate the conformation tensor  $\mathbf{c}$  from eqn.(5.17);
3. Calculate free energy change from eqn.(5.28);
4. Calculate function  $f$  from eqn.(5.7);
5. Calculate nuclei number per unit volume  $N$  from equations (5.4) to (5.6);
6. Calculate growth rate  $G$  from eqn.(5.2);
7. Calculate orientation tensor of semicrystalline phase from eqn.(5.31);
8. Calculate the dimensionality exponent  $m$  from eqn.(5.34);
9. Update viscosity, relaxation time, and density using equations (5.35), (5.32) and (6.5), respectively, and
10. Return to step 1 for next iteration until convergence is reached, then go to the next time step.

We point out here an inconsistency in our approach. The viscosity used in the flow analysis is, as explained above, based on the modified Cross equation eqn.(5.35), whereas the FENE-P model is used in the crystallization calculation. That is, a generalized Newtonian fluid model is used to calculate the flow kinematics, which in turn drive the viscoelastic calculation. Such a decoupled approach was first used in injection molding simulation by Baaijens [9]. Baaijens compared flow induced residual stress results obtained with the decoupled approach with a full viscoelastic simulation using the Leonov model. The results differed by around 10%, and Baaijens concluded that the decoupled approach was satisfactory. Indeed a full viscoelastic simulation of injection molding under realistic conditions and realistic geometry is beyond our current computational capability. Thus for reasons of practicality we adopt the decoupled approach here and note that, in the context of injection molding, it has also been used successfully by other investigators ([199], [127]).

## 6.6 Validation of the Model

Injection molding is a complicated process and validation of any simulation model is difficult. As discussed in Chapter 2, the shrinkage and warpage depend on the pressure/time history as well as the properties of the injection molded material. Consequently, any validation must first deal with prediction of pressure and temperature.

### 6.6.1 Pressure

We return to the data of Luye [111] introduced in Chapter 2.

Figure 6.2 shows the measured and calculated pressure decay in the packing phase with two sets of parameters for the viscosity model. While both sets of parameters produce reasonable results, the pair  $\beta = 1$  and  $\beta_1 = 12$  give better agreement with the experimental data. This is not surprising, as the other pair,  $\beta = 0.05$  and  $\beta_1 = 9.2$ , gave better results with the different iPP used by Pantani et al. [125]. On a positive note, the viscosity of iPP does not seem to be too sensitive to the choice of parameters in the viscosity model.

### 6.6.2 Temperature

A semi-analytical, non-invasive technique for measurement of temperature profiles across the thickness of an injection molded part has been developed by Le Bot [21]. It relies on measurement of heat flux normal to the plane at the point for which the temperature profile is required. Inverse methods are used to determine the thermal contact resistance, conductivity and temperature profile through the thickness. Le Bot [21] and Delaunay et al. [36] have used this technique on the Solvay iPP (PHV 252) used in our crystallinity model development. Details of the mold and technique

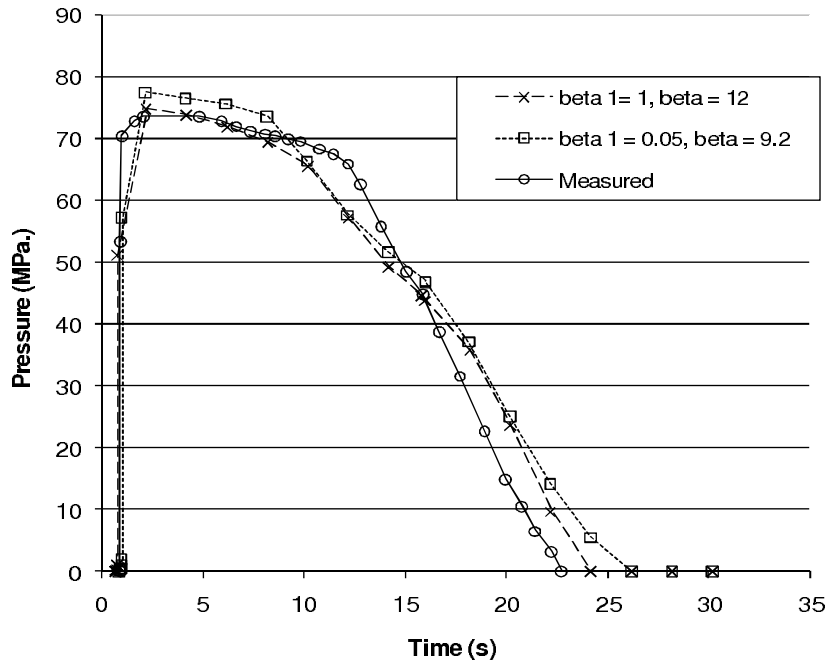


**Figure 6.2:** Pressure vs time for various values of  $\beta$  and  $\beta_1$  and the experimental data of Luye [111].

may be found in [111], [21], [36]. Figure 6.3, taken from [36], shows the temperature profile through the thickness of a 3mm thick injection molded plate at various times. The molding conditions are given in Table (6.1)

**Table 6.1:** Molding Parameters for 3mm plate

Molding Parameter	Value
Melt temperature	220°C
Injection time	1 s
Mold coolant temperature	40°C
Coolant flow rate	7 l/min
Nozzle holding pressure	40 MPa
Holding time	15 s
Total cooling time (holding time + cooling time)	40s

Due to Newton's law of cooling we expect the temperature at the midplane of the molding to decrease proportionally to the temperature difference. Yet between 10 and 15s we see that the expected temperature drop is not evident. We surmise that the smaller than expected temperature drop between the contours at 10 and 15s is due to the material crystallizing.

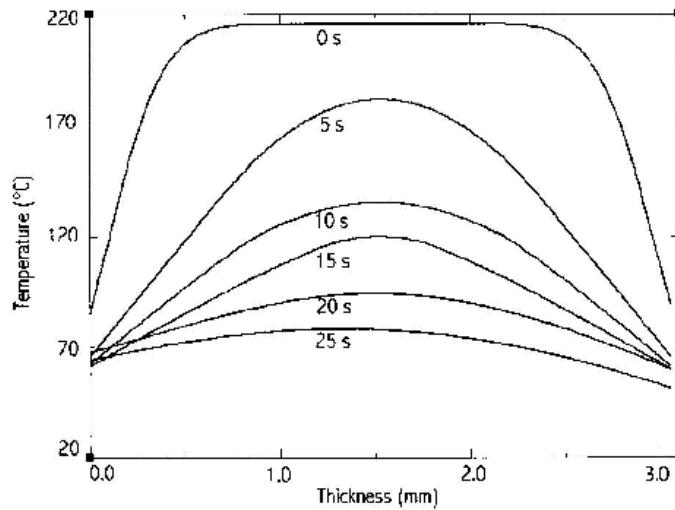


**Figure 6.3:** Experimental temperature profiles, across the thickness of the molding, at various times from [36].

Figure 6.4 shows the results of simulation for the molding parameters in Table 6.1 above [36]. It shows the calculated temperature vs. time curve at the midplane of the molding at the position of the flux transducer that produced the curves in Figure 6.3. Also shown are the temperatures at the midplane from Figure 6.3. A change in shape

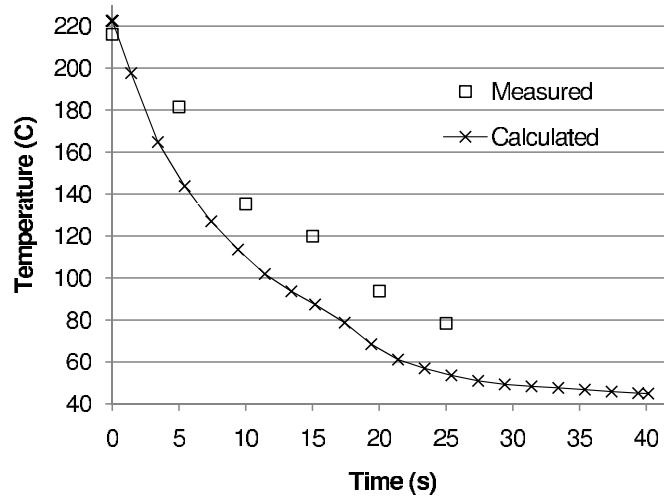


**Figure 6.4:** Calculated temperature distribution vs time at the midpoint of the molding considered by Delaunay [36].

of the calculated curve is evident between 10 and 20 s – as in the experimental data. While the comparison lacks precision, it does demonstrate that the crystallization kinetics are reasonably accounted for in the simulation. The calculated temperature

values do not compare well to the measured data. However, it should be remembered that the simulation uses a fixed coolant temperature of 40°C.

The temperature of the mold wall from Fig. 6.3 shows that the mold-wall temperature is initially around 80°C and then reduces to under 70°C. We conclude that the actual temperature within the part and at the mold wall is very difficult to determine but there is an effect due to crystallization between 10 - 20s that is seen in both experimental and calculated data.





# Conclusions and Further Work

---

In this chapter we summarize the work presented in earlier chapters and indicate further areas of development.

## 7.1 The Geometry Problem

The geometry problem involves performing flow and warpage analyses on a 3D solid geometry. A solution by way of the Dual Domain Finite Element Method was developed in Chapter 3.

The Dual Domain technique, in which a surface mesh on a 3D object may be used for analysis is a considerable step forward in injection molding simulation. For the first time, it is possible for designers and analysts to interface directly to the 3D geometry. It is an effective method of overcoming the need to create a midplane model without incurring the human interaction time or the computing resource problems associated with 3D FEA with volumetric elements. Indeed, the dual domain technique overcomes the problem of full 3D analysis. As most injection molded parts are thin-walled, it is necessary to have a fine grid in the thickness direction to capture the high thermal gradients. Dual domain typically allows 20 grid points in this direction thereby allowing accurate analysis on thin-walled geometries - which cover a large proportion of injection molded parts. The alternative method, full 3D analysis using volumetric elements, would lead to huge models and extremely long run times.

The commercial benefit of introducing this technique deserves attention [96]. Figure 7.1 shows the Moldflow licences in each year. It is apparent that the dual domain technique had an important affect on the utilization of injection molding simulation.

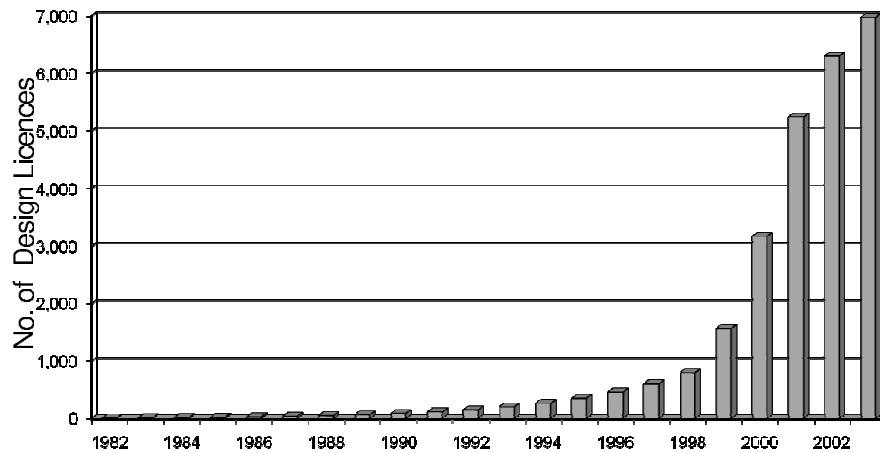


**Figure 7.1:** Moldflow licence sales increased with the introduction of the dual domain method in 1997.

## 7.2 The Material Data Problem

Here the problem is that it is impossible to determine material properties at the conditions experienced in molding. Moreover, to make simulation feasible, approximations such as the "no-flow" or "transition" temperature have been introduced. In Chapter 4 a model was introduced that "corrected" shrinkages calculated with a simple model that uses readily available material data. Despite its simplicity, the model significantly improves prediction of shrinkage for a wide range of materials.

In Chapter 5, we took a different approach to this problem. Here we used more sophisticated material modeling to transform data obtained under laboratory conditions into data required for simulation. Central to this is the introduction of crystallization kinetics in the simulation. In particular, the "no-flow" or "transition" temperature concept is removed by the use of a suspension model for viscosity. This relates viscosity to the amount of crystallization, and so allows viscosity to depend on rate of cooling, temperature, shear rate and the free energy of the melt. The latter term accounts for flow induced crystallinity.

In Chapter 6 we described some simple models to predict properties such as viscosity, thermal conductivity, specific heat and density. These models used the crystallization calculation and removed the problem of a fixed no-flow or transition temperature. We gave some validation for temperature and pressure for a specific iPP (Solvay PHV 252).

## 7.3 Future Development

Before discussing areas of improvement, we note that Chapters 5 and 6 of the thesis were based on a single iPP (Solvay PHV 252). This raises the question of applica-

bility to other materials. Although it is not easy to get a full set of characterization data and validation data for a given material, as we had with the Solvay material, our material characterization and modeling methods have been applied to other materials. Some of this work has been presented at scientific conferences. Hadinata et al. [68] provided some pressure vs time traces from simulation, using the theory in this thesis, for two materials, with experimental data using a different geometry to that used by Luye [111] and presented here. One material was an iPP (Borealis, Austria, HD 601CF), the other a 30% by weight glass filled PA6 (UBE, Japan, 1015GC6). Consequently, we think the methods described here are applicable to many other materials.

### 7.3.1 The Geometry Problem

The proposed geometry solution is an effective solution. Certainly it has limitations, due to the assumption that the part be thin-walled. To counter this a hybrid approach may be useful. Such a method could use the dual domain technique for the thin sections and a full 3D analysis in areas that are truly 3D [177]. Such a technique is the subject of a patent application by Kennedy and Yu [176].

### 7.3.2 Prediction of Properties

The prediction of properties is worthy of more work. Our model for morphology is capable of being used to predict many properties. Its success will depend on our ability to estimate properties for the amorphous matrix and semi-crystalline inclusions. Given this, micromechanical models may be used to predict a wide range of properties such as:

- thermal conductivity;
- thermal expansion coefficient;
- mechanical properties, and
- viscosity.

### 7.3.3 Thermal Conductivity

In Chapter 6 we discussed the anisotropy of thermal conductivity predicted theoretically by van den Brule [26] and subsequently experimentally verified by Venerus et al. [160] and Schieber [138]. Their work has focussed on amorphous materials. The situation for semi-crystalline materials is unclear. In the absence of rigorous scientific data, we note that the approach in Chapter 5 provides a means by which thermal conductivity of semi-crystalline materials may be predicted. Given the morphology

predicted by the model presented in Chapter 5, and by assuming properties of the semi-crystalline and amorphous phases, micromechanical models can provide the conductivity of the processed material. As a result, the thermal conductivity in the amorphous and solid phases would be tensor quantities.

### 7.3.4 Thermal Expansion Coefficient

Thermal expansion coefficient is a key property for warpage prediction. As for thermal conductivity, the methods presented may be used with assumed properties of the semi-crystalline and amorphous phases, to provide the coefficient of expansion for the processed material.

### 7.3.5 Mechanical properties

Micromechanical models have long been used in simulation to predict mechanical properties of short-fiber reinforced thermoplastics. In a similar way, they may be used to predict the mechanical properties of semicrystalline materials.

Our efforts have been directed to predicting the morphology of the material and hence its ultimate properties. For some processes, this may not be necessary. Henrichsen and McHugh [72] have shown a correlation between the stress in the amorphous phase and properties. Using the same additive stress rule as employed here, eqn.(5.8), Henrichsen and McHugh [72] demonstrate a correlation between elongation at break and yield stress with the quantity

$$\frac{\tau_{a_{ii}}}{\tau_{a_{ii}} + \tau_{c_{ii}}} \quad (7.1)$$

where  $\tau_{a_{ii}}$  and  $\tau_{c_{ii}}$  are the components of the stress in the amorphous and semi-crystalline phases respectively. Schrauwen [140] discusses the relationship between lamellar thickness and yield stress. However he notes the lack of a model that relates yield stress to levels of crystallinity. Perhaps the work of Henrichsen and McHugh [72] can be useful here. If so, more sophisticated models of mechanical behavior could be used with semi-crystalline materials.

Mykhaylyk et al. [121] have recently shown that a certain amount of work is required to create oriented crystalline structures. Using a blend of hydrogenated polybutadienes with components having short and long molecules, they introduce the idea of critical work  $w_c$  that is required to produce oriented structures. Of particular interest, is their finding that  $w_c$  is independent of shear rate, provided that the shear rate is above the inverse Rouse time of the long molecules. The authors claim the criterion has been tested with other polymers. Should these claims be true, the use of critical work could improve morphology modeling. Instead of using eqn.(5.1) with  $m = 4 - 3 \langle \mathbf{uu} \rangle : \langle \mathbf{uu} \rangle$ . We could replace eqn.(5.1) with the following equation for

spherulitic growth

$$\alpha_f = \frac{4\pi}{3} \int_0^t \dot{N}(s) \left[ \int_s^t G(u) du \right]^3 ds \quad (7.2)$$

and, in the event the work criterion was satisfied, use

$$\alpha_f = g \int_0^t \dot{N}(s) \left[ \int_s^t G(u) du \right]^1 ds \quad (7.3)$$

where  $g$  is a constant to be determined for the oriented structures. This area requires further investigation.

Khanna [99] has pointed out that poor transparency and lower impact resistance is associated with larger spherulite size. This should be compared with the observations of Figure 5.2, where we show the size of crystallites as functions of process conditions. A correlation of these results with measured properties may reveal some relationships.

### 7.3.6 Viscosity

The applicability of the suspension model should be reviewed. We have good results with iPP and have reported good results with PA6 [68]. Interestingly the values of  $b$  and  $b_1$  in eqn.(5.35) were the same for these two materials. Nevertheless, the suspension model needs to be evaluated with other polymer systems.

## 7.4 Additives

Very few polymers are used in their pure form. Additives including nucleating agents and colorants are very common. Lamberti et al. [107] have looked at the effect of sodium benzoate on crystallization. Our research with the CRC has started to look at the effect of organic and inorganic colorants. It appears that the methods of characterization required for the crystallization model presented here can capture the effects of colorants on crystallization and properties [69]. Nevertheless, we have only begun, and much work remains to be done.



## References

- [1] Feature - 50 ideas that changed plastics. *Plastics Technology*, October, 2005.
- [2] S. Acierno, B. Palomba, H.H. Winter, and N. Grizzuti. Effect of molecular weight on the flow-induced crystallization of isotactic poly(1-butene). *Rheologica Acta*, 42:243–250, 2003.
- [3] S.G. Advani and C.L. Tucker III. The use of tensors to describe and predict fiber orientation in short fibre composites. *J. Rheol.*, 31:751–784, 1987.
- [4] C. Angelloz, R. Fulchiron, A. Douillard, B. Chabert, R. Fillit, A. Vautrin, and L. David. Crystallization of isotactic polypropylene under high pressure (gamma phase). *Macromolecules*, 33:4138–4145, 2000.
- [5] C. Austin. Filling of mold cavities. In E.C. Bernhardt, editor, *Computer Aided Engineering for Injection Molding*. Hanser, New York, 1983.
- [6] C.A. Austin. *Moldflow Design Principles*. Moldflow Pty. Ltd., Melbourne. Australia, 1985.
- [7] C.A. Austin. Private correspondence. 1988.
- [8] M. Avrami. Kinetics of phase change, i. general theory. *J. Chem. Phys.*, 7:1103–1112, 1939.
- [9] F.P.T. Baaijens. Calculation of residual stress in injection moulded products. *Rheol. Acta*, 30:284–299, 1991.
- [10] A. Bakharev, Z. Fan, F. Costa, S. Han, X. Jin, and P. Kennedy. Prediction of core shift effects using mold filling Simulation. *Soc. Plastics. Eng. Proc. of Annual Technical Conference (ANTEC)*, 2004.
- [11] I.T. Barrie. Understanding how an injection mold fills. *SPE Journal*, 27:64–69, 1971.
- [12] J.L. Batoz and P. Lardeur. A discrete shear triangular nine DOF element for the analysis of thick to very thin plates. *International J. Numerical Methods in Engineering*, 28:533–560, 1989.
- [13] P.G. Bergan and C.A. Felippa. A triangular membrane element with rotational degree of freedom. *Computer Methods in Applied Mechanics and Engineering*, 50:25–69, 1985.
- [14] R. B. Bird, C.F. Curtis, R.C. Armstrong, and O. Hassager. *Dynamics of Polymeric Liquids: Vol.2 Kinetic Theory*. John Wiley and Sons, New York, 1987.
- [15] R. Byron Bird. Teaching with FENE dumbbells. *Rheology Bulletin*, 76:10–12, 2007.
- [16] R.B. Bird, R.C. Armstrong, and O. Hassager. *Dynamics of Polymeric Liquids Vol. 1: Fluid Mechanics*. John Wiley and Sons, New York, 2nd edition, 1987.
- [17] A. Bogaerds. *Stability Analysis of Viscoelastic Flows*. PhD thesis, Technical University of Eindhoven, 2002.
- [18] F. Boitout, J.F. Agassant, and M. Vincent. Elastic calculation of residual stresses in injection molding. *Int. Polym. Processing*, 10:237–242, 1995.
- [19] H.C. Booij. The energy storage in the Rouse model in an arbitrary flow field. *J. Chem. Phys.*, 80:4571–4572, 1984.



- [20] A.H.M. Boshouwers and J.J. Van der Werf. *A Simulation Code for the Filling Phase of the Injection Moulding Process of Thermoplastics*. PhD thesis, Technical University of Eindhoven, 1988.
- [21] P. Le Bot. *Comportement Thermiques Des Semi-Cristallins Injectes Application a la Prediction Des Retraits*. PhD thesis, Universite de Nantes, 1998.
- [22] K. Boutahar, C. Carrot, and J. Guillet. Polypropylene during crystallization from the melt as a model for the rheology of molten-filled polymers. *J. Applied Polymer Sci.*, 60:103–114, 1996.
- [23] K. Boutahar, C. Carrot, and J. Guillet. Crystallization of polyolefins from rheological measurements - relation between the transformed fraction and the dynamic moduli. *Macromolecules*, 31:1921–1929, 1998.
- [24] J. Braun, H. Wippel, G. Eder, and H. Janeschitz-Kriegl. Industrial solidification processes in polybutene-1. Part II - influence of shear flow. *Polym. Eng. Sci.*, 43:188–203, 2003.
- [25] V. Brucato, V. La Carrubba, S. Piccarolo, and G. Titomanlio. Solidification under pressure and high cooling rates. *Int. Polym. Processing*, XV:103–110, 2000.
- [26] B.H.A.A. Van Den Brule. A network theory for the thermal conductivity of an amorphous polymeric material. *Rheologica Acta*, 28:257–266, 1989.
- [27] T.E. Burton and M. Rezayat. POLYCOOL 2 a three-dimensional transient mold-cooling simulator. In L.T. Manzione, editor, *Applications of Computer Aided Engineering in Injection Molding*. Hanser, New York, 1987.
- [28] A.C. Bushman and A.J. McHugh. A continuum model for the dynamics of flow-induced crystallization. *J. Polym. Sci. Part B: Polymer Physics*, 34:2393–2407, 1996.
- [29] Hieber C.A, P.J. Wang, and K.K. Wang. Injection molding of a center-gated disk: Modelling and measurements for the filling and post filling stages including gapwise shrinkage. , *SPE Technical Papers*, 37:259–263, 1991.
- [30] S. Caren. GRAFTEK integrated CAD/CAM/CAE system. In L.T. Manzione, editor, *Applications of Computer Aided Engineering in Injection Molding*. Hanser, New York, 1987.
- [31] L. Caspers. *VIp: An Integrated Approach to the Simulation of Injection Moulding*. PhD thesis, Technical University of Eindhoven, 1996.
- [32] R.Y. Chang and W.H. Yang. Numerical simulation of mold filling in injection molding using a three-dimensional finite volume approach. *Int. J. Numerical Meth. Fluids*, 37:125–148, 2001.
- [33] H.H. Chiang, C.A. Hieber, and K.K. Wang. A unified simulation of the filling and post filling stages in injection molding. Part I: Formulation and Part II: Experimental verification. *Polym. Eng. Sci.*, 31:116–139, 1991.
- [34] D.H. Chung and T.H. Kwon. Invariant-based optimal fitting closure approximation for the numerical prediction of flow-induced fiber orientation. *J. Rheology*, 46:169–194, 2002.
- [35] S. Coppola, N. Grizzuti, and P.L. Maffettone. Microrheological modeling of flow-induced crystallization. *Macromolecules*, 34:5030–5036, 2001.

- 
- [36] D. Delaunay, P. Le Bot, R. Fulchiron, J.F. Luye, and G. Regnier. Nature of contact between polymer and mold in injection molding. Part i: Influence of a non-perfect thermal contact. *Polym. Eng. Sci.*, 40:1682–1691, 2000.
- [37] D. Delaunay, P. LeBot, R. Fulchiron, J.F. Luye, and G. Regnier. Nature of contact between polymer and mold in injection molding. Part II: Influence of mold deflection on pressure history and shrinkage. *Polym. Eng. Sci.*, 40:1692–1700, 2000.
- [38] M.H.E. Van der Beek, G.W.M. Peters, and H.E.H. Meijer. A dilatometer to measure the influence of cooling rate and melt shearing on specific volume. *Inter. Polymer Proc.*, 20:111 – 120, 2005.
- [39] M.H.E. Van der Beek, G.W.M. Peters, and H.E.H. Meijer. Influence of shear flow on the specific volume and the crystalline morphology of isotactic polypropylene. *Macromolecules*, 39:1805–1814, 2006.
- [40] R.J. Donaghy, R.W. McCune, S.J. Bridgett, C.G. Armstrong, D.J. Robinson, and R.M. McKeag. Dimensional reduction of analysis models. In *Proc. 5th International Meshing Roundtable*, pages 307–320, Pittsburgh, USA, 1996. Sandia National Laboratories.
- [41] L.H. Donnell. *Beams, Plates and Shells*. McGraw Hill, New York, 1976.
- [42] A.K. Doufas, I.S. Dairanieh, and A.J. McHugh. A continuum model for flow-induced crystallization of polymer melts. *J. Rheology*, 43:85–109, 1999.
- [43] A.K. Doufas and A.J. McHugh. Simulation of melt spinning including flow induced crystallization. Part II. Quantitative comparisons with PET spinline data. *J. Rheology*, 45:403–420, 2001.
- [44] A.K. Doufas, A.J. McHugh, and C. Miller. Simulation of melt spinning including flow-induced crystallization. part i. model development and predictions. *J. Non-Newtonian Fluid Mech.*, 92:27–66, 2000.
- [45] A.K. Doufas, A.J. McHugh, C. Miller, and A. Immaneni. Simulation of melt spinning including flow-induced crystallization. part II. quantitative comparisons with industrial spinline data. *J. Non-Newtonian Fluid Mech.*, 92:81–103, 2000.
- [46] L.F. Douven. *Towards the Computation of Properties of Injection Moulded Products: Flow and Thermally Induced Stresses in Amorphous Thermoplastics*. PhD thesis, Technical University of Eindhoven, 1991.
- [47] D. Dray-Bensahkoun. *Prediction Des Proprietes Thermo-Elastiques D'un Composite Injecte et Charge de Fibres Courtes*. PhD thesis, Ecole Nationale Superieure d'Arts et Metiers, Paris, 2006.
- [48] C. Duplay, B. Monasse, J.M. Haudin, and J.L. Costa. Shear-induced crystallization of polypropylene: Influence of molecular weight. *J. Mater. Sci.*, 35:6093–6103, 2000.
- [49] G. Eder and H. Janeschitz-Kriegl. Crystallization. in *Materials Science and Technology, Vol. 18, Processing of Polymers*, H.E.H. Meijer (Ed.), Wiley-VCH, New York, 1997, pages 269–342, 1997.
- [50] G. Eder, H. Janeschitz-Kriegl, and S. Liedauer. Crystallization processes in quiescent and moving polymer melts under heat transfer conditions. *Prog. Polym. Sci.*, 15:629–714, 1990.

- [51] X.-J. Fan. Viscosity, first normal stress difference and molecular stretching in dilute polymer solutions. *J. Non-Newtonian Fluid Mech.*, 17:125–144, 1985.
- [52] X.J. Fan, N. Phan-Thien, and R. Zheng. A direct simulation of fibre suspensions. *J. Non-Newtonian Fluid Mech.*, 74:113–136, 1998.
- [53] X.J. Fan, N. Phan-Thien, and R. Zheng. Simulation of fiber suspension flows by the brownian configuration field method. *J. Non-Newtonian Fluid Mech.*, 84:257–274, 1999.
- [54] Z. Fan, C. Kietzmann, S.R. Ray, F.S. Costa, and P.K. Kennedy. Three dimensional cooling and warpage simulation for the injection over-molding process. *Proc. Soc. Plastics Eng. Annual Technical Conference (ANTEC)*, 2005.
- [55] Z. Fan, B. Lin, F. Costa, X. Jin, R. Zheng, and P. Kennedy. Three dimensional warpage simulation for injection molding. *Proc. Soc. Plastics Eng. Annual Technical Conference (ANTEC)*, 2005.
- [56] Z. Fan, R. Zheng, P. Kennedy, H. Yu, and A. Bakharev. Warpage analysis of solid geometry. *Society of Plastics Engineers, Technical Papers, ANTEC 2000*, 46, 2000.
- [57] Z.L. Fan, R. Zheng, H. Yu, and P. Kennedy. Apparatus and method for structural analysis. *US Patent No. 6704693*, 2004.
- [58] J. Feng, C. V. Chaubal, and L. G. Leal. Closure approximations for the Doi theory: Which to use in simulating complex flows of liquid crystalline polymers? *J. Rheology*, 42:1095–1119, 1998.
- [59] E.C. Ferreira, N.M. Neves, R. Muschalle, and A.S. Pouzada. Friction properties of thermoplastics in injection molding. *Proc. Soc. Plastics Eng. Annual Technical Conference, ANTEC*, 2001.
- [60] F. Folgar and C.L. Tucker III. Orientation behaviour of fibres in concentrated suspensions. *J. Reinf. Plastics Compos.*, 3:98–119, 1984.
- [61] C. Friedl. Progress towards true 3D analysis for injection molding. *Soc. Plastics Eng., Proc. Annual Technical Conference (ANTEC)*, 42, 1996.
- [62] C. Friedl, H. Burke, P. Kennedy, N. McCaffrey, and R. Thomas. *SWIS 0.3 Manual*. Moldflow Pty. Ltd. Melbourne, Australia, 1990.
- [63] R. Fulchiron, E. Koscher, G. Poutot, D. Delaunay, and G. Regnier. Analysis of the pressure effect on the crystallization kinetics: Dilatometric measurements and thermal gradient modelling. *J. Macromolecular Science - Physics*, 40:297–314, 2001.
- [64] A. Garcia-Rejon. Advances in blow moulding process optimization. Technical Report Rapra Review Reports, Vol.7, No.10, Report 82, RAPRA, 1995.
- [65] Freedonia Group. Injection moulded plastics. Technical Report R 154-1198, Freedonia Group, Cleveland Ohio, 2004.
- [66] X. Guo, A.I. Isayev, and L. Guo. Crystallinity and microstructure in injection molding of isotactic polypropylenes. Part 1: A new approach to modeling and model parameters. *Polym. Eng. Sci.*, 39:2096–2114, 1999.
- [67] M.E. Gurtin. *An Introduction to Continuum Mechanics*. Academic Press, San Diego, 1981.

- [68] C. Hadinata, R. Zheng, C. Friedl, P.K. Kennedy, P. Zhu, and G. Edward. Material characterization for injection molding simulation. *Proc. 23rd Annual Conference of the Polymer Processing Society, Salvador, Brazil, 2007.*
- [69] C. Hadinata, R. Zheng, P.K. Kennedy, P. Zhu, G. Edward, D. Lee Wo, and R.I. Tanner. The effects of additives on material properties and shrinkage characteristics. *Proc. 24th Annual Meeting Polymer Proc. Soc., Salerno, Italy, 2008.*
- [70] S. Han and K.K. Wang. Use of the fast-cool PVT data for shrinkage analysis in injection molding. *Int. Polym. Processing, XVII:67–75, 2002.*
- [71] J. He and P. Zoller. Crystallization of polypropylene, nylon 66 and poly(ethylene terephthalate) at pressure to 200 MPa.: Kinematics and characterization of products. *J. Polym. Sci. part : Polym. Phys., 32:1049–1067, 1994.*
- [72] L.K. Henrichsen and A.J. McHugh. Analysis of film blowing with flow-enhanced crystallization: Part 1 Steady-state behavior. *Int. Polym. Processing, 22:179–189, 2007.*
- [73] J.-F. Héту, Y. Lauzé, and A. Garcia-Rejon. Three dimensional finite element simulation of mold filling processes. In S.F. Shen and P. Dawson, editors, *Simulation of Materials Processing: Theory, Methods and Applications, Numiform 95, Rotterdam, 1995.* Balkema.
- [74] C.A. Hieber and S.F. Shen. A finite element / finite difference simulation of the injection molding filling process. *J. Non-Newtonian Fluid Mech., 7:1–32, 1980.*
- [75] K. Himasekhar, C.A. Hieber, and K.K. Wang. Computer aided design software for cooling system in injection molding. *SPE Technical Papers, 35:352–355, 1989.*
- [76] J.D. Hoffman and R.L. Miller. Kinetics of crystallization from the melt and chain folding in polyethylene fractions revisited: Theory and experiment. *Polymer, 38:3151–3212, 1997.*
- [77] [Http://Www-03.Ibm.Com/Ibm/History/Documents/Pdf/1970-1984.Pdf.](http://Www-03.Ibm.Com/Ibm/History/Documents/Pdf/1970-1984.Pdf)
- [78] [Http://Www-03.Ibm.Com/Ibm/History/Documents/Pdf/Pcpress.Pdf.](http://Www-03.Ibm.Com/Ibm/History/Documents/Pdf/Pcpress.Pdf)
- [79] [Http://Www.Moldex3d.Com/En/Cooverview/A01.Php.](http://Www.Moldex3d.Com/En/Cooverview/A01.Php) 2008.
- [80] T. Huang and M.R. Kamal. Morphological modeling of polymer solidification. *Polymer Eng. Sci., 40:1796–1808, 2000.*
- [81] R.R. Huilgol and N. Phan-Thien. *Fluid Mechanics of Viscoelasticity.* Elsevier, Amsterdam, 1997.
- [82] K.S. Hyun, M.A. Spalding, and C.E. Hinton. Theoretical and experimental analysis of solids conveying in single-screw extruders. , *Proc. Soc. Plastics Eng. Annual Technical Conference (ANTEC), 1996.*
- [83] A.I. Isayev. Orientation, residual stresses and volumetric effects. In A.I. Isayev, editor, *Injection and Compression Molding Fundamentals*, pages 227–328. Marcel Dekker Inc., New York, 1987.
- [84] A.I. Isayev, C.A. Hieber, and D.L. Crouthamel. Residual stresses in the injection molding of amorphous polymers. *SPE Technical Papers, 27:110–113, 1981.*
- [85] F. Jay, B. Monasse, and J.M. Haudin. Shear-induced crystallization of polypropylenes: Effect of molecular weight. *J. Mater. Sci., 34:2089–2102, 1999.*



- [86] K.K. Kabanemi and M.J. Crochet. Thermoviscoelastic calculation of residual stresses and residual shapes of injection moulded parts. *Inter. Polymer Process.*, 7:60–70, 1992.
- [87] M. Kamal. The McGill University model (McKam-II): A comprehensive, integrated computer simulation of the injection molding process. In L.T. Manzione, editor, *Application of Computer Aided Engineering in Injection Molding*. Hanser, New York, 1987.
- [88] M.R. Kamal and S. Kenig. The injection molding of thermoplastics Part II: Experimental test of the model. *Polym. Eng. Sci.*, 12:302–308, 1972.
- [89] J. A. Karjalainen. Computer simulation of injection mould cooling. *Acta Universitatis Ouluensis*, Ser. C 43, 1987.
- [90] A. Keller and H. Kolnaar. Flow induced orientation and structure formation. in *Materials Science and Technology, Vol. 18, Processing of Polymers*, H.E.H. Meijer (Ed.), Wiley-VCH, New York, 1997, pages 189–268, 1997.
- [91] O. Kemmann, L. Weber, C. Jeggy, O. Magotte, and F. Dupret. Simulation of the micro injection molding process. *Soc. Plastics Engineers, Proc. Annual Technical Conference (ANTEC)*, 2000.
- [92] P. Kennedy. *Flow Analysis of Injection Molds*. Hanser, New York, 1995.
- [93] P. Kennedy and H. Yu. Plastic CAE analysis of solid geometry. *Society of Plastics Engineers, Technical Papers*, 43, 1997.
- [94] P. Kennedy and R. Zheng. Prediction of flow-induced crystallization in injection molding. *Proc. 19th Annual Meeting Polymer Processing Soc., Melbourne*, 2003.
- [95] P.K. Kennedy. *Flow Analysis Reference Manual*. Moldflow Pty. Ltd., Melbourne, Australia, 1993.
- [96] P.K. Kennedy. History of injection molding simulation. In M. R. Kamal, A. Isayev, and S.H. Liu, editors, *Injection Molding Handbook*. Hanser Gardner, to appear, 2008.
- [97] P.K. Kennedy and R. Zheng. Crystallization and simulation of injection molding. *Polymer Crystallization and Structure Formation in Processing*, Johannes Kepler University, Linz, Austria, Sep 19-20, 2003.
- [98] P.K. Kennedy and R. Zheng. Shrinkage of injection molded material. In J. Greener R. Wimberger-Friedl, editor, *Precision Injection Molding: Process, Materials and Applications*. Hanser Gardner, Munich, 2006.
- [99] Y. Khanna. Rheological mechanism and overview of nucleated crystallization kinetics. *Macromolecules*, 26:3639–3643, 1993.
- [100] B.V. Koen. *Discussion of the Method: Conducting the Engineer's Approach to Problem Solving*. Oxford University Press, New York, 2003.
- [101] A.N. Kolmogoroff. On the statistics of the crystallization process in metals. *Bull. Akad. Sci. USSR, Class Sci., Math. Nat.*, 1:355–359, 1937.
- [102] E. Koscher. *Effets Du Cisaillement sur la Crystallisation Du Polypropylene: Aspects Cinetiques et Morphologiques*. PhD thesis, Universite "Claude Bernard" Lyon I, 2002.

- 
- [103] E. Koscher and R. Fulchiron. Influence of shear on polypropylene crystallization : Morphology development and kinetics. *Polymer*, 43:6931–6942, 2002.
- [104] G. Kumaraswamy, A.M. Issaian, and J.A. Kornfield. Shear enhanced crystallization in isotactic polypropylene. 1. Correspondence between in situ rheo optics and ex situ structure determination. *Macromolecules*, 32:7537–7547, 1999.
- [105] T.H. Kwon, S.F. Shen, and K.K. Wang. Computer aided cooling system design for injection molding. *SPE Technical Papers*, 32:110–115, 1986.
- [106] P.G. Lafleur and M.R. Kamal. A structure-oriented computer simulation of the injection molding of viscoelastic crystalline polymers Part i: Model with fountain flow, packing, solidification. *Polym. Eng. Sci.*, 26:92–102, 1986.
- [107] G. Lamberti, G.W.M. Peters, and G. Titomanlio. Crystallinity and linear rheological properties of polymers. *Int. Polym. Processing*, 22:303–310, 2007.
- [108] E.H. Lee, T.G. Rogers, and T.C. Woo. Residual stresses in a glass plate cooled symmetrically from both surfaces. *J. American Ceramic Soc.*, 48:480–487, 1965.
- [109] V. Leo and CH. Cuvelliez. The effect of the packing parameters, gate geometry and mold elasticity on the final dimensions of a molded part. *Polym. Eng. Sci.*, 36:1961–1971, 1996.
- [110] H.A. Lord and G. Williams. Mold-filling studies for the injection molding of thermoplastic materials. Part II: The transient flow of plastic materials in the cavities of injection-molding dies. *Polym. Eng. Sci.*, 15:569–582, 1975.
- [111] J. F. Luye. *Etude Thermophysique Du Refroidissement Du Polypropylene Injecte*. PhD thesis, L'Ecole Nationale Supérieure D'Arts et Metiers, Paris, 1999.
- [112] J.F. Luyé, G. Régnier, P. Le Bot, D. Delaunay, and R. Fulchiron. PVT measurement methodology for semicrystalline polymers to simulate injection-molding process. *J. Applied Polym. Sci.*, 79:302–311, 1999.
- [113] H. Mavridis, A.N. Hrymak, and J. Vlachopoulos. Finite element simulation of fountain flow in injection molding. *Polym. Eng. Sci.*, 26:449–454, 1986.
- [114] H. Mavridis, A.N. Hrymak, and J. Vlachopoulos. The effect of fountain flow on molecular orientation in injection molding. *J. Rheology*, 32:639–663, 1988.
- [115] T. C. B. McLeish and R. G. Larson. Molecular constitutive equations for a class of branched polymers: The Pom-Pom polymer. *J. Rheology*, 42:81–110, 1998.
- [116] H.E.H. Meijer. Processing for properties. In H.E.H. Meijer, editor, *Processing of Polymers*, pages 3–75. Elsevier, 1997.
- [117] A.B. Metzner. Rheology of suspensions in polymeric liquids. *J. Rheol.*, 29:739–755, 1985.
- [118] Moldflow. *SWIS Manual*. Moldflow Pty. Ltd., Melbourne, 1988.
- [119] G. Moore. Cramming more components onto integrated circuits. *Electronics*, 38, 1965.
- [120] P.A. Moysey and M.R. Thompson. Investigation of solids transport in a single-screw extruder using a 3D discrete particle simulation. *Polym. Eng. Sci.*, 44:2203–2215, 2004.
- [121] O. Mykhaylyk, P. Chambon, R.S. Graham, J.P.A. Fairclough, P.D. Olmsted, and A.J. Ryan. The specific work of flow as a criterion for orientation in polymer crystallization. *Macromolecules*, To appear June 2008.

- [122] R. Nakano. Apparatus and method for analyzing a process of fluid flow, an apparatus and method for analyzing an injection molding process, an injection molded product, and a production method of the injection molded product. *US Patent No. 5835379*, 1998.
- [123] R. Nakano. Apparatus for analyzing a process of fluid flow, and a production method of an injection molded product. *US Patent No. 6161057*, 2000.
- [124] R. Pantani, I. Coccorullo, V. Speranza, and G. Titomanlio. Modeling of morphology evolution in the injection molding process of thermoplastic polymers. *Prog. Polymer Sci.*, 30:1185–1222, 2005.
- [125] R. Pantani, V. Speranza, and G. Titomanlio. Relevance of crystallization kinetics in the simulation of the injection molding process. *Int. Polymer Process.*, 16:61–71, 2001.
- [126] A. Peterlin. *J. Polym. Sci., Polym. Lett.*, 4B:287–291, 1966.
- [127] G.W.M. Peters, F.H.M. Swartjes, and H.E.H. Meijer. A recoverable strain-based model for flow-induced crystallization. *Macromol. Symp.*, 185:277–292, 2002.
- [128] E. Pichelin and T. Coupez. Finite element solution of the 3D mold filling problem for viscous incompressible fluid. *Comput. Methods Appl. Mech. Eng.*, 163:359–371, 1998.
- [129] V. Rajupalem, K. Talwar, and C. Friedl. Three-dimensional simulation of the injection molding process. *Society of Plastics Engineers, Technical Papers*, 43, 1997.
- [130] M. Rezayat and T.E. Burton. A boundary integral formulation for complex three-dimensional geometries. *Int. J. Numer. Meth. Eng.*, 29:262–273, 1990.
- [131] M. Rezayat and R.O. Stafford. A thermoviscoelastic model for residual stress in injection moulded thermoplastics. *Polym. Eng. Sci.*, 31:393–398, 1991.
- [132] S. Richardson. Hele-Shaw flows with a free boundary produced by the injection of fluid into a narrow channel. *J. Fluid Mech.*, 56:609–618, 1972.
- [133] I.I. Rubin. *Injection Molding Theory and Practice*. John Wiley and Sons, New York, 1972.
- [134] P.G. Saffmann and G.I. Taylor. The penetration of a fluid into a porous medium or Hele-Shaw cell containing a more viscous fluid. *Proc. Royal Soc. London, A* 245:312–329, 1958.
- [135] D.B.J. Samoy. Private correspondence. March 2008.
- [136] N. Santhanam. *Analysis of Residual Stresses and Post-Molding Deformation in Injection-Molded Components*. PhD thesis, Cornell University, 1992.
- [137] N. Santhanam and K.K. Wang. A theoretical and experimental investigation of warpage in injection molding. *SPE Technical Papers*, 36:270–273, 1990.
- [138] J.D. Schieber, D.C. Venerus, K. Bush, V. Balasubramanian, and S. Smoukov. Measurement of anisotropic energy transport in flowing polymers by using a holographic technique. *Proc. Nat. Acad. Sci.*, 101:13142–13146, 2004.
- [139] W. Schneider, A. Köppl, and J. Berger. Non-isothermal crystallization, crystallization in polymers. *Int. Polym. Processing*, 2:151–154, 1988.
- [140] B. Schrauwen. *Deformation and Failure of Semi-Crystalline Polymer Systems: Influence of Micro and Molecular Structure*. PhD thesis, Technische Universiteit Eindhoven, 2003.

- 
- [141] F. Schwarzl and A. J. Staverman. Time-temperature dependence of linear viscoelastic behavior. *Journal of Applied Physics*, 23(8):838–843, 1952.
- [142] M. Seti, D.W. Thurman, J.P. Oberhauser, and J.A. Kornfield. Shear-mediated crystallization of isotactic polypropylene: The role of long chain-long chain overlap. *Macromolecules*, 35:2583–2594, 2002.
- [143] J. Shoemaker. *Moldflow Design Guide - A Reference for Plastics Engineers*. Hanser, Munich, 2006.
- [144] K.J. Singh. Mold cooling. In E.C. Bernhardt, editor, *Computer Aided Engineering for Injection Molding*. Hanser, New York, 1983.
- [145] C.W.M Sitters. *Numerical Solution of Injection Moulding*. PhD thesis, Technical University of Eindhoven, 1988.
- [146] J. Stevenson. An experimental study and simulation of disk filling by injection molding. *Soc. Plastics Engineers, Tech. Papers*, 22:282–288, 1976.
- [147] F.H.M. Swartjes. *Stress Induced Crystallization in Elongational Flow*. PhD thesis, Technical University of Eindhoven, 2001.
- [148] Moldflow Computer Aided Software Engineering System. ClearCase. 2005.
- [149] Z. Tadmor and I. Klein. *Engineering Principles of Plasticating Extrusion*. Van Nostrand Reinhold and Co., New York, 1970.
- [150] K. Talwar, F. Costa, V. Rajupalem, L. Antanovski, and C. Friedl. Three-dimensional simulation of plastic injection molding. *Society of Plastics Engineers, Technical Papers*, 46, 1998.
- [151] R.I. Tanner. *Engineering Rheology*. Oxford University Press, London, 2000.
- [152] R.I. Tanner. A suspension model for low shear rate polymer solidification. *J. Non-Newtonian Fluid Mech.*, 102:397–408, 2002.
- [153] R.I. Tanner. On the flow of crystallizing polymers, I. Linear regime. *J. Non-Newtonian Fluid Mech.*, 42:243–250, 2003.
- [154] G. Titomanlio, V. Brucato, and M.R. Kamal. Mechanism of cooling stress build-up in injection molding of thermoplastic polymers. *Inter. Polym. Processing*, 1:55–59, 1987.
- [155] G. Titomanlio, V. Speranza, and V. Brucato. On the simulation of thermoplastic injection moulding process. *Int. Polym. Processing*, 10:55–61, 1995.
- [156] G. Titomanlio, V. Speranza, and V. Brucato. On the simulation of thermoplastic injection moulding process II - Relevance of interaction between flow and crystallization. *Int. Polym. Processing*, 12:45–53, 1997.
- [157] H.L. Toor, R.L. Ballman, and L. Cooper. Predicting mold flow by electronic computer. *Modern Plastics*, December, 1960.
- [158] C.L. Tucker and E. Liang. Stiffness predictions for unidirectional short-fiber composites: Review and evaluation. *Composites Science and Technology*, 59:655–671, 1999.
- [159] Verein Deutscher Maschinenbau-Anstalten (VDMA). *Kenndaten Fur Die Verarbeitung Thermoplastischer Kunststoffe. Teil 1, Thermodynamik*. Carl Hanser Verlag, Munich, 1979.



- [160] D.C. Venerus, J.D. Schieber, V. Balasubramanian, K. Bush, and S. Smoukov. Anisotropic thermal conduction in a polymer liquid subjected to shear flow. *Physical Rev. Lett.*, 93:098301-1 – 098301-4, 2004.
- [161] D.C. Venerus, J.D. Schieber, H. Iddir, J.D. Guzman, and A.W. Broedman. Anisotropic thermal conduction in deforming polymer melts. *Soc. Plast. Eng. Proc. Annual Tech Conf. (ANTEC 2000)*, 2000.
- [162] D.C. Venerus, J.D. Schieber, H. Iddir, J.D. Guzman, and A.W. Broerman. Measurement of thermal diffusivity in polymer melts using forced Rayleigh light scattering. *J. Polymer Sci. Part B: Polym. Phys.*, 37:1069-1078, 1999.
- [163] W.M.H. Verbeeten, G.W.M. Peters, and F. Baaijens. Differential constitutive equations for polymer melts: The extended pom-pom model. *J. Rheol.*, 45:823-843, 2001.
- [164] S. Vleeshouwers and H.E.H. Meijer. A rheological study of shear induced crystallization. *Rheologica Acta*, 35:391-399, 1996.
- [165] S.F. Walsh. Shrinkage and warpage prediction for injection molded components. *J. Reinforced Plastic. Compos.*, 12:769-777, 1993.
- [166] H.P. Wang and H.S. Lee. Numerical techniques for free and moving boundary problems. In C.L. Tucker, editor, *Computer Modeling for Polymer Processing*. Hanser, Munich, 1989.
- [167] V.W. Wang and C.A. Hieber. Post filling simulation of injection molding and its applications. *SPE Technical Papers*, 34:290-293, 1988.
- [168] V.W. Wang, C.A. Hieber, and K.K. Wang. C-FLOW a CAE package with high level interactive graphics. In L.T. Manzione, editor, *Applications of Computer Aided Engineering in Injection Molding*. Hanser, New York, 1987.
- [169] I.M. Ward. *Mechanical Properties of Solid Polymers*. John Wiley and Sons, London, 1971.
- [170] I.M. Ward. *Structure and Properties of Oriented Polymers*. John Wiley and Sons, New York, 1975.
- [171] E. Wassner and R.D. Maier. Shear-induced crystallization of polypropylene melts. *Proc. XIII Inter. Congress Rheol., Cambridge, (D.M. Bindings et al. Eds.)*, 1:83-85, 2000.
- [172] L.E. Wedgewood and R.B. Bird. From molecular models to the solution of flow problems. *Ind. Eng. Chem. Res.*, 27:1313-1320, 1988.
- [173] T. Wiegmann and M. Oehmke. Measuring the PVT behavior of polymers. *Soc. Plastic Eng., Proc. Annual Technical Conference (ANTEC)*, 37:1646-1650, 1991.
- [174] G. Williams and H.A. Lord. Mold filling studies for the injection molding of thermoplastic materials. Part i: The flow of plastic materials in hot- and cold-walled circular channels. *Polym. Eng. Sci.*, 15:553-568, 1975.
- [175] J.A. Yamamuro, D. Penumadu, and G.A. Campbell. Modeling solids conveying in polymer extruders. *Int. Polym. Processing*, 13:3-8, 1998.
- [176] H. Yu and P.K. Kennedy. Apparatus and methods for performing process simulation using a hybrid model. *US Patent Application No. 20040210429*, 2004.

- 
- [177] H. Yu, C. Kietzmann, P. Cook, S. Xu, F. Costa, and P. Kennedy. A new method for simulation of injection molding. *Proc. Soc. Plastics Eng. Annual Tech. Conference (ANTEC)*, 2004.
- [178] H. Yu and A.R. Thomas. Method for modelling three-dimensional objects and simulation of fluid flow. *European Patent No. EP 0968473*, 2005.
- [179] H. Yu and R. Thomas. Method for modelling three dimension objects and simulation of fluid flow. *United States Patent No. 6096088*, 2000.
- [180] L. Yu, J. Lee, and K. Koelling. Flow and heat transfer simulation of injection molding with microstructures. *Polym. Eng. Sci.*, 44:1866–1876, 2004.
- [181] R. Zheng and P. Kennedy. Numerical simulation of crystallization in injection molding. In *Proc. 6th World Congress of Chemical Engineering*, Melbourne, September 2001.
- [182] R. Zheng and P. Kennedy. Modeling flow-induced crystallization. *Proc. 22nd Annual Meeting Polymer Proc. Soc., Melbourne*, 2003.
- [183] R. Zheng, P. Kennedy, X.J. Fan, N. Phan-Thien, and R.I. Tanner. Brownian dynamics simulation of non-dilute fibre suspension flows in a center-gated disk. *Soc. Plastics Engineers, Annual Technical Conference (ANTEC) Proceedings*, 2000.
- [184] R. Zheng, P. Kennedy, N. Phan-Thien, and X.J. Fan. Thermoviscoelastic simulation of thermally and pressure induced stresses in injection moulding for the prediction of shrinkage and warpage for fibre-reinforced thermoplastics. *J. Non-Newtonian Fluid Mech.*, 84:159–190, 1999.
- [185] R. Zheng, P. K. Kennedy, and R.I. Tanner. Apparatus and methods for predicting properties of processed material. *US Patent Application No. 20040230411*, 2004.
- [186] R. Zheng and P.K. Kennedy. A model for post-flow induced crystallization: General equations and predictions. *J. Rheology*, 48:823–842, 2004.
- [187] R. Zheng and P.K. Kennedy. Anisotropic thermal conduction in injection molding. *Proc. 22nd Annual Conference of the Polymer Processing Soc., Yamagata, Japan.*, 2006.
- [188] R. Zheng and P.K. Kennedy. Impact of flow on crystallization and impact of crystallization on flow in injection molding. *Proc. 2006 Academic Workshop on Advanced Forming Technology and Materials Processing, Shanghai, China*, pages 222–230, 2006.
- [189] R. Zheng, N. McCaffrey, K. Winch, H. Yu, and P. Kennedy. Predicting warpage of injection moulded fibre-reinforced plastics. *J. Thermoplastic Compos. Materials*, 9:90–106, 1996.
- [190] P. Zhu and G. Edward. Distribution of shish-kebab structure of isotactic polypropylene under shear in the presence of nucleating agent. *Macromolecules*, 37:2658–2660, 2004.
- [191] P. Zhu and G. Edward. Morphological distribution of injection-moulded isotactic polypropylene: A study of synchrotron small angle x-ray scattering. *Polymer*, 45:2603–2613, 2004.
- [192] P. Zhu, A. Phillips, J. Tung, and G. Edward. Orientation distribution of sheared isotactic polypropylene plates through thickness in the presence of sodium benzoate. *J. Applied Phys.*, 97, 2005.

- [193] P. Zhu, J. Tung, and G. Edward. Effects of sodium benzoate on distributions of lamellar structures of sheared isotactic polypropylene: A study using small angle synchrotron x-ray scattering. *Polymer*, 46:10960–10969, 2005.
- [194] P. Zhu, J. Tung, A. Phillips, and G. Edward. Morphological development of oriented isotactic polypropylene in the presence of a nucleating agent. *Macromolecules*, 39:1821–1831, 2006.
- [195] A. Ziabicki. *Fundamentals of Fiber Formation*. Wiley, New York, 1976.
- [196] A. Ziabicki. Crystallization of polymers in variable external conditions. II, Effect of cooling in the absence of stress and orientation. *Colloid Polym. Sci.*, 274:705–716, 1996.
- [197] P. Zoller, P. Bolli, V. Pahud, and H. Ackermann. Apparatus for measuring pressure-volume-temperature relationships of polymers to 350°C and 2200 kg/cm<sup>2</sup>. *Rev. Sci. Instruments*, 47:948–952, 1976.
- [198] H. Zuidema. *Flow Induced Crystallinity of Polymers, Applications to Injection Molding*. PhD thesis, Technical University of Eindhoven, 2000.
- [199] H. Zuidema, G.W.M. Peters, and H.E.H. Meijer. Development and validation of a recoverable strain-based model on flow induced crystallization of polymers. *Macromol. Theory Simul.*, 4:14–24, 2001.

# Samenvatting

---

Van alle numerieke modellen ontwikkeld voor vormgevingsprocessen van polymeren, zijn modellen voor het spuitgietproces veruit het meest succesvol. Reden daarvoor zijn de hoge kosten voor het ontwikkelen en maken van spuitgietmatrijzen, gekoppeld aan de kans op kostbare matrijswijzigingen ten gevolge van problemen die zich pas voordoen in de gebruiksfase. Dit maakt spuitgietsimulaties een bijzonder waardevol numeriek gereedschap waarmee dit soort kosten grotendeels kunnen worden voorkomen. Bij andere vormgevingsprocessen zijn de gereedschapskosten veel lager, of zijn problemen oplosbaar zijn door middel van het veranderen van de procescondities. Daarvoor zijn besparingen veel lager en dus zijn numerieke simulaties daar minder interessant.

Ondanks dit duidelijke succes van spuitgietsimulaties worden nog steeds te weinig polymere producten op enige wijze numeriek geanalyseerd. Daarnaast worden steeds hogere eisen gesteld aan de kwaliteit van voorspellingen van krimp en kromtrekken van producten.

Dit proefschrift behandelt punten ter verbetering en reikt oplossingen aan die er toe kunnen leiden dat het gebruik van numerieke modellen zal toenemen en de kwaliteit van de voorspellingen verder zal verbeteren.

Een belangrijk issue, ook commercieel, is het gebruik van de Hele-Shaw benadering in de modelvorming, wat toelaatbaar is voor dunwandige producten. Hiermee reduceren de behoudswetten voor massa en impuls tot twee vergelijkingen in het middenvlak tussen de productwanden omdat de druk in dikterichting constant wordt verondersteld. Met een rooster van driehoekselementen in het middenvlak kan het systeem relatief eenvoudig worden opgelost, gebruikmakend van de Eindige Elementen Methode. Dit is een elegante en efficiënte aanpak in termen van een numerieke oplossing, maar wel een die van de gebruiker vraagt om een 3D productgeometrie te vertalen in een representatie in het middenvlak. Dit is geen eenvoudige en een, veelal, interactieve taak die, daarom, veel tijd kan vergen. We noemen dit het geometrie probleem.

Spuitgietsimulaties vereisen materiaolgegevens zoals viscositeit, specifieke warmte, warmtegeleidingscoëfficiënt en dichtheid. Deze grootheden worden meestal gemeeten onder goed gecontroleerde laboratorium omstandigheden. Echter, bij de simula-

ties wordt deze data gebruikt voor totaal verschillende condities. Dus rijst de vraag hoe betrouwbaar deze data zijn voor het gebruik bij deze simulaties. We noemen dit het materiaalprobleem.

Beide problemen komen in dit proefschrift aan de orde. Hoofdstuk 1 geeft een overzicht van de geschiedenis van spuitgietsimulaties vanuit zowel een academische als commercieel oogpunt. Het blijkt dat de ontwikkeling van programmatuur sterk beïnvloed wordt door externe factoren zoals de beschikbare computercapaciteit en de benaderingen die gebruikt worden bij het formuleren van het wiskundige model.

Hoofdstuk 2 definieert de twee eerder genoemde problemen: het geometrie probleem en het materiaalprobleem.

De oplossing van het geometrie probleem wordt in hoofdstuk 3 gepresenteerd. Gebruikmakend van de, in de huidige CAD/CAM pakketten standaard, "3D Solid Modeling" wordt de DDFEA methode, "Dual Domain Finite Element Analysis", gepresenteerd. Oorspronkelijk ontwikkeld voor het stromingsprobleem tijdens het vullen van het product, wordt de methode uitgebreid naar het domein van structurele analyse, om ook kromtrekken van een product te berekenen. DDFEA maakt gebruik van het feit dat de meeste spuitgietproducten dunwandig zijn en is veel efficiënter dan een volledige 3D analyse.

Hoofdstuk 4 presenteert een praktische methode om een deel van de aan materiaaldata gerelateerde problemen, gekoppeld aan krimpvoorspellingen, te omzeilen. Deze aanpak wordt de CRIMS methode genoemd, "Corrected Residual In-Mold Stress". De aanpak is in essentie gebaseerd op een eenvoudig theoretisch model voor krimp, waarvan de parameters worden bepaald via een set gestandaardiseerde metingen. Voor een brede range van materialen geeft deze pragmatische procedure een drastische verbetering van krimpvoorspellingen.

Hoofdstuk 5 beschrijft een recente poging om de voorspelling van kromtrekken te verbeteren door middel van een meer volledige fysische beschrijving van het spuitgietproces. In het bijzonder betreft dit de beschrijving van de kristallisatiekinetiek en de daaruit resulterende morfologie van semikristallijnen polymeren. Uiteindelijk willen we, in de toekomst, op basis van de berekende morfologie, eindeigenschappen van een product voorspellen.

In Hoofdstuk 6 vindt de eerste uitwerking plaats naar modellen voor het voorspellen van materiaaleigenschappen gebaseerd op kristallisatiekinetiek en morfologie. Het is de bedoeling data, verkregen onder laboratorium condities, te gebruiken voor spuitgietcondities zoals gebruikt bij de simulaties. Er wordt een eerste poging gepresenteerd deze aanpak te valideren.

Tenslotte wordt het onderzoek zoals gepresenteerd in deze thesis, in Hoofdstuk 7 samengevat en aansluitend worden voorstellen gedaan voor toekomstig onderzoek.

# Dankwoord

---

There are many people to thank for my being able to submit this thesis.

First is Colin Austin – the founder of Moldflow. He took a big risk in hiring a mathematician with no knowledge of plastics in 1987. Thanks are also due to the Moldflow staff with whom I have worked over the years. It is from these interactions that I have learnt so much about polymers. Special thanks are due to Roland Thomas, Chris Friedl, Huagang Yu and Zhiliang Fan who have taught me many things over the years and continue to do so today. I offer very special thanks to my friend and colleague Rong Zheng. We have worked together since Rong began at Moldflow and he is an unending source of both inspiration and knowledge.

On the personal side, I want to thank my wife Pauline, and my boys, Anthony and William. Over the years they have put up with me spending time on the "never-ending thesis" rather than with them. I offer my thanks for their support and apologize for the times I was at home, but not really there for them, due to my preoccupation with a full time job and the thesis.

I thank my parents, Ken and Alice, for instilling a love of learning in all areas – particularly, music, literature and science. I hope I can, in turn, pass this special gift to my children.

Special thanks are also due to my promotor Prof. Han Meijer. After visiting his lab at Eindhoven in 1997 and spending an afternoon with him and Prof. Frank Baaijens, I realized that Eindhoven was a very special place. It is an honor for me to submit the thesis here. Thanks are also due to my co-promoters, Dr. Gerrit Peters and Dr. Patrick Anderson for encouraging me to submit a thesis, one night in the Portuguese town of Guimarães. I also acknowledge their help in preparing the thesis. Finally, I want to thank a fellow student – Carmela Tufano (Linda) – who assisted me greatly with the preparation of the thesis and the necessary formalities.



# Curriculum Vitae

---

Peter Kennedy was born on 22nd November 1955 in Melbourne, Australia. After his secondary school education he received a Bachelor of Science degree with Honours in Mathematics from La Trobe University in Melbourne with a thesis entitled, "Functional Equations and a Proof of Sterling's Theorem".

In 1984, he received a Diploma of Education from Melbourne University in Mathematics. After teaching secondary school mathematics at Upfield High School he joined Moldflow Pty. Ltd., with responsibility for documentation and training, in 1987.

He authored a book entitled "Flow Analysis of Injection Molds", which was published by Carl Hanser Verlag in 1995.

Since 2004, he has served as an Executive Vice President and Chief Technology Officer for Moldflow Corporation.





# Notes <sup>1</sup>

---

---

<sup>1</sup>Write your note/domande/osservazioni/complimenti/notes/questions/remarks/compliments/notities/vragen/opmerkingen/complimenten qui/here/hier!



